

Development of Simple Methods for RNA Biomarker Extraction and Detection

By

Nicholas M. Adams

Dissertation

Submitted to the Faculty of the
Graduate School of Vanderbilt University
in partial fulfillment of the requirements

for the degree of

DOCTOR OF PHILOSOPHY

in

Chemical and Physical Biology

May, 2014

Nashville, Tennessee

Approved:

David W. Wright

Frederick R. Haselton

Brain O. Bachmann

Terence S. Dermody

Andrew J. Link

Lawrence J. Marnett

To Farrah for her love and enthusiasm for our journey,
and to Pyper and Marley for keeping it all in perspective

And to Mike for his determination, courage, and heart
in the face of opposition

*What of us round pegs, with dogma's square holes,
where education's lathe is proficient
in yielding rods fit for paradigm's woes?
When thoughts inscribed in the box are content,
who'll question that which gave shape to the norm?
Why must it be square, not some other form?*

– Nick Adams

ACKNOWLEDGEMENTS

The work presented in this dissertation could not have been accomplished without the persistent help of many individuals. With that said, I would like to acknowledge all those that made this work possible. Funding support for the instruments, materials, and reagents used to conduct the research was provided by a combination of foundations, government entities, and institutions including the Bill and Melinda Gates Foundation, the National Institutes of Health, the National Science Foundation, and Vanderbilt University. The National Science Foundation Graduate Research Fellowship Program, the Bill and Melinda Gates Foundation, the National Institutes of Health Training Grant in Vascular Disease, and Vanderbilt University Fellowship provided personal financial support and covered tuition costs.

I feel indebted to my graduate mentors, David Wright and Rick Haselton. These two fall to opposite ends of almost every personality and style spectrum I can imagine. As a true demonstration of the *yin-yang* concept, their combined co-mentorship has benefitted me more than either of them could have done on their own. David has mastered the art of graduate student mentorship with his ability to give students enough guidance and resources to make them feel supported while leaving them space to grow and develop confidence in their abilities. His fiery ambition combined with his blind faith in my potential pushed me toward goals that I would not have thought to achieve. David has truly looked out for and supported my career trajectory. Rick has mastered the art of forgetting the perceptions and dogmas that are developed, established, and reaffirmed throughout the scientific community. He has the unique ability to look at the world with a fresh pair of eyes every day. The result of this ability is unconstrained generation of creative, brilliant, and sometimes even outright

crazy ideas and approaches to solving scientific and technological problems. Rick also has the coveted patience to listen more than he talks. Because of the unique and complementary attributes of David and Rick, I found my years in graduate school enriched with great opportunities, insightful instruction, and personal growth.

A number of individuals that I have worked with during my graduate tenure deserve acknowledgement. Many collaborators were key in making this work possible; these include Darryl Bornhop, Ian Olmsted, Besik Kankia, John Williams, and Jim Crowe. I would also like to thank those that worked along side me and helped pave the way for the research I completed; these include Jonas Perez, Amy Klemm, Hali Bordelon, Josh Swartz, and Keersten Davis. My productivity as a graduate student was greatly increased by a number of undergraduate researchers, graduate rotation students, and laboratory technicians that directly contributed to the projects that I worked on and whose efforts produced many of the results presented in this dissertation; these include Grant Zimmerman, Ricardo Francis, Cat Majors, Sheba Wariso, Amy Creecy, Lana Thomas, Jesus Benito, Philip Short, Abraham Wang, and Alison Caprioli. A special acknowledgement must be made to the rest of my lab mates, as they have made me a better researcher and communicator of scientific ideas; these include Anh Hoang, Reese Harry, Becca Sandlin, Stephen Jackson, Chris Gulka, Matt Bryant, Jenny Nesbitt, Kim Fong, Adam Ryan Travis, Anna Bitting, Joseph Conrad, Nicholas Wright, Wes Bauer, Alexis Wong, Lauren Gibson, and Philip Budge. These guys have been a lot of fun, and I consider each of them to be close friends that I will lean on throughout my life and career. I would also like to thank my thesis committee for their mentorship, guidance, input, and critical observations of my work; these include Brian Bachmann, Terry Dermody, Andy Link, and Larry Marnett.

One man, David Jones, incorrigibly altered my trajectory through academia many years ago. Jones is the most eloquent instructor, writer, and thinker I have met. He is an academic shaman, a man of great wisdom, and a man with a deep appreciation for, and understanding of, the value of serendipitous paths through life. He is artfully disruptive of traditional thought and social norms. Had I not had the calamitous fortune of crossing paths with Jones, I may very well have been happily, albeit blindly, practicing dentistry or selling real estate by now. Maybe I would have ended up a banker, a true working class hero. For all I know, I may have ended up a rich man. But because of his importunate influence, I have embarked on a career in science, a career of persistent failure, little recognition, and even less recompense. And now that my eyes have been opened, I can never look back. Fo'real.

My family consists of the most important people in the world to me. My deepest feelings of gratitude are reserved for my wife, Farrah, who has supported me during these years with enthusiasm and love, and who is supportive of all my foolish pursuits. She is an amazing, hard working, and committed mother of our one-year-old twin girls, Pyper and Marley. If Pyper and Marley can develop a mere portion of the character of their mother, they can expect to have a tremendous influence on the world. Already they happen to be the sweetest girls on the planet. I would like to thank my great parents for raising me with the freedom to think for myself. I thank my mom for her unconditional love for people. And I thank my dad for his selfless desire for his sons' success. All of my most desirable traits and values can be credited to the nature and nurture of my wonderful parents. I thank my brother Jordan for his example of well-placed ambition, confidence, and focus. The man built a successful welding business from the ground up overnight without knowing how to weld the day that he set out to do it. If I could emulate his unwavering pertinacity in my career, as he

has done for his own, I could expect to be at the top of the field in no time. And lastly, I hope to portray my great appreciation and respect for my younger brother, Mike. Mike has a persistent determination to achieve great things in life that makes *The Little Engine That Could* appear weak and pessimistic. When Mike stares up at the figurative mountains ahead of him I imagine that his motto is not “I Think I Can,” it is “I Know I Can.” He is a creative problem solver with exceptional work ethic and desire to overcome all challenges that he is faced with. And on top of it all, Mike has a heart of gold. I hope I can become more like him.

Lastly, I am inclined to mention my gratitude for the experience I have had as a graduate student. I feel that this experience will likely have the furthest reaching impact not because of the contributions I have made to the body of science, but because of what it has done to me. Contrary to the traditional education system, where learning is lathed with rigid class schedules, inflexible writing templates, and standardized exams, graduate school has allotted freedom. The academic environment that has surrounded and supported my work has provided the resources to unbox my mind through its reinforcement for creativity. The basis of my decisions of which laboratory to join, mentors to choose, and projects to claim was to capitalize on these resources. Because of this, I have learned to question “dogma’s square holes” and to consider ideas beyond the constraints of conventional thought. Graduate school has allowed me to draw from my experience and interdisciplinary perspective to attempt to solve complex problems using simple and unconventional approaches. I will always cherish this time in graduate school as a time of great growth and development as a scientist.

TABLE OF CONTENTS

	Page
DEDICATION	ii
ACKNOWLEDGEMENTS	iv
LIST OF TABLES	xi
LIST OF FIGURES	xi
Chapter	
I. INTRODUCTION	1
The burden of infectious diseases	1
Simple RNA biomarker detection methods are needed	2
Current molecular diagnostic methods are complex	3
Self-contained format simplifies complex methods	5
Overview of the body of the dissertation	6
Statement of Dissertation	8
Part I. Self-contained format for nucleic acid extraction	
II. DESIGN CRITERIA FOR DEVELOPING LOW-RESOURCE MAGNETIC BEAD ASSAYS USING SURFACE TENSION VALVES	13
Abstract	13
Introduction	14
Materials and Methods	17
Results	27
Discussion and Conclusions	35
Acknowledgments	45
III. DEVELOPMENT OF A LOW RESOURCE RNA EXTRACTION CASSETTE	46

Abstract.....	46
Introduction.....	47
Materials and Methods.....	49
Results.....	57
Discussion.....	62
Conclusion	67
Acknowledgments.....	67

Part II. Isothermal methods for nucleic acid detection

IV. THE EFFECT OF HYBRIDIZATION-INDUCED SECONDARY STRUCTURE ALTERATIONS ON RNA DETECTION USING BACKSCATTERING INTERFEROMETRY.....	70
Abstract.....	70
Introduction.....	71
Materials and Methods.....	74
Results.....	80
Discussion and Conclusions	93
Acknowledgements.....	98
V. QUADRUPLEX PRIMING AMPLIFICATION FOR THE DETECTION OF mRNA FROM SURROGATE PATIENT SAMPLES	99
Abstract.....	99
Introduction.....	100
Experimental Section.....	105
Results And Discussion	111
Conclusions.....	124
Acknowledgments.....	126
VI. TOWARD THE DEVELOPMENT OF A COMPLETE DIAGNOSTIC DEVICE .	127
Abstract.....	127

Introduction.....	128
Progress made toward a complete diagnostic device.....	128
Next steps for the development of a complete diagnostic device.....	131
REFERENCES	140
Appendix	
A. Supplementary Data.....	149
B. Illustrations of Concepts and Designs for Biomarker Extraction and Detection.....	155
C. Nucleic Acid Extraction Protocols and Reagents	167
D. Synthesis of the Respiratory Syncytial Virus RNA Biomarker Protocol	171
E. HEp-2 Cell Culture Protocol.....	174
F. Respiratory Syncytial Virus Culture Protocol	178
G. RNA and DNA Gel Electrophoresis Protocol	182
H. Circular Dichroism Spectroscopy of Nucleic Acids Protocol	184
I. Nanomaterial Functionalization and Evaluation Protocols.....	187
CURRICULUM VITAE.....	197

LIST OF TABLES

Table	Page
1. List of the probe sequences used in the BSI studies	76
2. Summary of binding curve slopes and limits of detection for each BSI probe	82
3. List of oligonucleotide sequences used in the QPA studies	105

LIST OF FIGURES

Figure	Page
1. Illustration of the self-contained format for extraction of RNA biomarkers	15
2. Selected video images of magnetic beads under the influence of the magnetic field.....	16
3. The properties of the materials tested in these studies span a wide range of values	19
4. The effect of material properties on the stability of the surface tension valve	29
5. The effect of interface orientation and fluid on the force required to pull beads	31
6. The effect of material properties on force required to pull beads.....	32
7. The effect of the material properties on the amount of solution carryover	35
8. Comparison of valve stability and penetrability for various material configurations	38
9. Design of the preliminary extraction method	53
10. Design of the continuous tubing extraction cassette.....	55
11. Comparison of RNA yields from nasal wash samples using five extraction methods	57
12. RNA recovered from buffer or cell lysates using extraction cassette or RNeasy kit	58
13. RNA extracted from RSV-infected cells using extraction cassette and RNeasy kit.....	59
14. Post-extraction distribution of RNA processing solutions after RNA extraction.....	60
15. Limit of detection of RNA after extraction using extraction cassette or RNeasy kit	61

16. Mechanism for RNA detection using backscattering interferometry (BSI)	72
17. BSI response using various lengths of DNA probes for the RNA target.....	81
18. BSI response using various combinations of DNA probes for the RNA target.....	83
19. Saturation curves of target RNA using increasing concentrations of DNA probes.....	84
20. BSI specificity for mismatched targets or RNA targets in complex samples.....	85
21. DNA probes generate a range of binding responses.....	87
22. BSI response using LNA and DNA probes	89
23. Degree of A-form character of nucleic acid hybrids corresponds with BSI signal	91
24. Degree of A-form character of TFE-treated DNA corresponds with BSI signal	92
25. Description of the quadruplex priming amplification (QPA) method	102
26. Schematic of the integrated self-contained mRNA extraction and QPA assay	104
27. 6-MI-labeled G-quadruplex as an effective molecular sensor	112
28. Optimal QPA signal determined by testing a range of conditions.....	114
29. QPA is a linear and quantitative amplification method when measured in real-time	115
30. Increase in fluorescence is proportional to the concentration of interface reagents.....	116
31. Self-contained format extracts mRNA and associates them with interface reagents	118
32. QPA performs well when heated within the self-contained format in a water bath.....	121
33. Depiction of prototype automated sample processor based on self-contained format	129
34. Illustration of the basic sample introduction method.....	131
35. Conceptual summary of the major integration components	133
36. Depiction of Qiagen's ESElog fluorescence detector system.....	135
37. Interface components for converting biomarkers to standardized DNA output.....	138

Chapter I

INTRODUCTION

The global burden of infectious diseases

Infectious diseases were the cause of almost half of all deaths in on the African continent and approximately one-sixth of all deaths worldwide in 2011 (1). Some of the most prevalent infectious diseases, which account for the vast majority of these deaths, include respiratory virus infections, HIV, tuberculosis, and malaria. In the United States, respiratory infections are among the most common reasons for which patients seek medical attention, accounting for 20% of all visits to primary care physicians and resulting in approximately 20,000 deaths and 114,000 hospitalizations (2,3). The burden of infectious diseases could be greatly reduced if effective medical treatment and management strategies were implemented, especially in low- and middle-income countries.

Effective clinical management strategies for infectious diseases are dependent on rapid and accurate diagnosis. Currently, the most common methods of diagnosis include identifying symptoms that are consistent with a specific disease and culturing cells or viruses from a patient sample. Because of the high overlap of clinical manifestations amongst different classes of infectious diseases, symptom-based diagnosis can be difficult and often requires a more definitive means of diagnosis, which oftentimes requires patient samples to be sent out to a clinical laboratory. Cell and virus cultures require trained personnel and can take several days to get a result. It is therefore simpler for physicians to prescribe antibiotics for symptoms consistent with an infection than to wait for the results of a cell culture or a report from a clinical laboratory. Consequently, more antibiotic prescriptions are written for

respiratory infections than for any other indication, despite the fact that viruses (i.e., rhinovirus, coronavirus, adenovirus, influenza, etc.) account for the majority of respiratory infections (2). The result has been an overuse of antibiotics, which has led to soaring rates of antibiotic-resistant strains of bacteria in the United States. These issues and many others could be mitigated if infections could be diagnosed quickly and conveniently in a clinician's office. Rapid and accurate diagnostics for respiratory viruses would also assist physicians in implementing other clinical management strategies, such as isolating infected patients to prevent nosocomial spread of infections.

Simple RNA biomarker detection methods are needed

For illnesses that advance as a result of the rapid pathogen doubling times, it is critical that the time-to-diagnosis be minimized. Pathogen biomarkers, or biological indicators of infection, have been identified to assist in diagnosing such illnesses. A pathogen biomarker is, in general, a biological molecule that is produced by a pathogen in an infected patient and can be used as a means for detecting the presence of the pathogen (4). Biomarkers are characterized as less expensive, more rapid, or more accessible to detect than the pathogen itself, and can therefore be used as surrogates for the pathogen (5). One advantage of properly characterized biomarkers is that their presence can be objectively measured using standardized detection methods; therefore, conclusions about the cause of an illness can be generated with less bias compared to more subjective diagnostic methods for infectious diseases, such as symptom monitoring, cell or virus culture, cell staining, or light microscopy. Biomarker detection methods also can be automated, thus reducing the potential for human error in the process of diagnosing a disease.

Ribonucleic acid (RNA) biomarkers have been established for a variety of pathogens. Human pathogens produce unique sequences of RNA as part of their natural life cycle. These RNA sequences have been exploited as “barcodes” of sorts for characterizing and identifying pathogen species and have become especially useful for pathogen detection and diagnosis of illnesses that result from pathogen infection. Another advantage of RNA as a biomarker of disease is that it is produced in great abundance during infection. For example, some viruses have been found to produce between 1,000 and 10,000 copies of a single unique sequence of RNA per virus particle (6,7). Because RNA has become a standard biomarker of disease for many pathogen infections, methods for detecting RNA from patient samples, or molecular diagnostic methods, are valuable. Molecular diagnostic methods that are simple and rapid are especially desirable in settings with limited access to laboratory resources and trained personnel.

Many places that could benefit from molecular diagnostics are unable to support the personnel or maintain and operate the equipment required for biomarker detection methods. This includes a wide range of health care facilities, from rural health outposts in developing countries to local clinics in developed countries. Throughout this dissertation, I describe any setting that is limited because of training, electricity, or financial constraints broadly as resource-limited settings or low-resource settings. In general, these terms are used to describe places that could benefit from laboratory-based diagnostics but that do not have the resources to access them.

Current molecular diagnostic methods are complex

Many molecular diagnostic methods are used to extract and detect RNA biomarkers found in patient samples for diagnosing pathogenic infections. These methods often involve

multiple steps to perform and commonly require expensive laboratory equipment or trained technicians. For example, reverse transcriptase-polymerase chain reaction (RT-PCR) is commonly used to identify RNA disease biomarkers from patient samples (8-10). Because of its sensitivity, specificity, and relatively rapid time-to-answer, it has become the gold-standard for RNA detection in clinical laboratories. The effectiveness of RT-PCR, however, is dependent on both the quality and quantity of nucleic acid template (11) and the absence of contaminants and interfering biological molecules (12). Therefore, complex and time-consuming sample preparation strategies are required to extract RNA from patient samples in preparation for RT-PCR. Furthermore, RT-PCR requires an expensive thermocycler to amplify and detect the target RNA and a computer with software to interpret the results. Because of these requirements, RT-PCR is generally conducted in large clinical laboratories with trained personnel and the resources to purchase and maintain expensive equipment and instruments. Therefore, in its current form, RT-PCR is oftentimes unavailable in many settings (13,14). Isothermal nucleic acid amplification approaches have been developed to function at a single temperature, and therefore do not require a thermocycler. Some isothermal approaches have been demonstrated to be as effective as traditional PCR and have the potential to be a simpler and less expensive alternative (13,15).

Simple rapid diagnostic tests based on lateral flow sample processing and antibody binding, which function much like common pregnancy tests, have been developed for resource-limited settings. Despite being easy to use, they are not effective in many cases because of their lack of specificity and sensitivity. This is because of two primary reasons: non-target molecules present in patient samples often interfere with detection, and target biomarkers are often present at low abundance (7,14,16,17). Therefore, methods for purifying

and detecting biomarkers of disease in patient samples are needed in settings with limited access to laboratory resources and trained personnel.

Magnetic bead-based methods have been developed for a variety of biological and biochemical applications such as biomolecule extraction, amplification, and detection, because, in part, they enhance the flexibility and simplicity the solid phase assay format (18-23). Despite their success, magnetic bead-based assays still generally require relatively complex procedures that involve dispensing multiple solutions or transferring the beads between solutions. For settings where trained personnel are not available or specialized laboratory equipment is too cumbersome for the application, such as in point-of-care diagnostics, extensive solution handling can reduce assay efficacy and, in many cases, is not feasible. Because of these obstacles, simple, self-contained formats for magnetic bead-based applications are highly desirable.

Self-contained format simplifies complex methods

The focus of this dissertation is on the development and evaluation of simple methods to extract and quantify RNA biomarkers from patient samples that are suitable for settings that lack the resources of a diagnostic laboratory. The physical format that I developed for processing RNA from complex samples is based on the simple idea that magnetic beads can capture RNA on their surface and be magnetically pulled across immiscible fluid separators, or surface tension valves, contained within small diameter tubing. Surface tension valves are fluids that are immiscible with processing solutions and prevent adjacent solutions from intermixing when arrayed within millimeter-diameter tubing. The valve mechanism is established by selective passage of magnetic beads at the surface tension valve interface. The enabling features of this physical format are that i) processing solutions (i.e., RNA binding

solutions, wash buffers, etc.) injected into a continuous length of small-diameter tubing and separated by immiscible fluid separators, or surface tension valves, remain isolated from one another, ii) magnetic beads under a magnetic field gradient can be transported across the surface tension barrier of the fluid separators, and iii) magnetic beads passing between adjacent solutions through a surface tension interface do not intermix the solutions. Because of these features, the format enables sample processing without pipetting, centrifugation, or other laboratory instrumentation.

Our laboratories have demonstrated the use of this self-contained format as a simple and effective format for conducting biological assays, such as extracting RNA, DNA, and proteins from complex samples (7,16,17). The format has also been shown to effectively integrate with simple RNA detection methods, including an interferometric method called backscattering interferometry (BSI) and an isothermal nucleic acid amplification reaction called quadruplex priming amplification (QPA) (24,25). The culmination of the efforts presented in this dissertation demonstrates that the self-contained format is an effective platform for the development of a complete diagnostic device with the potential to be implemented in resource-limited settings.

Overview of the body of the dissertation

The body of this dissertation covers four major research themes aimed at overcoming barriers to the development of diagnostic tests suitable for resource-limited settings. The findings of each of these research themes are the basis for the following four chapters, which are broken into two major parts. Chapters II and III and describes the design, development, and evaluation of a self-contained format for extracting RNA biomarkers from complex samples. Chapters IV and V and describes the development of simple methods for detecting

RNA biomarkers that are demonstrated to be compatible with the self-contained extraction format. The final chapter, chapter VI, describes the current state of progress toward developing a complete automated diagnostic device and outlines some additional steps that may be considered to produce a functional device. Concise summaries of the material and findings are provided at the beginning of each chapter.

Statement of Dissertation

It was once described to me that getting a Ph.D. degree consisted of becoming a extremely proficient, even a world expert, in a subfield of scientific research that is so specialized and focused on minutiae that it loses any practical relevance to society. I understand how that perception could be developed by a casual observer, as I have many times become so buried in a project that its context within the ‘big picture’ has become eclipsed by the layers of material that seem to settle on top of me. For the purpose this dissertation, however, I have reflected extensively on the impact that my research has made or has the potential to make to advance science and technology. For this exercise, I borrowed criteria for gauging the importance of science from Arturo Casadevall, Editor in Chief of the journal *mBio* and a major proponent of impactful science. Important science, he argues, should be sizable, practical, integrated, and new, which form the acronym “SPIN” (26). I will assess the importance of the work that I have completed during my graduate tenure using these criteria, and to put my own “SPIN” on the assessment, I will discuss them in the reverse order.

New. My research efforts have produced novel contributions in the fields of biomarker extraction and detection. This includes the development and characterization of a novel self-contained sample processing design and insights into the mechanism of backscattering interferometry (BSI) signal generation for detecting nucleic acids (7,24,27). The self-contained format is a new design for a biomarker extraction and detection format and has distinct advantages over other approaches to biomarker extraction and detection. First, it does not involve pipetting or other fluid transport steps in its operation. Second, the order of the processing steps is controlled by the order of the reagents contained within the

processing tubing. Third, the small diameter of the tube increases binding rates by decreasing the effective reaction volume and the distance target molecules must travel to interact with molecular capture elements. Furthermore, to characterize the physical performance of this format, I contributed to the development of a new dimensionless number that describes the relationship between the magnetic forces and surface tension forces that act on the beads, and can be used to predict whether magnetic beads will cross the solution/valve interface under the influence of a given magnetic field gradient (see Chapter II) (27).

My involvement on a project that employed BSI for RNA detection also contributed to the greater body of science by resulting in new insights about the factors involved in BSI signal generation. BSI had been used to successfully monitor binding interactions of a variety of biological molecules with high sensitivity, but had never before been used to detect and quantify RNA. I developed a unique method for detecting RNA based on refractive index shifts that result from DNA probes binding specific RNA targets as measured by BSI. In doing this, our laboratories observed for the first time that nucleic acid secondary structure alterations (from B-form to A-form) significantly changed the refractive index of a biological solution and produced a large BSI signal (see Chapter IV) (24).

Integrated. Important science may also integrate past knowledge with new knowledge to create something impactful. The research that I have conducted is interdisciplinary, integrating knowledge of biology, chemistry, and engineering to overcome challenges in the field of low-resource diagnostics. The physical format of the self-contained sample processor is a key enabler of integrated sample processing and biomarker detection. This is most clearly demonstrated in our work with quadruplex priming amplification (QPA) and our work with BSI. QPA was previously developed as a molecular sensor, limited to detecting a

unique template DNA sequence (28,29). Using the self-contained format and a novel mRNA-QPA integration reagent, I enabled mRNA detection using QPA (see Chapter V) (25). Similarly, BSI was previously developed to detect a variety of analytes in relatively complex solutions, but could not effectively detect RNA biomarkers contained within a complex surrogate patient sample. Only by extracting the RNA from the sample using the self-contained cassette was BSI able to effectively detect the specific biomarker sequence (see Chapter IV) (24).

Practical. Because the projects I have worked on are generally application driven, the outcomes have apparent practical benefits to society. The self-contained format is a simple, inexpensive, and disposable platform that enables complex assays to be performed by untrained users in settings lacking conventional laboratory equipment and materials (see Chapters II and III) (7,27). These features make the assay particularly practical for implementation in the field of low-resource diagnostics. The platform has the potential to be developed into a diagnostic device suitable for settings that lack laboratory resources and trained personnel (see Chapters V and VI) (25). The development of an automated device for reducing the number of steps that are completed by the end user is the focus of our current efforts. We expect that the culmination of these efforts will result in the development of a simple diagnostic device for a variety of diseases that could be implemented in resource-limited settings.

Sizeable. Research that is sizable must have the potential to impact a great number of people. Improving the methods for detecting infectious diseases that plague the developing world would impact a large number of people and is a major research thrust in the field of global health. The development of the self-contained RNA extraction format and integrated

detection assays has the potential to make complex and sensitive diagnostic assays accessible to the developing world by simplifying the process for the end user. The self-contained format for simplifying sample processing may also have the flexibility to extend beyond biomarker extraction and detection assays (see Chapter II) (27). Solid phase-based methods seem readily adaptable to this format and may benefit from the simplicity offered by the magnetic transport of beads through stationary solutions. The assay processing steps are self-contained, reducing the potential for contamination during processing with the use of an externally applied magnetic field to move the functionalized beads, which has some clear advantages in the greater fields of automated biopolymer synthesis, high throughput screening assays, or industrial quality control.

Part I. Self-contained format for nucleic acid extraction

Chapter II

DESIGN CRITERIA FOR DEVELOPING LOW-RESOURCE MAGNETIC BEAD ASSAYS USING SURFACE TENSION VALVES

Abstract

In this chapter, I outline the design and characterization of the physical parameters of our simple, self-contained assay format based on magnetic beads and surface tension valves (27). This self-contained format has the potential to facilitate the application of laboratory-based sample processing assays in low-resource settings and significantly reduce the time, expertise, and infrastructure required. The technology is enabled by immiscible fluid barriers, or surface tension valves, which stably separate adjacent processing solutions within millimeter-diameter tubing and simultaneously permit the transit of magnetic beads across the interfaces. I identify the physical parameters of the materials that maximize fluid stability and bead transport and minimize solution carryover. I found that fluid stability is maximized with ≤ 0.8 mm i.d. tubing, valve fluids of similar density to the adjacent solutions, and tubing with ≤ 20 dyn/cm surface energy. Maximizing bead transport was achieved using ≥ 2.4 mm i.d. tubing, mineral oil valve fluid, and a mass of 1 - 3 mg beads. The amount of solution carryover across a surface tension valve was minimized using ≤ 0.2 mg of beads, tubing with ≤ 20 dyn/cm surface energy, and air separators. Combining our experimental results into a single plot using two dimensionless numbers identified the most favorable parameter space for valve stability and bead transport. At the end of this chapter, a strategy is presented for developing additional self-contained assays based on magnetic beads and surface tension valves for low-resource diagnostic applications.

Introduction

Magnetic bead-based methods have been developed for a variety of biological and biochemical applications such as biomolecule extraction, amplification, and detection, because, in part, they enhance the flexibility and simplicity the solid phase assay format (18-23). Perhaps one of the clearest examples of the utility of magnetic beads is the development of automated, high-throughput, parallel extraction of nucleic acids from biological samples in a 96-well plate format (30), a process that would be too cumbersome or inefficient using a traditional column-based solid phase format. Despite their success, magnetic bead-based assays still generally require relatively complex procedures that involve dispensing multiple solutions or transferring the beads between solutions. For settings where trained personnel are not available or specialized laboratory equipment is too cumbersome for the application, such as in point-of-care diagnostics, extensive solution handling can reduce assay efficacy and, in many cases, is not feasible. Because these obstacles are faced in low-resource settings, simple, self-contained formats for magnetic bead-based applications are highly desirable.

The development of multiphase fluidic systems for fluid separation and manipulation has also been used for simplifying and automating chemical and biological assays. In microfluidic systems, controlled fluid-fluid interfaces and microencapsulation of assay components and reagents have been applied to a variety of methods, including large-scale parallelization of chemical screening and high-throughput nucleic acid sequencing (31). Multiphase microfluidic systems feature robust fluid separation and permit controlled manipulation of assay reagents. These characteristics make multiphase microfluidics a desirable platform for developing technologies to be used in low-resource settings.

Our laboratories have exploited the simplicity of magnetic bead-based assays and the robustness of multiphase fluidics to develop methods for the extraction of RNA, DNA, or protein biomarkers in a simple, self-contained format suitable for use in a low-resource environment (7,16). The analogous commercial kits for nucleic acid or protein extraction require centrifugation and extensive solution handling or pipetting, whereas the self-contained assays our laboratories have developed have a much simpler user interface. The assay is carried out within a single length of 1.6 mm inner diameter (i.d.) tubing containing pre-arrayed processing solutions and magnetic beads (Figure 1). The biological sample is added to the first processing solution through the end of the tube using a transfer bulb or by syringe injection through the tubing wall, and then functionalized beads are mixed with the sample using an externally applied magnetic field to selectively capture the biomarker of interest. As the beads are moved from one solution to the next through surface tension valves, the valves maintain their integrity and no solution intermixing occurs. To ensure that the magnetic beads mix properly, the magnetic field is moved back and forth along the length of the tube to disperse the beads throughout the solution.

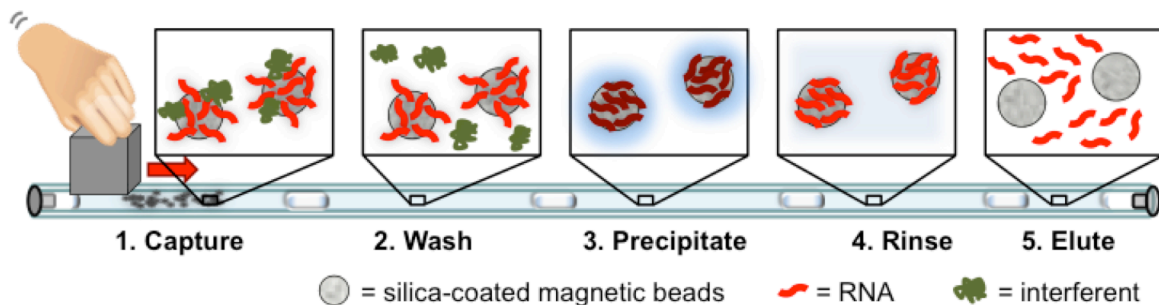


Figure 1. Illustration of the self-contained format for extraction of RNA biomarkers. Surface tension valves separate unique processing solutions arrayed within a single length of 1.6 mm i.d. tubing. Functionalized magnetic beads used to capture the biomarker of interest are drawn through the surface tension valves into each processing solution using an externally applied magnetic field (i.e., a permanent cube magnet).

Surface tension valves are fluids that are immiscible with processing solutions and prevent adjacent solutions from intermixing when arrayed within millimeter-diameter tubing. The valve mechanism is established by selective passage of magnetic beads at the surface tension valve interface. Magnetic beads under the influence of a sufficiently strong magnetic field gradient traverse the immiscible phase when a sufficient mass of beads is gathered at the interface (Figure 2). The surface tension valve format inverts the classical solid-phase assay format by immobilizing the assay solutions and making the solid phase the movable entity. The advantages of this format are in its simplicity; using preloaded assay solutions separated by immiscible surface tension valves, cumbersome liquid handling and dispensing steps are eliminated and the assay is carried out by simply manipulating the transit of magnetic particles through the various processing solutions using a magnetic field. This inverted solid phase format based on magnetic beads and stationary fluids separated by surface tension forces has been developed for a number of applications (32-36). Other laboratory-based magnetic bead assays, such as enzyme-linked immunosorbent assays (ELISAs) or onbead isothermal polymerase chain reaction (PCR), could potentially benefit from the simplicity and flexibility of this format for applications in low-resource settings. In

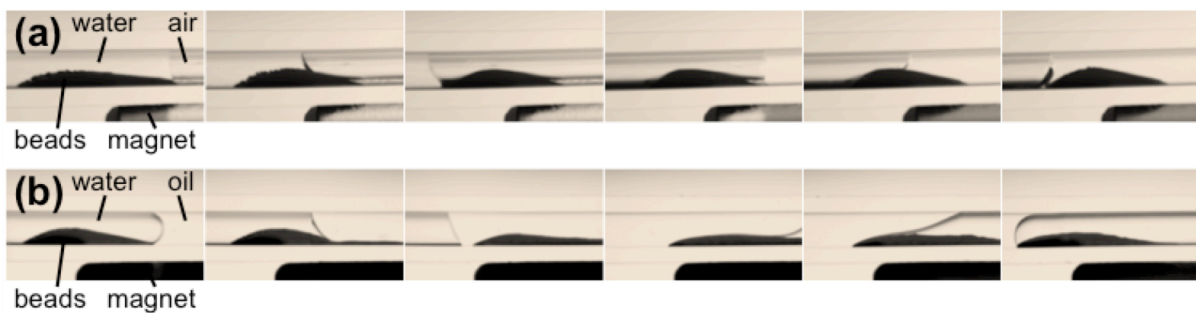


Figure 2. Selected video images of magnetic beads under the influence of the magnetic field of a permanent magnet moving from one solution to the next through an air surface tension valve (A) or a mineral oil surface tension valve (B).

this chapter, I identify and characterize the key physical design constraints for developing a self-contained format suitable for magnetic bead-based assays.

Materials and Methods

Materials

Tygon R-3603 tubing (0.8, 1.6, 2.4, 3.2 and 4.8 mm i.d.) and Chemfluor fluorinated ethylene propylene (FEP) tubing (1.6 mm i.d.) were purchased from Fisher Scientific. Glass tubing (1.6 mm i.d.) was purchased from the Vanderbilt Glass Shop. Siliconized glass was produced using Sigmacote SL-2 (Sigma-Aldrich) following the manufacturer's protocol. Briefly, the glass was cleaned using a piranha solution (3 H₂SO₄ : 1 H₂O₂). The glass was then submerged in Sigmacote solution for approximately 1 minute then allowed to dry. The coated glass was then rinsed with water and baked at 100 °C for 1 hour. The silicon coating was validated by a characteristic ~100° contact angle with water. Dynabeads MyOne Silane beads were purchased from Life Technologies (cat. # 370-02D). MagAttract Suspension E beads were purchased as part of the MagAttract RNA Tissue Mini M48 Kit from Qiagen (cat. # 959236), and AccuBead beads were purchased from Bioneer Corporation (cat. # TS-1010-2). The solutions that were selected for these studies are common nucleic acid extraction buffers and span a range of surface tension values. These solutions were GuHCl buffer (4 M guanidine hydrochloride, 25 mM sodium citrate, pH 7.0), 50% EtOH GuSCN buffer (50% ethanol, 2 M guanidine thiocyanate, 25 mM sodium citrate, pH 7.0), 80% EtOH buffer (80% ethanol, 5 mM potassium phosphate, pH 8.5), and deionized water. The surface tension valve fluids used in these studies include air or molecular biology grade mineral oil (Bio-Rad). A

2.54 cm cube magnet (Emovendo, SKU # M1CU) was used to transport the magnetic beads through the solutions in the tubing.

The range of surface and interfacial tensions of the solution/valve interfaces used in these studies spans from ~ 0 to 72 dyn/cm, and the range of surface energies of the tubing tested spans the range of commercially available materials (~ 20 to 42 dyn/cm) (Figure 3A and B). Photographs comparing the configurations used in these studies are shown in Figure 3C. The most notable difference among the tubes is the curvature of the menisci, which reflect the large range of solid/liquid/gas interactions evaluated in these studies. Tubes were prepared by loading them with solutions serially through one end of the tube using a pipette. Unless otherwise noted, the baseline experimental configuration for these studies is an 8 cm length of 1.6 mm i.d. Tygon R-3603 tubing preloaded with two 75 μ L water aliquots separated by a 1 cm air gap (valve). The tubing was plugged on both ends using plastic end caps. Solution carryover and magnetic force studies were performed using 1 mg of Dynabeads MyOne Silane.

Surface energy measurements

The surface energy of the materials used in these studies was calculated using the Zisman method. Contact angles of several test liquids spanning a range of surface tensions, including distilled water, glycerol, formamide, ethylene glycol, 1-bromonaphthalene, and

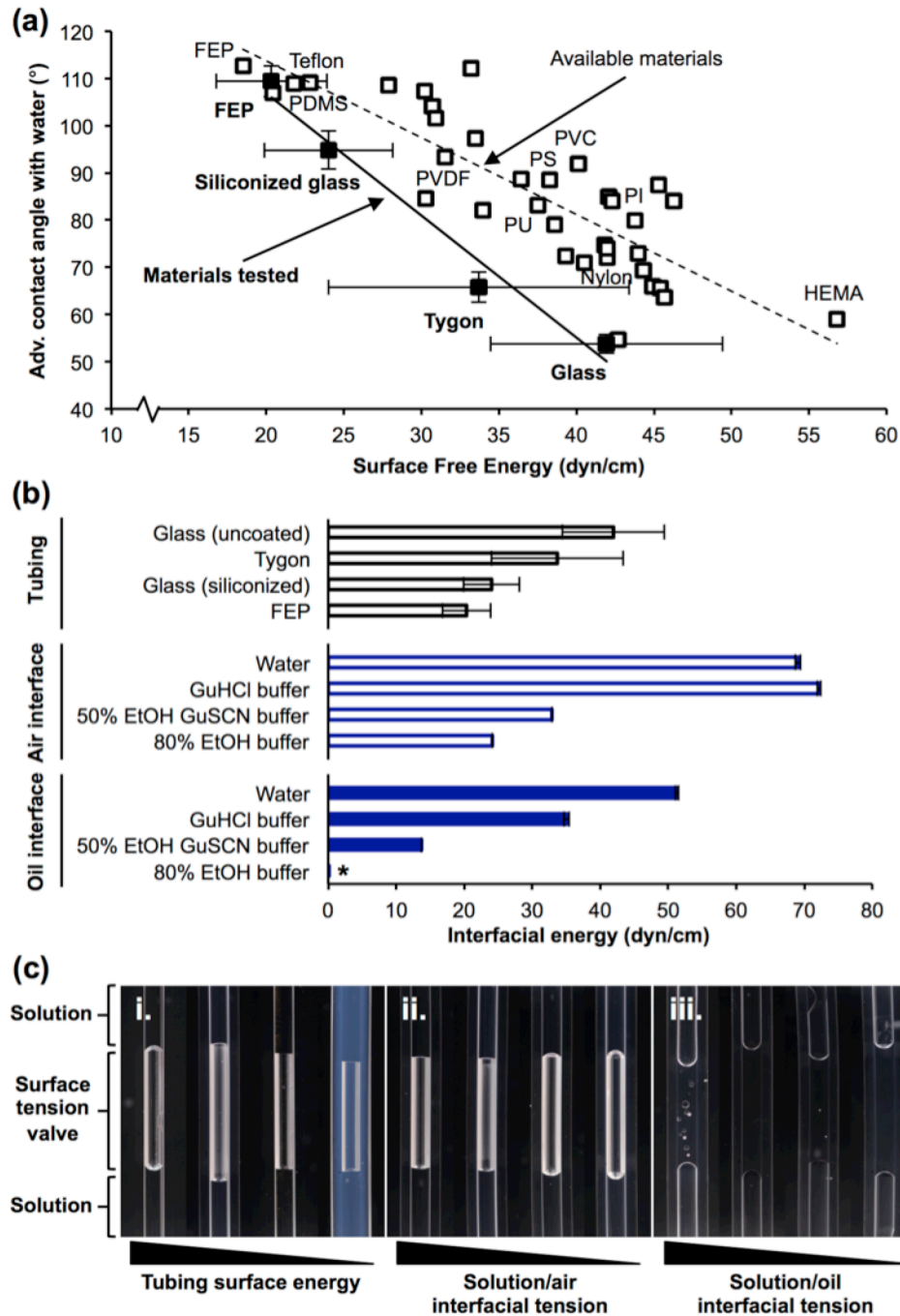


Figure 3. The properties of the materials tested in these studies span a wide range of values. A) The surface free energy of the various materials is related to the advancing contact angle with water. The surface free energies of the materials used in these studies (solid squares) span the range of available materials (open squares). B) Tubing, solutions, and valve types tested span a wide range of interfacial energies. C) Images showing the curvature of the menisci for tubing materials, solutions, and valve fluids evaluated in these studies. From left to right: i. water and an air valve in tubing of decreasing surface energies. ii. Tygon tubing and an air valve with solutions of decreasing interfacial tensions. iii. Tygon tubing and a mineral oil valve with solutions of decreasing interfacial tensions.

diiodomethane, on the surface of each material were recorded using a standard goniometer (Rame-Hart Inst., model # 200-F4). Three angle measurements were taken from four separate ~ 2 μL drops placed on each material. The surfaces of the materials were cleaned after each test liquid by rinsing with deionized water and then 100% ethanol. The surface energy of each material was calculated using the Zisman plots created using the DROPImage Standard V. 2.4 software (Rame-Hart Inst.).

Interfacial tension measurements

Interfacial tension of the solutions used in these studies was determined by using a Sigma 700 Tensiometer (Biolin Sci.) using the Du Nouy ring method. The Du Nouy ring was lowered into 30 mL of each test liquid and the force data was collected and analyzed using the Attension Sigma software (Biolin Sci.). Each measurement was repeated 25 times for each solution. For interfacial surface tension between the liquids and mineral oil, the same protocol was followed except that 30 mL of mineral oil was layered on top of each solution tested, and the ring was lowered into the mineral oil layer before measurements were made. The ring was washed thoroughly after each test with 100% ethanol. The readings through the layers of 80% EtOH buffer and mineral oil were approximately zero, because the two solutions swirled together during the measurements. Therefore, the interfacial tension of the 80% EtOH buffer interfaced with mineral oil was approximated as 0 dyn/cm.

Valve stability measurements

To produce an effective acceleration, or body force, in the x , y , or z direction of the tube, a centrifuge suitable for spinning the tubes was constructed. The centrifuge was used for

measuring the relative centrifugal force (RCF) at which the surface tension valve fails. A motor interfaced with Labview software was used to spin the tubes containing the surface tension valve at defined speeds, which were converted to RCF through the following relationship: $RCF = 1.12r \left(\frac{RPM}{1000} \right)^2$. Tubes were prepared by loading a solution containing Brilliant Blue dye on one side of a surface tension valve with a solution containing no dye on the other side of the valve. Rotational velocity was gradually increased until the valve failed as defined by blue color appearing in the clear solution on the opposite side of the valve. The stability values are reported in terms of the g-force that caused the valve to fail when applied in the direction perpendicular to the tubing wall, which is the orientation that is most likely to cause the valve to fail. The effects of the properties of the surface tension valves on valve failure were determined for different tubing types and diameters, valve contents and lengths, and solution contents. This method was validated using the impact-based drop method to evaluate valve stability. The baseline configuration used in these studies was 1.6 mm i.d. Tygon tubing loaded with two 75 μ L volumes of water separated by an air valve, unless otherwise noted.

Valve penetrability measurements

The force required to move a group of beads through the surface tension valve in the linear tubing, where the movement is constrained to the x direction only ($F_{m,x}$), was calculated using the following equation described by Gijs (37):

$$F_{m,x} = \frac{v\chi_v}{\mu_o} \left(B_x \frac{\partial}{\partial x} + B_y \frac{\partial}{\partial y} + B_z \frac{\partial}{\partial z} \right) B_x$$

where V is the volume occupied by the magnetic beads (m^3), χ_v is the volume susceptibility (CGS), μ_0 is the permeability of free space ($4\pi \times 10^{-7} \text{ T}\cdot\text{m}/\text{A}$), and B is the magnetic field along the axis of the tube through which the beads are pulled (T/m). Volume (V) was measured as the bulk volume that the particles occupied under the influence of a magnetic field. The values were calculated by measuring the cylindrical volume that a known mass of beads occupied in a short length of 1.6 mm i.d. tubing. Volume susceptibility (χ_v) of the magnetic particles was calculated by measuring the magnetic susceptibility of the beads using an Alfa Aesar Magnetic Susceptibility Balance Mark 1. This was done by taking 1 mg of Dynal beads, MagAttract beads, or Bioneer beads and diluting them into 114 mg silica gel, which is the amount required to fill the standard size glass tubes to the required ~ 3 cm height. The calibration constant was calculated using the manganese chloride standard supplied by the manufacturer. The blank was made using 114 mg silica gel without beads added. The tube was rinsed with water between each sample, dried at 100°C for 10 min, and the magnetic susceptibility of the empty tube was measured to verify that residual magnetic beads had been removed after each wash. Each sample was measured three times, removing and repacking the beads between each measurement. Mass susceptibility (χ_g) was calculated using the following equation:

$$\chi_g = \frac{C_{bal} \times (R - R_0) \times l}{10^9 \times m}$$

where C_{bal} is the calibration constant, R is the sample value, R_0 is the blank value, l is the length (cm) of sample in tube, and m is the mass of magnetic sample in the tube. This was converted to volume susceptibility (χ_v) using the following conversion factor: $\chi_v = \chi_g d$, where d is the bulk density of the beads in the presence of a magnetic field.

To measure the force required to pull the beads through the solution/valve interface, an apparatus was developed to measure x , y , and z coordinates of the magnetic field (B) of a 2.54 cm cube permanent magnet (Emovendo, SKU# M1CU) at 0.5 mm intervals along the axis of the tube using a F.W. Bell series 9900 gaussmeter. The values for the x , y , and z coordinates were plotted as a function of distance from the edge of the magnet. The gradient of the magnetic field for the x , y , and z coordinates $\left(B_{(x,y,z)} \frac{\partial}{\partial(x,y,z)}\right)$ was approximated using the slope of the lines between two consecutive magnetic field measurements. Because the gradient of the magnetic field in the y and z coordinates was approximately zero, the $B_y \frac{\partial}{\partial y}$ and $B_z \frac{\partial}{\partial z}$ terms of the magnetic force equation were set to zero.

To measure the force required to pull the beads through a surface tension valve, a preloaded tube containing magnetic beads was slowly moved toward the 2.54 cm cube magnet along the x coordinate of the measured magnetic field until the point at which the beads pulled through the valve interface. The distance of the interface from the magnet was recorded and used to approximate the magnetic field strength (B_x) and the magnetic field gradient ($B_x \frac{\partial}{\partial x}$) at that distance. The magnetic force requirement values for 1 mg Dynabeads MyOne Silane beads moving from water into an air valve in Tygon R-3603 tubing were validated using a second permanent magnet, one-fourth the size of the magnet described above (1.27 cm cube), in a manner similar to the methods described above. The baseline experimental configuration used in these studies was 1.6 mm i.d. Tygon tubing loaded with 75 μ L volume of water and another 75 μ L volume of water containing 1 mg Dynabeads MyOne Silane beads separated by an air valve, unless otherwise noted.

Solution carryover measurements

Carryover volume was measured using a fluorescence-based assay. In these studies, fluorescein was added to each solution tested and standard curves were made for small volumes of each solution diluted into water. The standard curves for each solution had R^2 values > 0.98 and consisted of at least five data points. Tubes were loaded with a test solution containing fluorescein and water separated by an air or mineral oil valve. Using a permanent magnet, beads were pulled from the fluorescein-containing solution, through the valve, and into the water solution. Then the beads were mixed with the water and removed from the water. The amount of liquid carryover associated with the beads was measured by plotting the value of fluorescence that was introduced into the water on the standard curve of fluorescein in the corresponding solutions diluted into water. The effect of material properties on solution carryover was determined for different tubing types, valve contents and lengths, bead types and masses, and solution contents. The solution carryover values for 1 mg Dynabeads MyOne Silane beads moving from water into an air valve in 1.6 mm i.d. Tygon R-3603 tubing were validated using a solution mass measurement. The baseline experimental configuration used in these studies was 1.6 mm i.d. Tygon tubing loaded with 75 μ L volume of water and another 75 μ L volume of water containing 1 mg Dynabeads MyOne Silane beads separated by an air valve, unless otherwise noted.

Imaging

Digital photographs of the fluids within the tubing for the various configurations tested were collected using a Nikon D100 D-SLR camera with a 60 mm AF Micro Nikkor lens and three Kenko extension tubes (58 mm total extension length). Videos of the magnetic beads

crossing the surface tension valves were recorded using a Nikon D800 D-SLR camera with the lens and extension tubes used for collecting the images.

Electron micrographs of the three bead types were collected using a Hitachi scanning electron microscope at 3000× zoom with a 3 kV beam strength, a working distance of 14 mm, and an objective aperture position of 2. Bead samples were prepared by pipetting 5 μL of each bead suspension directly onto an aluminum specimen mount and drying at 80 °C overnight.

Preliminary valve stability studies

An impact-based drop method was used to validate the valve failure values recorded using the centrifuge method described above. The surface tension valve failed when the preloaded tubing was dropped from a height of 1.05 m onto a solid surface without any impact-dampening materials. The impact force that caused the valve to fail was approximated assuming a conservative impact time of 15.4 ms. Both the centrifugation and impact methods yielded similar failure values for the baseline configuration of 28.8 ± 0.24 g and 30.1 ± 4.6 g, respectively. The greater error associated with the impact method could be attributed to uncontrollable experimental variables, such as the angle of the tubing at impact, vibrations in the tubing after impact, and bouncing of the tubing after impact. Because there was significantly more experimental error using the impact method, the centrifugation method was used for the valve stability studies.

Preliminary valve penetrability studies

In preliminary studies, two permanent magnets were tested to determine if the method of measurement could be applied to different sizes of permanent magnets. A 2.54 cm and a 1.27 cm cube neodymium magnets were used, each having different magnetic strengths and magnetic field gradients. Both magnets yielded similar force measurements, validating the method for determining force produced on the beads under a measured magnetic field gradient. The force required to pull 1 mg Dynabeads MyOne Silane beads from water into the air valve within 1.6 mm i.d. Tygon R-3603 tubing was $326 \pm 78 \mu\text{N}$ using the 2.54 mm cube magnet and 362 ± 124 using the 1.27 mm cube magnet. The relatively large error associated with these measurements is attributed to the sub-millimeter differences between measurements at close proximity to the magnet, where the magnetic field gradient is the steepest. Accordingly, there is greater error using the smaller magnet, for which the magnetic field is steeper than the large magnet. The large magnet was used for further force measurement studies.

Preliminary carryover studies

To validate the fluorescence-based method for measuring solution carryover, a mass-based method was used. Within the tubing, beads were pulled from water and into the air space at the end of the tubing, and the section of tubing containing the beads with the associated carryover solution was cut out using a razor blade. The section of tubing was then quickly weighed, and the average of three measurements was recorded. The tubing containing the beads were then dried for 30 min at 100 °C in an oven, placed at room temperature for 30 min, and then weighed again three times. The difference between the

averages of the measurements was used to determine the amount of water carryover associated with the beads. In baseline configuration studies, both the fluorescence and mass-based methods yielded similar carryover values of $1.31 \pm 0.01 \mu\text{L}$ and $1.26 \pm 0.21 \mu\text{L}$, respectively. The greater error associated with the mass-based method is most probably the result of the lack of precision of the balance for low masses ($\sim 1 \text{ mg}$). Also, the more volatile liquids (i.e., those with 50% or 80% ethanol) evaporate from the beads too quickly to make accurate measurements using the mass-based method. Consequently, the fluorescence-based method was used in subsequent carryover studies.

Results

In experimental evaluations of the self-contained format based on surface tension valves I sought to identify physical parameters that i) maximized valve stability, ii) enhanced valve penetrability by magnetic beads, and iii) minimized the carryover of one processing solution to the next. Each of these characteristics is essential for developing an assay format that is simple, robust and effective outside of a laboratory setting. The greatest utility is achieved with a stable preloaded assay format, which could be transported and stored for long periods of time. Similarly, enhancing valve penetrability minimizes the magnetic force required for processing and yields the most effective format for reproducible assay results. Finally, carryover between processing steps is minimized as it can contaminate and negatively impact downstream chemistries and molecular interactions. Factors that affect each of these performance characteristics are detailed in the following sections.

Valve fluid stability

Tubing diameter has a substantial effect on valve stability. Valves prepared in the smallest commercially available diameter of Tygon R-3603 tubing (0.8 mm i.d.) were extremely stable and did not fail at 84.9 g (the highest RCF tested), which is equivalent to dropping the tubing from a height of ~8.4 m assuming no air drag (Figure 4A). The stability drops off exponentially with increasing tubing diameters up to 4.8 mm (surface tension valves can not be supported in tubing with a 5.6 mm diameter or greater). The effect of the surface energy of the tubing material was not as striking but suggests a linear, inverse relationship between valve stability and tubing surface energy (Figure 4B). Valves prepared in FEP tubing, which has the lowest surface energy of the tubing materials tested (20.3 dyn/cm), were the most stable, failing at 48.2 g. Valves prepared in glass tubing, which has the highest surface energy of those tested (42 dyn/cm), on the other hand, were the least stable, failing at 22.5 g.

Valve fluid also had a substantial effect on valve stability. Overall, valves prepared with mineral oil were significantly more stable than those prepared with air (Figure 4C and D). Additionally, mineral oil valve stability decreased, whereas air valve stability increased, with increasing interfacial tension. The most stable valve tested under these conditions was mineral oil interfaced with 80% EtOH buffer, which did not fail at the highest RCF tested (80 g), whereas the least stable valve was air interfaced with 80% EtOH buffer, which failed at 4.5 g (Figure 4C). The density difference between the solution and valve appears to predict valve stability for all the solution/valve combinations tested, particularly for solutions interfaced with mineral oil valves (Figure 4D).

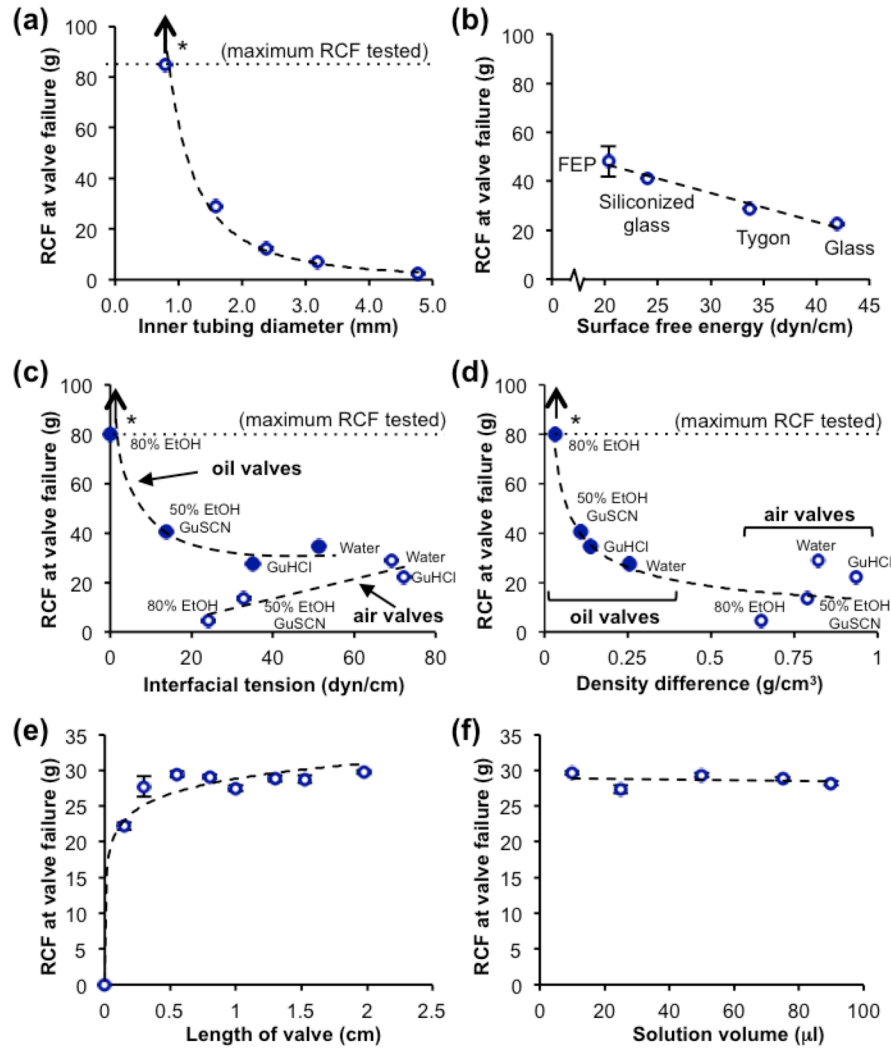


Figure 4. The effect of material properties on the stability of the surface tension valve. A) Surface tension valves within tubing with smaller inner diameter are much more stable than those within tubing with larger diameters. B) Surface tension valves within tubing with low surface energy are more stable than those within tubing with high surface energy. C) The stability of mineral oil valves decreases with increasing interfacial tension (solid circles), whereas the stability of air valves increases linearly with increasing interfacial tension (open circles). D) Surface tension valves interfaced with solutions of similar density are much more stable than those interfaced with solutions with a greater difference in density. E) Valve stability increases sharply with valve lengths smaller than 0.3 cm and remains consistent with longer valve lengths. F) The volume of water flanking the valve has little effect on the stability of the valve. *Valve did not fail at maximum RCF tested. (n = 3, mean \pm s.d.; if not visible, error bars are obscured by the symbols)

The effect of the length of the valve and the volume of the processing solutions on valve stability was also evaluated. Tygon R-3603 tubing (1.6 mm i.d.) was loaded with a range of air valve lengths up to 2 cm separating the two water solutions. I found that the smallest possible air valve, or separation gap, that can effectively prevent solution intermixing was 0.15 cm, which was slightly less stable than a 0.3 cm valve length, most likely because the opposing menisci of adjacent solutions are nearly touching. All valve lengths 0.3 cm or greater failed at approximately 29 g, suggesting that air separations greater than 0.3 cm offer no advantage for valve stability (Figure 4E). All solution volumes tested (10 - 90 μL water) had approximately the same stability, failing at approximately 29 g (Figure 4F). Although the tested range of valve lengths and solution volumes were limited by the design of the centrifuge, it is reasonable to assume that valve lengths and solution volumes greater than those tested would follow the established trend and also have little influence on the stability.

Valve penetrability

The force required to pull the beads from water into the air valve was much greater than the force to pull from the air valve into water ($372 \pm 78 \mu\text{N}$ and $52 \pm 8.7 \mu\text{N}$, respectively) (Figure 5). A similar trend was observed using a mineral oil valve ($18.7 \pm 8.2 \mu\text{N}$ and $1.6 \pm 0.3 \mu\text{N}$, respectively), although overall the forces were significantly smaller than those with the air valve. Additionally, the force required to pull beads along the tubing wall within an aqueous solution (i.e., the force required to overcome friction and drag) is the same as the force required to pull beads from an oil valve into water ($1.6 \pm 0.3 \mu\text{N}$), which is negligible compared to the forces required for beads to penetrate the solution/valve interface. Therefore,

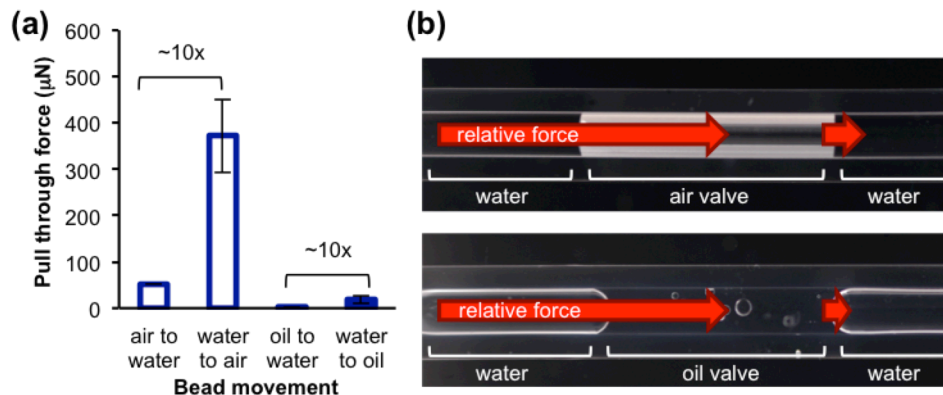


Figure 5. The effect of interface orientation and fluid on the force required to pull beads through the solution/valve interface. A) The force that is required to pull beads into or out of the the mineral oil valve (solid bars) is ~25-fold less than the force required to pull beads into or out of the air valve (open bars), respectively. B) The force required to pull the beads from water into the air (top panel) or mineral oil (bottom panel) valve is ~10-fold greater than the force required to pull the beads out of the valve into water. The length of the arrows indicates the normalized relative force required to pull beads through the valve interface. ($n = 3$, mean \pm s.d.; if not visible, error bars are obscured by the symbols)

the force required to pull the beads from the solution into the valve, through the solution/valve interface, is reported, since this is the largest of the forces and thus the limiting force for transporting beads.

The diameter of the tubing had a significant impact on valve penetrability. The force required to pull the beads through an air valve drops significantly with larger diameter tubing (Figure 6A). In 0.8 mm i.d. tubing, the required force is large and variable ($678 \pm 271 \mu\text{N}$), whereas in larger tubing diameters (2.4 to 4.8 mm i.d.) the required forces are much lower, in the range of ~60 to 100 μN . The effect of tubing surface energy was less conclusive. With the exception of Tygon R-3603 tubing, which has a force requirement of $326 \pm 78 \mu\text{N}$, there appears to be a positive correlation between surface energy of the tubing and force required to pull the beads through the valve (Figure 6B). The tubing with the lowest surface energy

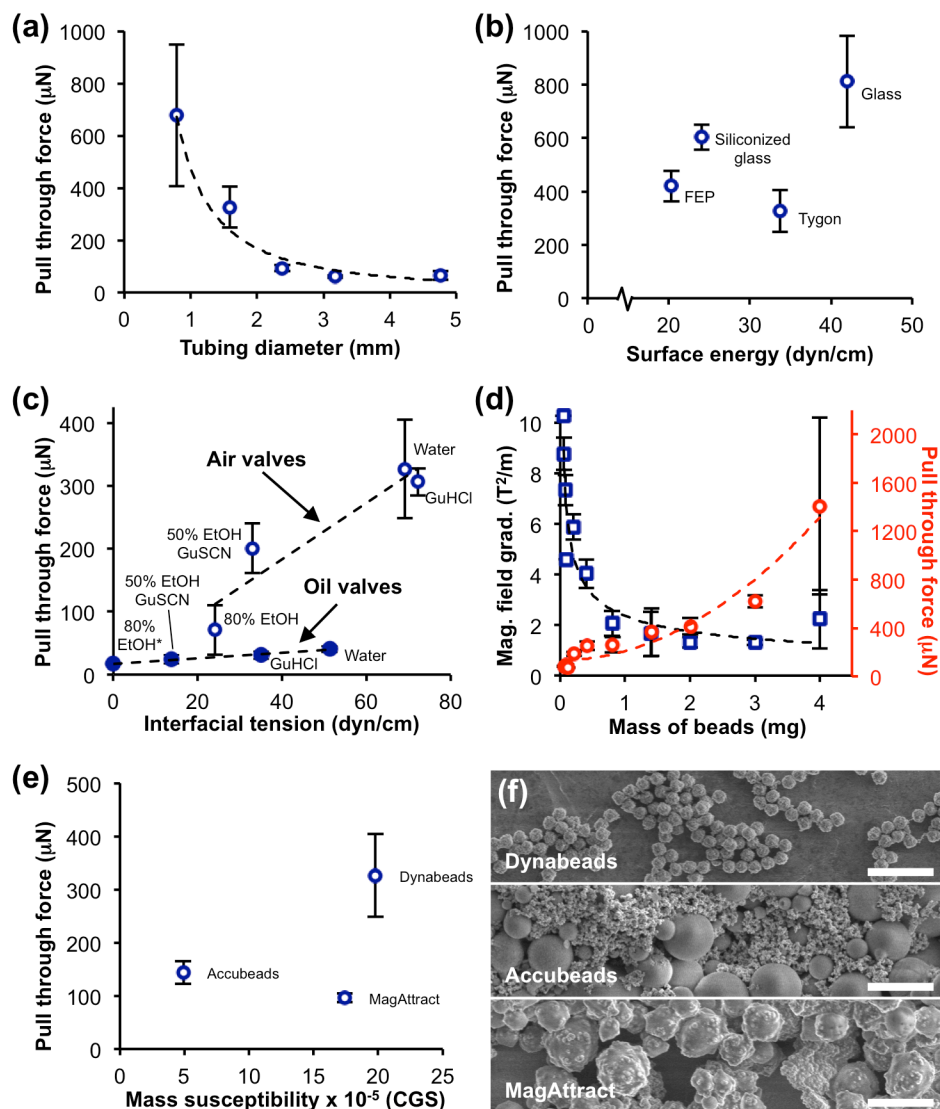


Figure 6. The effect of material properties on force required to pull beads through the solution/valve interface. A) The force required decreases when using tubing of a larger diameter. B) With the exception of Tygon tubing, the force required to pull beads across a surface tension valve increases with the surface energy of the tubing. C) The force required to pull beads through mineral oil valves (solid circles) is significantly less than the force required to pull beads across air valves (open circles). Force required increases with interfacial tension using with both types of valves. D) The magnetic field gradient along the x axis that is required to pull the beads through the valve (squares) increases with the amount of beads, whereas the magnetic field required (circles) decreases. E) The mass susceptibility of the bead used has little influence over the force required to pull beads across a surface tension valve. F) Scanning electron microscopy images of the three commercially available silica-coated magnetic beads (scale bars = $5 \mu\text{m}$). ($n = 3$, mean \pm s.d.; if not visible, error bars are obscured by the symbols)

(FEP) required a pull through force of $420 \pm 58 \mu\text{N}$, and the tubing with the highest surface energy (glass) required a pull through force of $812 \pm 172 \mu\text{N}$.

Overall, the force required to pull the beads through a mineral oil valve was significantly lower than the force required for air valves (Figure 6C). The force required to pull the beads through both mineral oil valves and air valves increased as the interfacial energy increased, though the increase was more substantial with air valves. The solution with the lowest interfacial energy (80% EtOH buffer solution interfaced with mineral oil) had a force requirement of just $17 \pm 0.8 \mu\text{N}$, whereas the solution with the highest interfacial energy (water interfaced with air) required $326 \pm 78 \mu\text{N}$.

Interestingly, the force required to pull beads through the valve increased with increasing bead mass, whereas the magnetic field gradient required decreased (Figure 6D). The bead mass range that has the lowest magnetic field gradient requirement is between 1 - 3 mg. Bead masses less than 1 mg become increasingly difficult to pull across the solution/valve interface with 0.048 mg being the minimum bead mass that can be pulled through the interface under the baseline experimental conditions. Masses much more than 3 mg fill the entire diameter of 1.6 mm tubing and increase the experimental error.

The force required to pull three commercially available bead types was also defined. Although one might expect that mass susceptibility would be inversely related to the force required for transport across a valve, there was no clear trend among the three types of beads tested (Figure 6E). It is interesting to note that despite having similar product descriptions, there was substantial variation in the morphology of these bead types as determined by scanning electron microscopy. The variability in force requirement appears to reflect their varying sizes and dispersity (Figure 6F): Dynabeads are relatively small, monodispersed (1.1

$\pm 0.07 \mu\text{m}$) silica-coated magnetite spheres; Accubeads are relatively large, polydispersed ($2.4 \pm 1.7 \mu\text{m}$) silica spheres trapped amidst magnetite crystals; and MagAttract beads are relatively large, polydispersed ($3.7 \pm 1.9 \mu\text{m}$) and amorphous silica-coated magnetite.

Solution carryover

The number of beads used had the greatest influence on the amount of liquid carried across the valve (Figure 7). Using increasing amounts of Dynabeads MyOne Silane beads, the carryover volume increased proportionally for the mass of beads tested (Figure 7B). Water carryover is $\sim 1.5 \mu\text{L}$ per milligram of beads, which equals ~ 3.6 femtoliters of water per bead, assuming that the beads are uniformly $1.15 \mu\text{m}$ in diameter, 3 g/cm^3 in density, and that there are 4.2×10^8 beads per milligram.

There was no clear relationship between surface free energy of the tubing or interfacial energy at the solution/valve interface to the carryover volume associated with the beads. The carryover volume using the four types of tubing was fairly similar and increased only modestly ($0.9 - 1.2 \mu\text{L}$) as the surface energy of the tubing increased (Figure 7C). Overall, the carryover volume associated with beads pulled through mineral oil valves was higher than with beads pulled through air valves, except with the 80% EtOH buffer solution, which had the same amount of carryover with air and mineral oil (Figure 7D, solid bars vs. open bars, respectively). The range of carryover volumes was $1.2 - 1.9 \mu\text{L}$ with air valves and $1.2 - 2.4 \mu\text{L}$ with mineral oil valves.

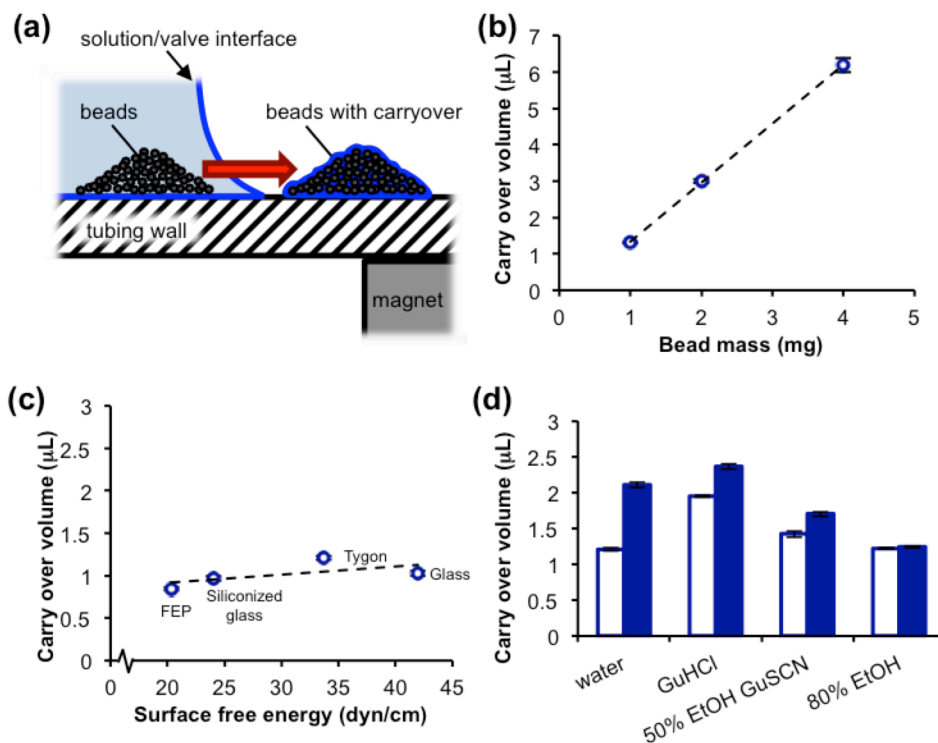


Figure 7. The effect of the material properties on the amount of solution carryover between solutions. A) Illustration of magnetic beads under the influence of a magnetic field moving from a solution through a surface tension valve within small-diameter tubing. As beads traverse the solution/valve interface, a small amount of solution is retained amidst the beads and is carried across the valve and into the next solution. B) The carryover volume increases linearly with an increased number of beads. C) The surface energy of the tubing has little effect on the carryover volume. D) In all solutions except 80% ethanol, there is more carryover when using mineral oil valves (solid bars) compared to air valves (open bars). ($n = 3$, mean \pm s.d.; if not visible, error bars are obscured by the symbols)

Discussion and Conclusions

Magnetic bead-based methods developed for biomarker isolation, amplification, and detection would be especially relevant for diagnostics in low resource settings; however, in many cases they are not used because of the prevalence of environmental contaminants and the limited access to trained personnel. Because the self-contained assay format described in this chapter is sealed from the environment and does not require extensive solution handling

or pipetting, it has the potential to facilitate the application of these magnetic bead-based assays in settings that lack laboratory resources (7,16). Furthermore, as demonstrated by the experimental results of these studies, the multiphase fluidic-based format has the flexibility to handle the diverse constraints and requirements of a variety of magnetic bead assays, such as biopolymer synthesis, high throughput screening assays, or industrial quality control.

The manipulation fluid-fluid interfaces for performing simplified and automated chemical and biological assays is of general interest, especially in the field of microfluidics. Consequently, the physical properties governing multiphase microfluidics are under investigation by many researchers. Some of the many aspects of the phenomena that control microdroplet formation were presented in a special collection of papers (38-41). Interestingly, some of the physical properties that influence fluid stability within our self-contained format, such as surface and interfacial tension and solution density difference at the fluid-fluid interface, are similar to those that govern microdroplet formation in multiphase microfluidics. In our system, additional variables and constraints associated with magnetic particles are discussed in the context of the multiphase fluidic system.

The self-contained sample processing format based on surface tension valves functions well because of three phenomena: i) solutions arrayed in millimeter-diameter tubing and separated by immiscible fluid spacers remain isolated from one another, ii) magnetic beads under a magnetic field gradient can be transported across the surface tension barrier of the fluid separators, and iii) magnetic beads passing between adjacent solutions through a surface tension interface do not intermix the solutions. Because of these phenomena, the tubing can be preloaded with processing solutions that are effectively separated by surface tension valves, and the assay can be carried out simply by moving the functionalized beads through

the solutions using an externally applied magnetic field. The results of these studies outline the physical design constraints for which these phenomena remain true. Based on these results, this discussion presents a generalized strategy for reconfiguring magnetic bead assays to the self-contained format.

The optimal design for the self-contained format would maximize valve stability, minimize the force required to pull beads through the valves, and minimize the solution carryover across the valve. Because the most useful relationships from a design standpoint are between valve stability and penetrability, the results for all the parameters tested in these studies are plotted in terms of their effects on these two performance characteristics (Figure 8). Valve stability is expressed in terms of a modified form of the Bond number ($\Delta\rho r^2 g / \sin \theta \gamma$), where $\Delta\rho$ is the difference in density across the valve interface (g/m^3), r is the radius of the tubing (m), g is the gravitational acceleration constant (9.8 m/s^2), θ is the contact angle of the solution on the tubing wall ($^\circ$), and γ is the interfacial tension at the solution/valve interface (N/m). The Bond number is a dimensionless relationship of the accelerative forces and the surface tension forces that determine whether the surface tension valve maintains the separation between two adjacent solutions in small diameter tubing. The Bond number is generally used to determine the stability of drops suspended in free solution. For these studies, I have modified the Bond number to make it more appropriate for the configuration of our fluids, which are interfaced with the solid surface of the inner tube wall. In our configuration, the gravitational acceleration acts opposite that of the vertical component of the interfacial tension, so by including the $\sin \theta$, only the vertical component of the interfacial tension is considered. Valve penetrability is expressed in terms of the Penetrability number ($F_{m,x} / l \cos \theta \gamma$), where $F_{m,x}$ is the force required to move a group of

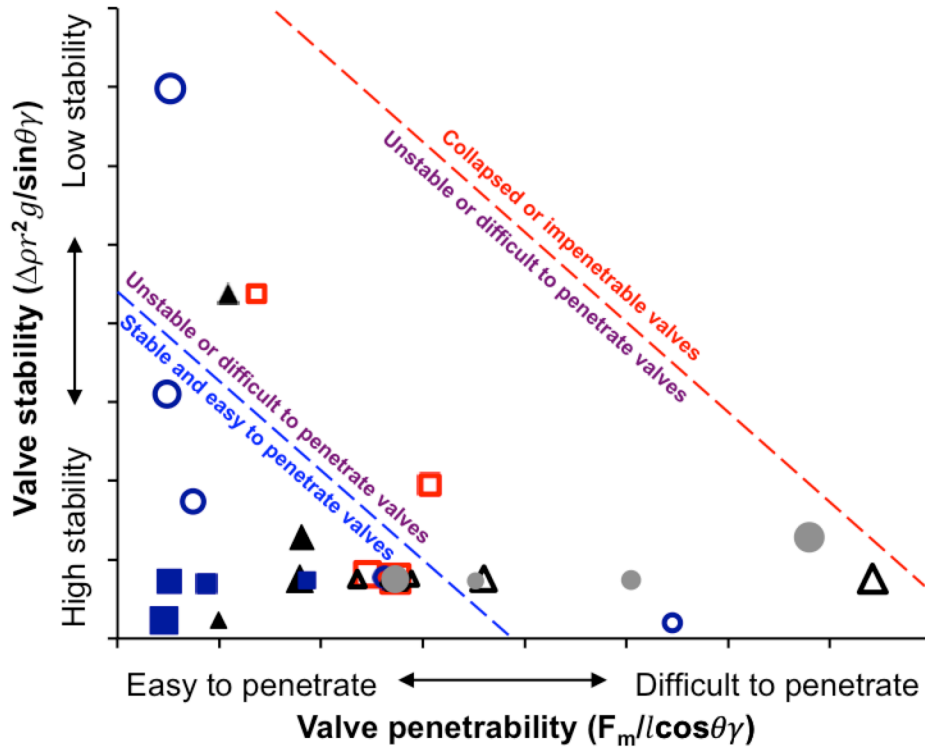


Figure 8. Comparison of the valve fluid stability and penetrability for various material configurations. Solutions interfaced with mineral oil valves (solid squares) are more stable and easier to penetrate than solutions interfaced with air valves (open squares). There are tradeoffs between stability and penetrability with the range of tubing diameters tested (open circles). Tubing surface energy (solid circles) and bead mass (open triangles) influence valve penetrability but not valve stability. The minimum mass of beads that can be pulled through a valve (solid triangles) can be optimized for valve stability and penetrability. The relative size of the symbols corresponds to the relative material property values (e.g., large solid squares have higher interfacial energy than smaller solid squares). The positions of the zone boundaries indicated by the dotted lines are approximations.

beads the x direction only through the surface tension valve interface (N), l is the contact line of the group of beads on the solution/valve interface (m), θ is the contact angle of the solution on the tubing wall ($^\circ$), and γ is the interfacial tension at the solution/valve interface (N/m). The Penetrability number is a dimensionless number that Rick Haselton and I developed to describe the relationship between the magnetic forces and surface tension forces that act on the beads to determine whether the magnetic beads cross the solution/valve

interface. Plotting the modified Bond number versus the Penetrability number is useful for identifying configurations that support a surface tension valve that is both highly stable and easy to penetrate with magnetic beads. For reference, the values that reflect the configuration used for our RNA extraction assay (refer to chapter III) are represented as the red open square symbols (see Figure 8). Plotting the modified Bond number versus the Penetrability number is also useful for determining the effect of changing a single parameter on these performance characteristics, and it can be utilized for identifying variables that can be manipulated when one variable is constrained by a particular internal or external constraint. The parameters that influence the stability and penetrability to the greatest degree, and are therefore the most important to optimize, span a range of values outside of the region identified as stable and easy to penetrate (Figure 8). In these studies, those parameters include tubing diameter, tubing surface energy, and bead mass (open circles, closed circles, and open triangles, respectively).

When reconfiguring a magnetic bead-based assay into the self-contained format, it is necessary to balance the physical design constraints of a configuration within the context of the chemical constraints of the assay, as the chemical composition of the processing solutions is connected to the function of a particular assay. For example, the surface tension and density of the processing solutions are intrinsically associated with the assay performance and are generally unalterable constraints for designing the physical format of the device. Consequently, an important step to designing a self-contained format for a particular assay is to identify the internal constraints of the assay. Internal constraints include the arrangement and volumes of the solutions, which influence the overall length of the tube; the compositions of the reagents, which influence the surface tension of the solutions; and the

analyte-binding capacity of the beads, which influences the amount of beads used. These factors must be taken into account when choosing materials for configuring the self-contained format, as the physical configuration for optimizing one performance indicator can conflict with the configuration for optimizing another.

It is clear that tubing material and diameter strongly influence the physical performance characteristics of this assay format. In general, tubing material of the lowest surface energy (i.e., the most hydrophobic) is preferred as it reduces the magnetic force required to pull beads through the valve (Figure 6B) and, to a lesser extent, increases the stability of the surface tension valve (Figure 4B). The choice of tubing diameter, on the other hand, must be considered as a tradeoff between valve stability and penetrability (see Figure 4A, Figure 6A, and Figure 8). Small diameter tubing maintains a stable valve but requires a very high magnetic force to move beads across the valve. The opposite is true with large diameter tubing, where the valves become less stable as the magnetic force requirement is minimized. The Penetrability number described above can explain these phenomena. The surface tension of the tubing material determines the contact angle (θ) of the solution with the tubing wall. With lower material surface tension the contact angle increases, which in turn decreases the Penetrability number (i.e. makes the surface tension valve easier to penetrate). Tubing diameter on the other hand, influences the contact line (l) of the group of beads on the solution/valve interface. With larger tubing diameters the contact line increases, which also decreases the Penetrability number. The use of 1.6 to 2.4 mm i.d. tubing with low surface energy appears to be optimal for maximizing both stability and penetrability. In contrast, valve length and solution volume within the ranges most likely to be used in biological assays, do not influence valve stability or penetrability (Figure 4E and F and data not show).

Another important design criterion is the immiscible fluid used to separate the processing solutions within the tubing. The fluid must provide an adequately stable barrier between solutions and permit the transit of the magnetic beads through the interface. I have found that separating processing solutions with air works well for practical reasons. Surface tension valves made from air are easier to load and more reproducibly separate solutions in millimeter-diameter tubing compared to those made with mineral oil, as mineral oil tends to inconveniently adhere to the surface of the tubing. Nevertheless, mineral oil works well for maximizing stability and minimizing bead pull through force (Figure 4C and Figure 6C, respectively). One of the most stable configurations tested was the use of the 80% EtOH buffer solution separated by a mineral oil valve. This combination is interesting as the 80% EtOH buffer solution has nearly the same density as the mineral oil valve used in these experiments (0.83 and 0.86 g/cm³, respectively). The modified Bond number can explain the high stability of this valve configuration. One of the variables represented in the modified Bond number is the difference in density between the fluids at the valve interface ($\Delta\rho$). Because there is such a low difference in density between the solution and the valve (0.03 g/cm³), the body force (g) acts on each fluid almost equally. This results in a lower value for the modified Bond number and a more stable solution/valve interface. Difference in density, however, is not predictive of valve stability with air valves (Figure 4D). It appears that with a liquid surface tension valve (i.e., mineral oil) interfaced with adjacent solutions, the density difference between the solution and valve has a dominating influence on valve stability, and with a gas surface tension valve (i.e., air) interfaced with adjacent solutions, the surface tension has a dominating influence on stability. Despite the convenience and reproducibility

of air separators for preloading processing solutions, applications that require high valve stability or valves that are easy to penetrate may benefit most from mineral oil valves.

Magnetic beads of an adequate mass under the influence of a sufficient magnetic field gradient can overcome surface tension barrier of the fluid separators and traverse the surface tension valve. A low magnetic force requirement is ideal, because the use of a small permanent magnet or an electromagnet is most desirable for the development of automated assay formats where limitations on magnet size or power requirements may exist. The force required to pull beads through the valve increased with increasing bead mass (Figure 6D). This positive correlation between pull-through force and bead mass was also observed by Shikida et al. (36). Interestingly, while the force required increased with increasing bead mass, the magnetic field gradient required decreased (Figure 6D). This is because a lower magnetic field gradient produces a much larger force on beads of increasing mass, as the force acting on the beads is directly proportional to both magnetic field gradient and bead mass. I have found that valve penetrability is maximized using a mass of approximately 1 - 3 mg beads in 1.6 mm i.d. tubing (Figure 6D). The minimum mass of beads that penetrated the water/air interface in 1.6 mm Tygon tubing and a magnetic field gradient of $\sim 10.2 \text{ T}^2/\text{m}$ was 0.048 mg. Because the magnetic force acting on the beads is directly related to bead mass, the magnetic force that can be generated for bead masses below this minimum threshold are not sufficient to overcome the surface tension forces of the meniscus. This minimum bead mass value is in the range of those determined by Shikida et al. using beads of much larger diameters (36). It was, however, observed that bead masses less than 0.2 mg require more time and effort to pull through the solution/valve interface. Some magnetic bead-based assays may require the use of low amounts of beads (i.e., $<0.2 \text{ mg}$) to optimize the surface

area available for binding the biomolecules of interest while limiting nonspecific binding of nonspecifically bound contaminants. Therefore, increasing the number of beads in a particular assay to reduce the magnetic field gradient required to pull the beads through a valve may have deleterious effects on the assay. I observed, however, that the Qiagen MagAttract beads required the least amount of force to move through the surface tension valves (Figure 6E), likely because of the relatively large size of the individual beads (see Figure 6D). Because the surface area to bead mass ratio decreases as the diameter of the beads increases, the use of larger beads may resolve this potential problem because of their lower surface area to mass ratio. Another way to facilitate valve penetration in the case that small masses of beads are to be used is to reduce the surface tension at the interface using a detergent. In a report of a 96-well plate mRNA extraction assay analogous to our continuous tubing design, Berry et al. use low concentrations of Triton X-100 to reduce the interfacial tension at the solution/valve interface (34). The group reported that the addition of 0.01 - 0.1% Triton X-100 did not interfere with the mRNA binding chemistry yet facilitated the magnetic transfer of the beads across the immiscible phase.

Although the integrity of the valve is maintained and the solutions do not intermix when beads traverse a surface tension valve, a relatively small volume of solution associated with the magnetic particles is carried to downstream solutions. Minimizing solution carryover is most desirable for the majority of bead-based assays, because it limits the amount of nonspecifically associated species that are carried over in the solution surrounding the beads that may interfere with the efficacy of the chemistry of the downstream solutions. In the case of the nucleic acid biomarker extraction assays developed in our laboratories and others, it has been reported that the carryover of GuSCN, GuHCl, or ethanol from upstream solutions

into the eluate can negatively impact the polymerase chain reaction (PCR) (35). The results of these studies indicate that the smallest amount of solution carryover is achieved with the fewest beads possible, as the amount of carryover is proportional to the number of beads used. Tubing surface energy, solution interfacial energy, and valve fluid had less impact on carryover; all carryover volumes fell between 1 - 2 μ L per milligram of beads for each configuration tested when using 1 mg Dynabeads (Figure 7C and D), which represents between 0.3% and 4% of the processing solution volumes used in the most common nucleic acid extraction assays. Notably, this carryover volume is approximately equivalent to that of the commercially available Dynabeads Silane viral NA (Invitrogen) kit.

Our laboratories have shown that this simple, self-contained format functions well for a variety of biomarker extraction assays (7,16). This format has many advantages for implementation in low-resource settings compared to laboratory-based assays. Foremost is the simplicity of the preloaded cassette. Because the tubing can be preloaded with assay solutions, the processing steps are self-contained, which reduces the potential for contamination during the assay with the use of an externally applied magnetic field to move the functionalized beads. The self-contained format also has the flexibility to interface with other assays, as the tubing permits direct injection or coupling to upstream and downstream systems for introducing or removing samples, reagents, or products. Furthermore, automated and multiplexed processing could be achieved by simply manipulating the magnetic field gradient using electronic motors or electromagnets. Because of these advantages, this self-contained format may be extended to simplify a variety of magnetic bead-based assays that have potential diagnostic applications.

Acknowledgments

The purchase of materials and regents for this project was supported by the Bill & Melinda Gates Foundation through the Grand Challenges in Global Health initiative in diagnostics. I thank the National Science Foundation Graduate Research Fellowship Program (DGE 0909667) for personal support during the time I worked on this project.

The work presented in this chapter could not have been completed without the efforts of several individuals. The initial concept of using surface tension valves to separate processing solutions is credited to Rick Haselton. Much of the data presented in this chapter was collected by Amy Creecy, Cat Major, and Sheba Wariso. A considerable amount of effort was contributed by way of experiment design and background research into mathematical describing fluids and magnetic field gradients by Rick Haselton and Cat Majors. David Wright provided many essential resources and expertise for carrying out these experiments.

Chapter III

DEVELOPMENT OF A LOW RESOURCE RNA EXTRACTION CASSETTE

Abstract

In this chapter, I describe the development of a self-contained RNA extraction cassette suitable for operation in a low resource setting (7). This is important, because the presence of interferents in biological samples is a barrier to the development of nucleic acid-based diagnostics. In a laboratory setting, the influence of these interferents can be minimized using an RNA or DNA extraction procedure. In low resource settings, limited access to specialized instrumentation and trained personnel presents challenges that impede sample preparation. As nucleic acid-based technologies move out of the laboratory setting, there is a need for new approaches to interface biological samples with these devices for point-of-care diagnostics. The continuous tubing extraction cassette that our laboratories developed contains processing solutions arrayed within a length of 1.6 mm inner diameter Tygon tubing. Processing solutions are separated by air gaps and held in place during processing by the surface tension forces at the liquid-air interface. RNA adsorbed to silica-coated magnetic particles is pulled by an external magnet through successive solutions to precipitate, wash and elute RNA in the final cassette solution. The efficiency of the continuous tubing extraction cassette was evaluated using quantitative reverse transcriptase PCR (qRT-PCR) following extraction of respiratory syncytial virus (RSV) RNA that is spiked into TE buffer or HEP-2 epithelial cell lysates. RNA was recovered from each sample matrix with 22.5 and 7.6% efficiency, respectively. Additionally, 3.6×10^5 RNA copies/ μ L

was recovered from RSV infected HEp-2 cells in a 50 μ L elution volume. An overall limit of detection after extraction was determined to be nearly identical (97.5%) to the RNeasy kit. These results indicate that the continuous tubing extraction cassette has the potential to be an effective sample preparation device in a low resource setting.

Introduction

Nucleic acid-based detection systems, such as quantitative PCR (qPCR), are attractive technologies for diagnosis of pathogens because of their sensitivity, specificity and relatively rapid time-to-answer. Many research groups have focused on the development of nucleic acid-based detection for low-resource settings (13). The effectiveness of PCR is dependent on both the quality and quantity of nucleic acid template (11) and the absence of interferents (12). For example, carbohydrates, proteins and lipids present in clinical samples have all been shown to inhibit PCR (42,43). In addition to various interferents, patient samples also contain nucleases, which directly reduce the number of nucleic acid targets present (43).

To maximize the efficiency of nucleic acid-based diagnostics, RNA can be extracted and concentrated into an interferent-free buffer prior to testing. One classic laboratory method uses a phenol-chloroform cocktail (44). This method is highly effective but is not as commonly utilized today because it is time consuming and requires the use of toxic organic chemicals. Several solid phase extraction kits are commercially available to purify RNA from patient samples. Many of these kits rely on selective RNA binding to silica-coated surfaces in the presence of ethanol and a chaotropic agent such as guanidinium thiocyanate (GuSCN) (45,46). GuSCN also denatures protein contaminants including nucleases that may be present in the sample (47,48). These kits are not cost effective for low resource use and

often require specialized laboratory equipment and trained technicians that are unavailable in a low resource setting. Additionally, many involve multiple steps that increase the chance of contamination of both the sample and technician.

There has been a growing interest in microfluidic technologies for sample preparation (13,49). Microfluidic devices are capable of overcoming many of the limitations of RNA extraction kits. These devices are fully self-contained, decreasing the chance for contamination of the sample or operator. The extractions are automated, reducing the skill required for operation. Additionally, many of these devices are suitable for integrating with downstream nucleic acid amplification and detection technologies (50,51). However, the small diameter of the microfluidic channels results in a small surface area of solid phase available for RNA adsorption and restricts the total sample volume that can be flowed through the chip. These features limit the total amount of RNA recovered (13) and therefore negatively impact the limit of detection. Additionally, manufacturing of these devices is often complex and difficult to perform on a large scale (13,52).

I developed a self-contained RNA extraction cassette suitable for operation in a low resource setting. A self-contained extraction cassette is pre-arrayed with processing solutions separated by air gaps, which our laboratories have defined as surface tension valves. Cells are lysed and RNA is extracted after selective adsorption to silica-coated magnetic particles in the presence of GuSCN and ethanol. The extraction process is similar to commercially available magnetic bead-based extraction kits. However, instead of residing in separate tubes, individual processing solutions are contained in a single small-diameter tube separated by surface tension valves. The solutions remain stationary due to strong capillary forces. RNA adsorbed to the silica-coated magnetic particles is pulled through each processing solution

using an externally applied magnetic field and is eluted from the particle surface in the final solution. This chapter describes the general performance characteristics of this approach. Since there is not a commercially available low resource alternative to our RNA extraction cassette, its performance is compared to laboratory-based commercial kits.

Materials and Methods

Preparation of RSV RNA N gene standards

Because our laboratories have experience with respiratory syncytial virus (RSV) diagnostics, we have chosen to develop our extraction cassette using RSV RNA. *Escherichia coli* DH5 α transformed with the pGBKT7 vector containing RSV N gene was generously provided by the Crowe Laboratory at Vanderbilt University. *E. coli* were grown for 18 hours on kanamycin agar plates at 37 °C. A single colony was isolated and transferred into 25 mL of Miller's LB broth with 50 μ g/mL kanamycin antibiotics and grown overnight on a rotating rack at 37 °C to an optical density of 0.6 - 0.8AU. The plasmid was extracted using a Qiagen Spin Miniprep Kit and linearized using the *Bss*HIII restriction enzyme. Linearization was confirmed by running both pre- and post-linearized plasmids on a 1% agarose gel. Linearized plasmid was recovered from the restriction digest by ethanol precipitation. The plasmid was then transcribed into RNA using a T7 MEGAscript transcription kit (Ambion, Austin, TX), and treated with DNase I. The expected RNA length was confirmed on a denaturing 2%-formaldehyde-1.2% agarose gel. The RNA was quantified by UV-Vis spectroscopy.

Preparation of RSV infected and uninfected HEp-2 cell lysates

Uninfected HEp-2 cell lysates were prepared from a confluent monolayer of HEp-2 cells from a T-150 media flask. The cells were harvested by scraping from the T150 flask and centrifuging at 500 g for 5 min. The pellet was resuspended into 8 mL denaturing solution (4 M guanidinium thiocyanate, 25 mM sodium citrate [pH 7.0] 0.5% N-lauroylsarcosine [Sarkosyl], 0.1 M 2-mercaptoethanol) and passed through a pipette tip 10 times. The cell lysates were stored at a concentration of approximately 3×10^6 lysed cells per mL in 1 mL aliquots at -80 °C.

Infected HEp-2 cell lysates were prepared by infecting confluent monolayer of HEp-2 cells in two T150 flasks with RSV strain A₂. After 4 days, one flask was harvested as described above and used to perform RSV RNA extractions from HEp-2 lysates. A plaque assay was performed on the second flask to quantify the concentration of infectious particles. To prepare the assay, cells were scraped from the T150 flask and centrifuged at 500 g for 5 min. The pellet was resuspended into 8 mL of media, and cells were lysed by 3 cycles of freezing in an ethanol and dry ice slurry and thawing in a 37 °C water bath. The cell lysate was centrifuged at 100 g for 5 min, and the supernatant was stored at -80 °C in 1 mL aliquots.

One hundred uL of the lysed cells was serially diluted, and each dilution added in triplicate to a confluent monolayer of HEp-2 cells in a 24-well plate. Plates were incubated at 37 °C for 1 h. 1 mL of sterile 0.75% methyl cellulose (w/v) was then added to each well and the plate was placed at 37 °C for an additional 4 days. The infected HEp-2 cells were fixed in 80% methanol at -20 °C for 1 h, washed 3 times with PBS, and blocked with a 5% milk solution for 1 h. One hundred fifty µl of 30 µg/mL anti-F protein primary antibody in 5%

powdered milk solution was added to each well. After 1 hour, wells were washed 3 times with PBS, and 150 μ l of 0.5 μ g/mL anti-mouse IgG HRP conjugate secondary antibody (Promega, Madison, WI) in 5% powdered milk solution was added for 1 hour. Wells were washed 5 times with PBS and 150 μ l of TrueBlue peroxidase substrate (KLP, Gaithersburg, MD) added for 20 min at room temperature. The plaque forming units (pfus) were quantified by averaging the plaques at the dilution that resulted in a countable number plaques and multiplying by the dilution factor.

Quantitative RT-PCR

An 82-bp fragment of the RSV N gene was amplified using forward primer 5'-GCTCTTAGCAAAGTCAAGTTGAAATGA-3' and reverse primer 5'-TGCTCCGTTGGATGGTGTATT-3' (53). Reactions were performed in a 25 μ L volume using 5 μ L of RNA template and the Clontech one-step RT-PCR kit according to manufacturer's instructions. Thermal cycling consisted of 48 $^{\circ}$ C for 20 minutes to synthesize cDNA, 95 $^{\circ}$ C for 3 minutes to inactivate the reverse transcriptase and activate Qtaq DNA polymerase, and 40 cycles of 95 $^{\circ}$ C for 15 s and 60 $^{\circ}$ C for 60 s using a Rotor-Gene Q thermal cycler (Qiagen, Germantown, MD). Product specificity was confirmed using melting curve analysis and gel electrophoresis. Data was collected and C_t values recorded by Rotor-Gene Q Software (Qiagen, Germantown, MD) and converted to number of copies of RNA per μ L using a standard curve.

RNA extraction using prototype capillary extraction cassette

Proof-of-principle studies were performed using 14 frozen de-identified nasal wash samples provided by Dr. John Williams' lab (Vanderbilt University Hospital, Nashville, TN). Use of specimens was approved by Vanderbilt University's IRB. At the time of collection, nasal swabs were placed in opti-MEM media (Invitrogen, Oslo, Norway) and frozen at -80 °C. Each sample was characterized by Williams' lab for respiratory syncytial virus (RSV) using RT-PCR after an extraction using Roche Total Nucleic Acid Extraction Kit (Basel, Switzerland). RT-PCR was performed using Roche LC Magna Pure machine (Basel, Switzerland). We obtained samples that tested positive for RSV as determined by a calculated cycle threshold (C_t). We also obtained samples that tested negative for RSV as determined by no calculated cycle threshold value within the cycles that were performed. Seven samples characterized as RSV positive and seven as RSV negative were selected at random from a total of 840 samples. Frozen samples were briefly thawed, divided and refrozen as 100 μ L aliquots to facilitate comparison across different RNA extraction methods.

A prototype extraction cassette (Figure 9) was constructed from glass capillary tubes and pipette tips. Glass capillary chambers (2 mm i.d.) were cut from 0.635 cm stock tubing into 80 mm lengths, and the ends were flared outward. Six capillary chambers were aligned linearly on the top of a horizontal aluminum stage using machined aluminum mounts. A 1000 μ L pipette tip was placed as a spacer in between each capillary chamber with the wide end of the pipette tip around the preceding capillary chamber and the narrow end resting inside the flared region of the next capillary chamber. Thus successive processing chambers were separated from one another by air spacers within the pipette tips. The first capillary

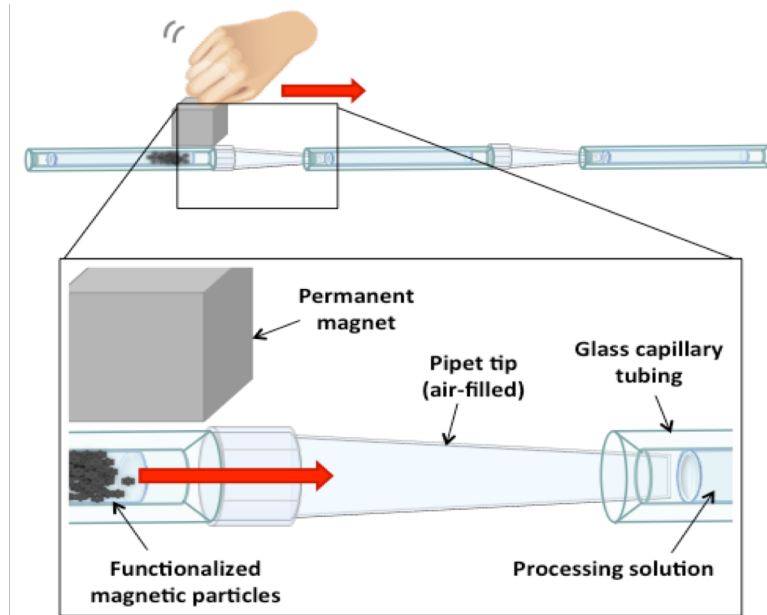


Figure 9. Design of the preliminary extraction method showing the processing solutions held in place in glass tubing and separated by air-filled pipette tips. RNA is adsorbed to silica-coated magnetic particles, which are pulled left to right through successive processing chambers using an external magnet. Following processing, the RNA is eluted in a final water chamber.

chamber was reserved for the RNA sample and was initially left empty. The remaining chambers were pre-filled with the processing reagents supplied in the MagAttract RNA Cell Mini M48 kit (Qiagen, Germantown, MD) as follows: 200 μL of “Buffer MW” wash buffer, 200 μL “Buffer RPE” wash buffer, 200 μL “Buffer RPE” wash buffer, 200 μL RNase/DNase free water, 30 μL RNase/DNase free water heated to 65 $^{\circ}\text{C}$ for elution of RNA. Thirty μL of nasal wash sample was added to 150 μL of “Buffer RLT” and homogenized by passage through a 20-gauge needle five times. Twenty μL of the MagAttract bead solution (Qiagen, Germantown, MD) was added to the homogenized sample, vortexed, and placed on a rotary mixer for 5 minutes at room temperature. The sample was then pipetted into chamber 1, shown on the left in Figure 9. A 2.54 cm cube of grade 40 NdFeB magnet (National Imports, Vienna, VA) was placed adjacent to the first capillary chamber and slowly pulled parallel to

the chambers at a rate of ~4 mm/second to pull the magnetic beads through each of the processing chambers. The total pull-through time was ~2 minutes. After reaching the final elution chamber, the beads were held to one side by the magnet and the eluent was collected. The recovery efficiency of RNA extraction was compared to the RNeasy Mini kit (Qiagen, Germantown, MD), Dynabeads mRNA Direct kit (Invitrogen, Oslo, Norway) used according to manufacturer's protocols, as well as the MagAttract RNA Cell Mini M48 kit (Qiagen, Germantown, MD) performed manually instead of with the Qiagen M48 BioRobot which was unavailable for these studies. The number of extracted RSV N gene RNA copies/ μL was calculated for the 7 RSV positive and 7 RSV negative nasal wash samples after 4 different extraction methods using a standard curve. The results were compared to the calculated copy numbers of RSV N gene RNA detectable in each sample prior to extraction.

RNA extraction using continuous tubing extraction cassette

The prototype design was simplified into a continuous tubing design using 8 processing solutions pre-arrayed within two feet of Tygon tubing (1.6 mm i.d.) (Figure 10). These solutions were chaotropic wash buffer (300 μL of 4 M guanidine hydrochloride, 25 mM sodium citrate, pH 7.0), RNA precipitation buffer (300 μL of 80% ethanol, 5 mM potassium phosphate, pH 8.5, 2), water wash (100 μL of molecular grade water, 3 \times), and RNA elution (50 μL of molecular grade water). Each solution was separated from the next by an air gap ~2 mm in length. Three types of extraction test samples were prepared: 5 μL of RSV N gene standard RNA in TE buffer at a concentration of 1×10^6 copies/ μL , 20 μL of HEp-2 cell lysates (2×10^3 cells/ μL) spiked with 5 μL of RNA standard, or 20 μL of RSV-infected HEp-2 cell lysates. Cell lysate samples were homogenized by passage through a 25

gauge needle five times. Prior to extraction, samples were added to 230 μL of RNA-silica binding buffer (230 μL of 2 M guanidine thiocyanate, 25 mM sodium citrate, pH 7.0, 50% ethanol) and 20 μL of silica-coated 1 μm diameter magnetic particles (3×10^6 particles/ μL) (Bioneer Inc., Alameda, CA) and placed on a rotating mixer for 5 minutes at room temperature. After mixing, the sample was loaded into the tubing and the tubing ends were capped. The particles were collected in the first chamber by the external magnet and pulled through the air valves and each successive chamber at ~ 4 mm/second using a 2 in. diameter neodymium ring magnet (Emovendo LLC, Petersburg, WV) as depicted in Figure 10. Particles were dispersed in the chaotropic wash and RNA precipitation solutions by rapidly moving the magnet back and forth before being recollected. In the water wash solutions, the particles were moved at ~ 8 mm/second to minimize RNA loss by elution during the wash.

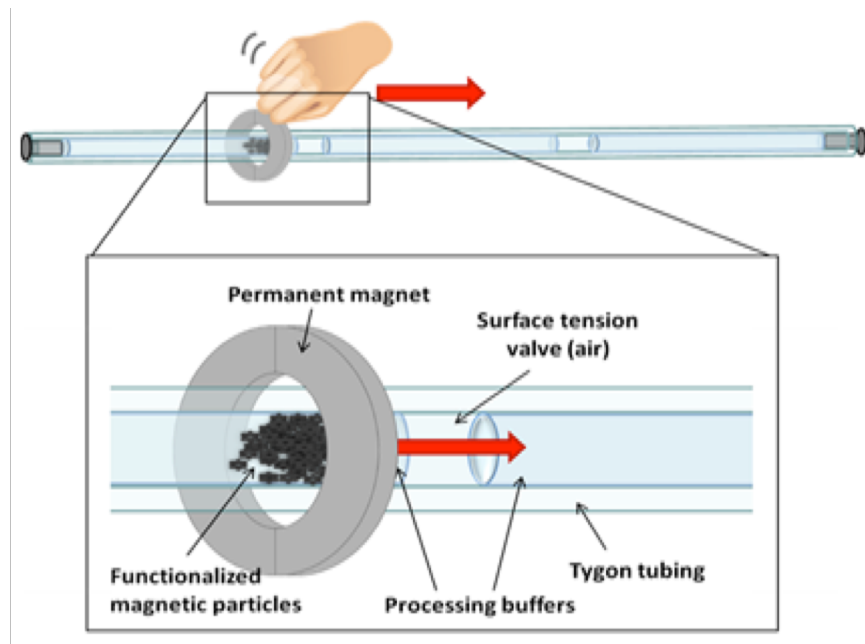


Figure 10. Design of the continuous tubing extraction cassette showing individual processing solutions separated by surface tension valves. An external magnet is used to pull RNA adsorbed to silica-coated magnetic particles through each processing solution. Following processing, the RNA is eluted in a final water chamber.

Finally, the particles were dispersed in the final elution chamber and incubated at room temperature for 5 minutes before removal. The final chamber contents were collected for RT-PCR analysis. Each RNA extraction was completed in ~15 minutes.

Continuous tubing extraction cassette limit of detection

The minimum quantity of target RNA added to the RSV negative cell lysates and detected by RT-PCR after RNA extraction was found for the continuous tubing extraction cassette and compared to the RNeasy kit. Twenty μL of uninfected HEp-2 cell lysate was spiked with 5 μL of RNA in TE buffer containing 0, 5×10^3 , 5×10^4 , 1×10^5 , 5×10^5 , 1×10^6 , and 5×10^6 copies of RSV N gene RNA standard and extracted by both methods as previously described. After extraction, the RNA was quantified by RT-PCR. The limit of detection was defined as 3σ above the mean value obtained for control extractions containing no RNA.

Post-extraction RNA distribution analysis

Extraction test samples were prepared using 5 μL of RSV RNA standard in TE buffer added to 230 μL of silica binding buffer as described above. Twenty μL of magnetic particles were added to the sample and mixed for 5 minutes. RNA was extracted using the extraction cassette as described above. After extraction, each chamber was removed by cutting the tubing with a razor blade. Each solution was purified with the RNeasy Mini kit according to manufacturer's protocol in order to remove PCR inhibitors. To account for RNA loss during the secondary RNA purification step, a control containing 5 μL of RSV RNA standard was purified from TE buffer using the RNeasy kit. The purified RNA was quantified by RT-PCR

analysis and normalized to the TE buffer control to account for loss during this second extraction. RNA remaining on magnetic particles after extraction was determined by recollecting the particles post-elution in 100 μ L of nuclease free water. The particles were placed on a rotary mixer for 12 hours at 4 $^{\circ}$ C. Particles were removed and RNA in solution was purified with the RNeasy Mini kit and quantified by RT-PCR.

Results

RNA extraction from aliquots of frozen nasal wash samples using the prototype extraction cassette shown in Figure 9 recovered 510 ± 800 RSV RNA copies per μ L (Figure 11 dark bars). Using the same sample aliquots, the commercial RNeasy Mini kit, Dynabeads mRNA Direct kit and MagAttract RNA Cell Mini M48 kit recovered $4,400 \pm 10,000$, $750 \pm 1,300$, and $940 \pm 1,000$ copies per μ L, respectively. In an unextracted RSV positive nasal

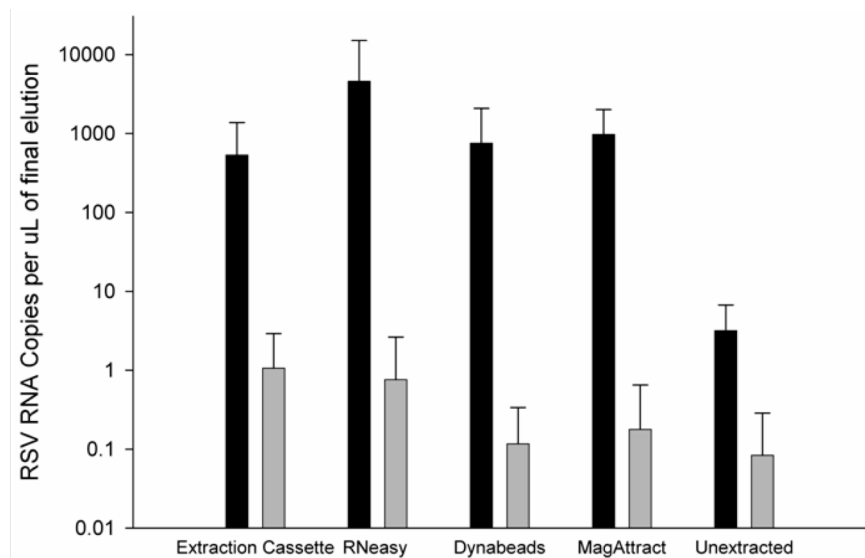


Figure 11. Comparison of RNA yields from nasal wash samples using five extraction methods. The number of copies of RNA per μ L extracted from RSV positive (black bars) and RSV negative (gray bars) nasal wash samples. Extractions were performed using prototype extraction cassette, RNeasy Mini kit, Dynabeads mRNA Direct kit, and the MagAttract RNA Cell Mini M48 kit (mean \pm s.d., n=7).

wash sample, 3 ± 3 RSV RNA copies were detected. In samples previously classified as RSV negative, an average of less than 1 copy of RSV RNA was detectable per μL for all methods (Figure 11, light bars).

Using the continuous tubing extraction cassette shown in Figure 10, extraction of an RSV N gene standard added to TE buffer was recovered at an efficiency of $22.5 \pm 19\%$ ($1.1 \pm 0.95 \times 10^6$ copies) (Figure 12A). Recovery efficiency was calculated by dividing the total number of copies extracted by the initial number of copies present in the sample and multiplying by 100%. In TE buffer, the RNeasy kit recovered $41 \pm 19\%$ ($2.1 \pm 0.95 \times 10^6$ copies). TE buffer does not contain PCR interferents so, as expected, the detection of unextracted standard RNA was 100% (Figure 12A, right bar).

In the more complex uninfected HEp-2 cell lysate sample matrix, the recovery efficiency of RNA was $7.6 \pm 4.8\%$ ($3.8 \pm 0.24 \times 10^5$ copies) using the extraction cassette, and $18.1 \pm 2.4\%$ ($9.1 \pm 1.2 \times 10^5$ copies) using the RNeasy kit (Figure 12B). The spiked cell

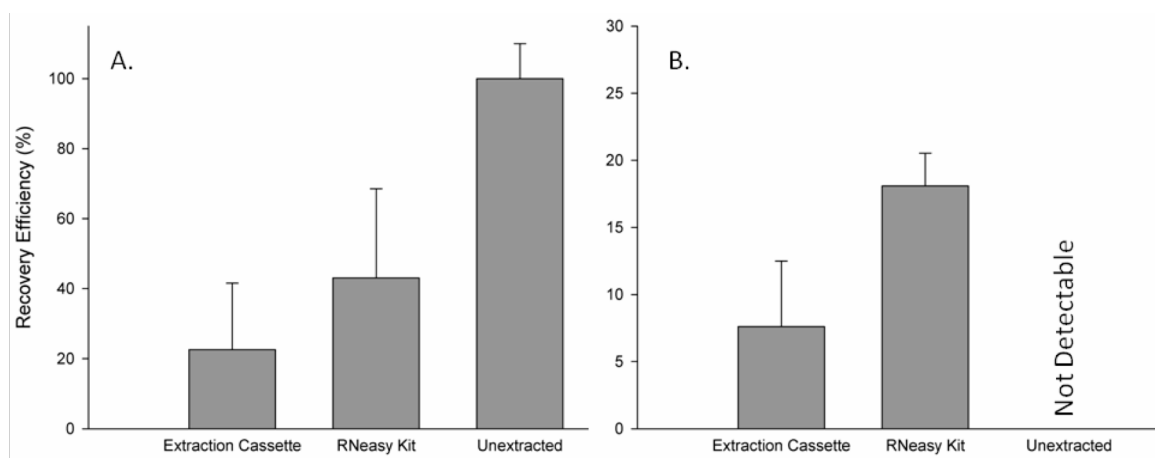


Figure 12. Comparison of the percent of RSV RNA recovered after addition to TE buffer (A) or HEp-2 cell lysates (B) using the extraction cassette (left bars), RNeasy kit (middle bars), or no extraction (right bars) (mean \pm s.d., $n = 9$). The recovery efficiency of the cassette was 55% and 42% of the RNeasy kit from TE buffer and HEp-2 cell lysates, respectively.

lysates evidently contained RT-PCR interferences since there was no amplification of the unextracted spiked sample by RT-PCR (Figure 12B, right bar).

Using the continuous tubing extraction cassette, RSV RNA extracted from RSV infected HEP-2 cell lysates containing 4.6×10^5 pfu/mL recovered $3.6 \pm 0.09 \times 10^5$ RNA copies per μL from the elution chamber compared to $1.2 \pm 0.07 \times 10^6$ copies per μL using the RNeasy kit (Figure 13, black bars). Less than 100 copies/ μL was reported in extractions obtained from uninfected cell lysates (Figure 13, gray bars), and RNA was not detectable for infected or uninfected cell lysates which were not extracted prior to RT-PCR ($C_t > 40$) (Figure 13, “Unextracted”).

For all methods, RNA loss during extraction was significant. A post-extraction examination of the distribution of RNA in the processing solutions was partially successful at identifying features responsible for this loss. In a separate series of continuous tubing extraction cassette experiments, 59.5% (3.0×10^6 copies) of RNA was accounted for in a

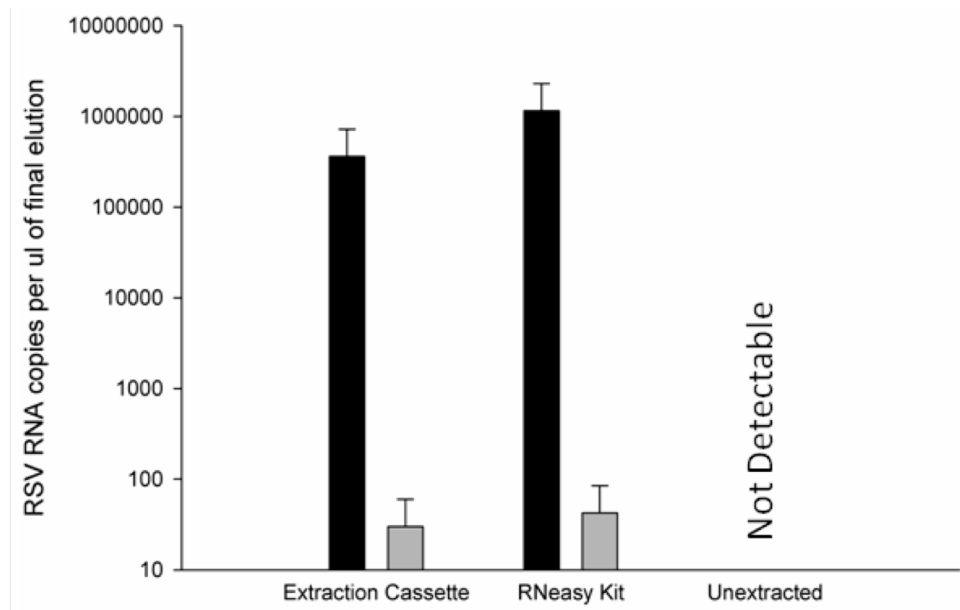


Figure 13. Comparison of RNA extracted from RSV infected (black bars) and uninfected (gray bars) HEP-2 cell lysates using the extraction cassette and RNeasy kit. Unextracted samples failed to report RSV RNA in either sample (mean \pm s.d, n = 3).

post-processing distribution analysis of RSV N gene standard added to TE buffer (Figure 14). Similar to the results found in Figure 12A, $28 \pm 4.5\%$ ($1.4 \pm 0.23 \times 10^6$ copies) of the RNA was recovered in the elution. Significant RNA was recoverable in the water wash solutions, which contained $21.7 \pm 4.6\%$ ($1.1 \pm 0.23 \times 10^6$ copies) of the initial RNA. An additional $7.8 \pm 3.5\%$ ($3.9 \pm 1.8 \times 10^5$ copies) of the RNA was recovered from the silica particles after 12 hours of further elution at 4°C . Less than 2% of the RNA was recoverable in the RNA-silica binding, chaotropic wash, and RNA precipitation solutions. The tube wall was also checked for RNA binding by washing with water post-extraction, and no detectable RNA could be recovered (data not shown). Approximately 40.5% (2.0×10^6 copies) could not be accounted for during the post processing distribution analysis.

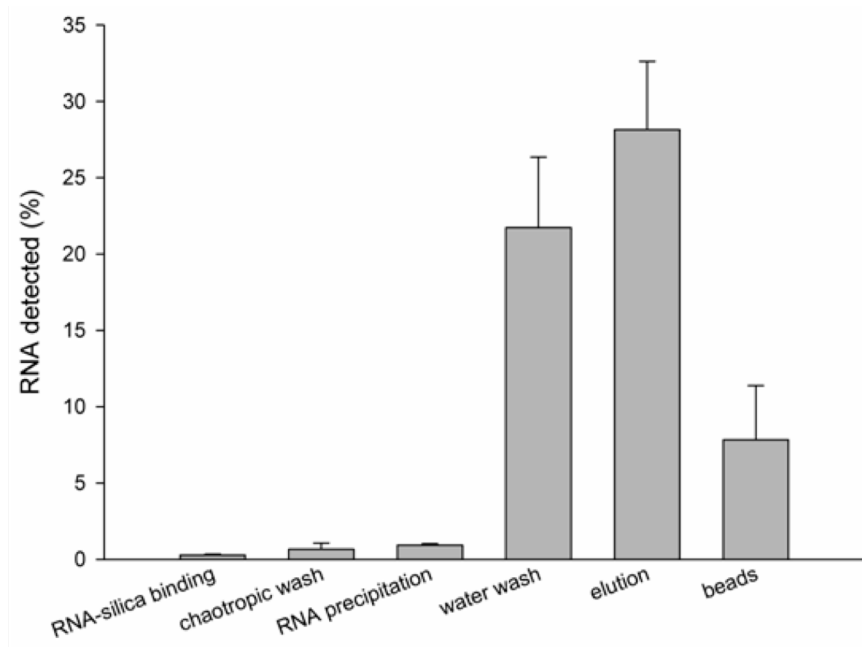


Figure 14. The post-extraction distribution of RNA in each processing solution after RNA extraction from TE buffer is shown. Insignificant amounts were recovered in the first three steps, but the water wash and silica particles contained significant RNA (mean \pm s.d., $n = 3$).

Continuous tubing extraction cassette limit of detection

The post-extraction limit of detection was established for the continuous tubing extraction cassette by determining the minimum RSV RNA copies in HEp-2 cell lysates detectable following an RNA extraction and RT-PCR. 5000 copies of RSV RNA spiked into HEp-2 cell lysates (e.g. 5 μ L of RNA at 1000 copies/uL into 20 uL of cell lysate) was the lowest concentration detectable by RT-PCR after sample extraction using both the continuous tubing extraction cassette and RNeasy kit (Figure 15). For the extraction cassette, 197 ± 8.5 copies were reported in the sample containing no RSV RNA, giving a 3 s.d. limit of detection target of roughly 222 copies. Cell lysates spiked with 5000 copies prior to extraction reported a value of 228 ± 58.5 copies per PCR reaction. Additionally, 461 ± 19.5 ,

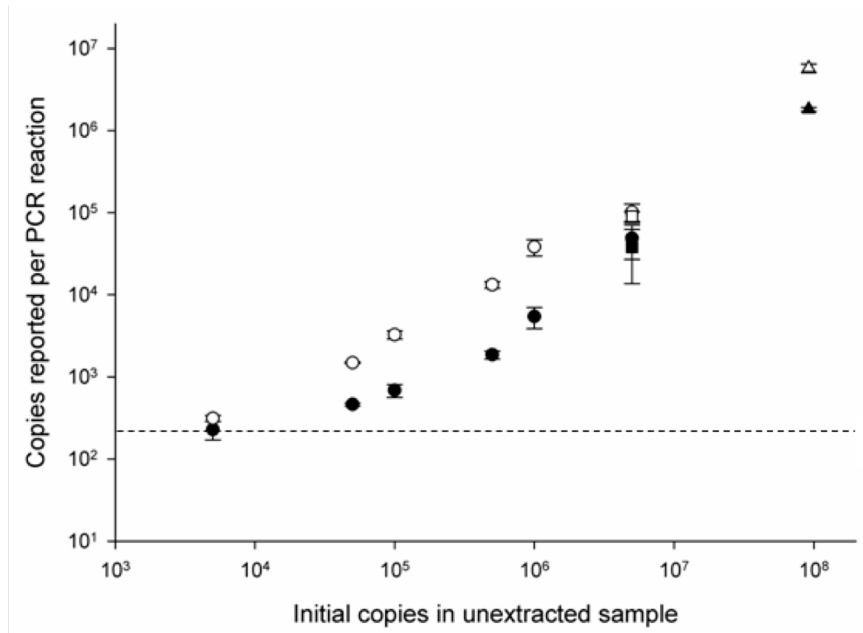


Figure 15. The limit of detection of RNA detectable by RT-PCR after extraction from HEp-2 cell lysates spiked with known amounts of RSV RNA using either the continuous tubing extraction cassette (\bullet) or the RNeasy kit (\circ) (mean \pm s.d, n=3). When a sample containing no copies of RNA was extracted, 197 ± 8.5 RNA copies were detected with the extraction cassette and 202 ± 9.5 copies were detected with the RNeasy kit. The limit of detection is shown for the continuous tubing extraction cassette (dotted line).

686 ± 123, 1857 ± 206, 5435 ± 1562, and 48,910 ± 22012 copies were reported from lysates spiked with 5×10^4 , 1×10^5 , 5×10^5 , 1×10^6 , and 5×10^6 copies respectively. Similarly, 202 ± 9.5 copies were reported in the sample containing no RSV RNA, and 312 ± 26.8 copies from lysates spiked with 5000 copies and extracted with the RNeasy kit. Finally, 1489 ± 27.7, 3250 ± 1240, 13233 ± 1240, 38345 ± 8526, and 101,505 ± 26,173 copies were reported from lysates spiked with 5×10^4 , 1×10^5 , 5×10^5 , 1×10^6 , and 5×10^6 copies respectively.

Discussion

One of the factors that limits nucleic acid-based detection is the need for patient sample preparation prior to testing (54). Sample preparation techniques mirroring the simple nucleic acid-based diagnostic devices currently being developed are necessary to make diagnosis practical at the point-of-care. Unfortunately, the operation of most existing commercial kits appropriate for RNA extraction and concentration require specialized laboratory equipment and trained laboratory personnel.

In agreement with previous studies, we found that without an initial extraction step, only purified RNA in solutions containing no interferents (e.g., TE buffer) can be directly detected by RT-PCR (Figure 12A). Direct amplification of viral RNA by RT-PCR prior to RNA extraction failed to accurately report the concentration of viral RNA in RSV-infected clinical nasal wash samples (Figure 11), HEp-2 cell lysates spiked with RSV RNA (Figure 12B), and RSV infected HEp-2 cell lysates (Figure 13). Direct amplification has been performed on patient samples by others but not without the need for more complex analysis (e.g., RT-PCR followed by flow cytometry) (55), which would be impractical in a low resource setting. Therefore, RSV false negatives are likely to be obtained when the extraction

step is omitted prior to RT-PCR, and sample preparation is necessary to achieve a low limit of detection.

A limit of detection study was performed using spiked cell lysate samples, and the results suggest that the proposed continuous tubing extraction cassette and the RNeasy kit have a limit of detection of ~ 200 copies per μL . This limit of detection is better than current clinical diagnostics, which have a lower limit of detection of $\sim 10^4$ pfu/mL or $\sim 10^5$ copies per μL . In combination with a point-of-care nucleic acid-based diagnostic, the proposed extraction cassette would be ideal in a low resource setting. Here, the estimate of 1 pfu equaling $\sim 10^4$ copies of RSV RNA is based on the split culture characterization studies of RSV-infected HEp-2 cells. With a factor or two improvement in the extraction process or optimization of the RT-PCR, lower limits at or below the RSV infectious dose 50 (dose that will infect 50% of subjects, ~ 100 copies per μL) are likely achievable.

Currently, there are no commercially available low resource nucleic acid extraction devices for comparison to the proposed method. However, several laboratory-based commercial kits are available, and we compared the proposed low resource method to these approaches. Somewhat surprisingly, the proposed low resource method performed well in comparison with established laboratory-based methods. As shown in Figure 12, $\sim 22.5\%$ of the RNA is recovered by the current design under idealized conditions (spiked TE buffer). More complex sample matrices such as cell lysates or nasal wash samples evidently contain components that inhibit RT-PCR or make RNA recovery more difficult. All extraction methods tested had lower extraction efficiencies when used to extract RNA from cell lysates. For example, compared to extraction from TE buffer, the recovery from spiked cell lysates

using the extraction cassette was reduced by 65%. Similarly, the recovery using the RNeasy kit was reduced by 57%.

The prototype design was tested with a small subset of previously collected de-identified nasal wash samples. These samples were labeled RSV positive or negative during the collection process (not part of this study) using a commercial laboratory RNA extraction process and RT-PCR. The testing of these samples was not designed as a blinded study and served as a simple validation of the basic extraction design. The evaluation of these samples with our prototype device indicated that the basic design performed similarly to commercially available kits (Figure 11) but in general recovered less than the other kits tested. All of the extraction methods used correctly classified the RSV positive and negative samples. However, the amount of RSV RNA present in these samples was quite variable as indicated by the coefficient of variation (s.d./mean) obtained with all of the extraction methods. The coefficients of variation were 157% (extraction prototype), 227% (RNeasy), 173% (Dynabeads), and 106% (MagAttract). This high variation was the major reason for using the HEp-2 cell lysates as a more controllable clinical sample analogue for further device development and testing. The error obtained with known starting RNA content is more indicative of variation inherent in the methods themselves. As Figure 13 indicates, under these more controlled conditions, the coefficient of variation is substantially reduced for both the extraction cassette at 6% and the RNeasy kit at 13%.

The inherent flexibility and stability of the extraction cassette provides a unique format for creating a low resource RNA extraction device. The device format can be easily modified to incorporate larger sample volumes and is suitable for large scale manufacturing. The continuous diameter of the tubing minimizes particle loss during sample pull-through by

eliminating locations where the particles can become trapped, a limitation of the original prototype design shown in Figure 9. In addition, the utilization of surface tension valves in the continuous tubing design serves to separate processing solutions within one continuous section of tubing, and allows the extraction process to be fully self-contained. Individual processing solutions are preloaded into the tubing, eliminating the need for sample handling and pipetting during the extraction process. This is advantageous as it minimizes the potential for contamination of the wash solutions, the extracted RNA, and the operator. The surface tension in the small diameter tubing holds each solution in place, and individual solutions remain undisturbed when magnetic particles pass through the air valves. The valves also minimize interferent carryover by preventing diffusion down the tubing, and separating the water wash into three successive steps also helped to minimize carryover.

Previous studies using a filament-antibody recognition assay found that high capillary forces held solutions within small diameter capillary tubes even in the presence of a moving filament (56). This fluid retention and separation are key to the continuous tubing design. The surface tension at this interface is affected by the surface properties of the tubing and the properties of the air/liquid interface. On-going studies are directed at better understanding the physical properties of the cassette such as the particle diameter, density, magnetic susceptibility, and surface chemistry that define this phenomenon and how they might be modified to improve device performance. A better understanding of these forces will enable more flexibility in future design improvements.

The performance of this approach and could be improved by reducing the overall loss of RNA during the extraction process. Unlike commercially available extraction kits, all of the required components in this study are known and have been chosen based on published

methods for RNA extraction. It is likely that further modifications to individual solutions will lead to an increase in the recovery efficiency. The post-extraction RNA distribution in the processing solutions suggests that RNA may be irreversibly bound to surfaces or degraded during processing. It is also possible that a component in the processing solutions inhibited RNeasy recovery. An estimation of the RNA distribution within each wash chamber allows us to identify potential locations for optimization (Figure 14). Significant quantities of RNA were lost during the water wash steps, which are necessary to remove the ethanol in the absence of centrifugation. For downstream RNA detection by RT-PCR, the ethanol must be removed prior to amplification; however, other nucleic acid-based detection strategies may not be inhibited by the presence of ethanol. In these cases, the water wash chambers could be reduced or eliminated and the recovery efficiency of the extraction cassette would be improved. Approximately 8% of the RNA still remained on the silica particles after a 5 minute elution in water. By increasing the elution time, the overall yield of the device could be improved by up to 8% in 12 hours, but the total extraction time would be dramatically increased. Minimal RNA was detected within the RNA-silica binding, chaotropic wash and RNA precipitation solutions. It is possible that additional RNA is bound to the inner wall of the tubing or located on particles that become trapped in the surface tension valves during magnetic pull-through.

The extraction cassette investigated in this chapter can potentially be utilized for sample preparation in a low resource setting. It is relatively inexpensive to produce at less than \$1.00 per extraction. A rough cost estimate based on current catalog prices of the chemicals and materials required for the continuous tubing design suggests that the most expensive items are the magnetic particles (about \$0.50) and the Tygon tubing (about \$0.30).

The recovery efficiency of this device is lower than we would like. However, the continuous tubing design can likely be further improved by solution and surface optimization studies. Its major advantages are that it can be performed without a laboratory centrifuge or access to a pipetter and without the skills necessary to operate these laboratory devices, keys to a low resource device.

Conclusion

In summary, a self-contained RNA extraction device suitable for the preparation of patient samples for RT-PCR analysis has been developed. An initial non-laboratory prototype design had a recovery efficiency between approximately 12% and 68% of laboratory-based commercially available kits. The continuous tubing extraction cassette design improved this to between 30% and 55% of the Qiagen RNeasy kit. The performance of this device along with its simplicity and flexibility suggests that it merits further evaluation as a sample preparation tool suitable for use in low resource settings where nucleic acid-based diagnostics must be utilized without specialized equipment, trained personnel, or even electricity.

Acknowledgments

The purchase of materials and reagents for this project was supported in part by a Vanderbilt University IDEAS Award and a National Institutes of Health R21 grant (EB009235). I thank the National Institutes of Health Training Grant in Mechanisms of Vascular Disease for personal support during the time I worked on this project.

The work presented in this chapter is the result of the efforts of several individuals. The initial concept of RNA extraction in a tube using surface tension valves to separate

processing solutions is credited to Rick Haselton. Much of the data was collected by Hali Bordelon and Amy Klemm. A considerable amount of effort was contributed by way of experiment design and background research into RNA extraction methods and reagents by Hali Bordelon and Patricia Russ. Hali also contributed significantly to writing of the manuscript that is the basis of this chapter. David Wright provided his immense body of knowledge to keep the project efforts in check with reality. And finally, this work could not have been completed without our great collaborators John Williams and Keipp Talbot, who collected and provided the RSV-infected nasal wash patient samples.

Part II. Isothermal methods for nucleic acid detection

Chapter IV

THE EFFECT OF HYBRIDIZATION-INDUCED SECONDARY STRUCTURE ALTERATIONS ON RNA DETECTION USING BACKSCATTERING INTERFEROMETRY

Abstract

Backscattering interferometry (BSI) has been used to successfully monitor molecular interactions without labeling and with high sensitivity. These properties suggest that this approach might be useful for detecting biomarkers of infection, such as RNA, which is the basis for the work described in this chapter (24). I identified interactions and characteristics of nucleic acid probes that maximize the BSI signal upon binding the respiratory syncytial virus nucleocapsid gene RNA biomarker. The number of base pairs formed upon the addition of oligonucleotide probes to a solution containing the viral RNA target correlated with the BSI signal magnitude. Using RNA folding software *mfold*, I found that the predicted number of unpaired nucleotides in the targeted regions of the RNA sequence generally correlated with BSI sensitivity. I also demonstrated that locked nucleic acid (LNA) probes improve sensitivity approximately four-fold compared to DNA probes of the same sequence. This enhancement in BSI performance was attributed to the increased A-form character of the LNA:RNA hybrid. A limit of detection of 624 pM, corresponding to $\sim 10^5$ target molecules, was achieved using nine distinct ~ 23 -mer DNA probes targeting regions distributed along the RNA target. I conclude that BSI has promise as an effective tool for sensitive RNA detection and provides a road map for further improving detection limits.

Introduction

The expression of single-stranded RNA is an essential part of the life cycle of human pathogens. RNA is found in great abundance during critical stages of infection. Some virus infections produce $10^3 - 10^4$ detectable RNA molecules per virion (6,7). Additionally, a high degree of pathogen-specificity can be found in sequences of expressed RNA. Pathogen species and strains can be identified based solely on the detection of RNA sequences as short as 16 nucleotides (57,58). Because of their abundance and species-specificity, RNA biomarkers are especially useful for pathogen detection and diagnosis of illnesses that result from infection. Our laboratories have developed an interferometric method for RNA detection based on specific interactions with unlabeled oligonucleotide probes in solution.

Many methods have been developed to detect RNA biomarkers. Reverse transcription followed by polymerase chain reaction (RT-PCR) is a common technique used to quantify RNA. Because of its sensitivity, it has become the gold-standard for RNA detection. PCR-based methods, however, typically require purification, denaturation, and time consuming amplification and labeling. Fluorescence-based methods, such as microarrays or molecular beacons, are also commonly used for detecting RNA targets using oligonucleotide probes (59), yet they often lack the sensitivity needed for diagnostic applications. Other nucleic acid probe-based methods developed for RNA detection include the biobarcode-assay (60), cantilever array sensors (61), and surface plasmon resonance (SPR) (62). These methods require complex probe synthesis procedures, nucleic acid labeling or immobilization, or specialized instrumentation and are deficient in terms of speed, sensitivity, convenience, and cost. There is, therefore, a need for methods that are simple, rapid, and sensitive for RNA detection. Backscattering interferometry (BSI) is a technology that circumvents the limitations of other detection methods as it has a simple instrumental design, does not require

molecular labeling or amplification, and can be performed in solution using microliter volumes in complex matrices.

BSI has been used to successfully monitor binding interactions of a variety of biological molecules with high sensitivity (63-69). The design of this unique interferometer is very simple. A He-Ne laser is used to illuminate a semicircular microfluidic channel containing less than 1 μL of analyte, creating a set of high contrast interference fringes of reflected and refracted light (Figure 16A). When a specific binding event occurs, the refractive index (RI) of the solution in the channel changes, causing these fringes to shift in a manner that is proportional to the concentration of the analyte (Figure 16B - C). Though BSI has been used to quantify protein biomarkers via antibody-antigen interactions (64), the work presented in this chapter represents the first demonstration of its use for detecting and

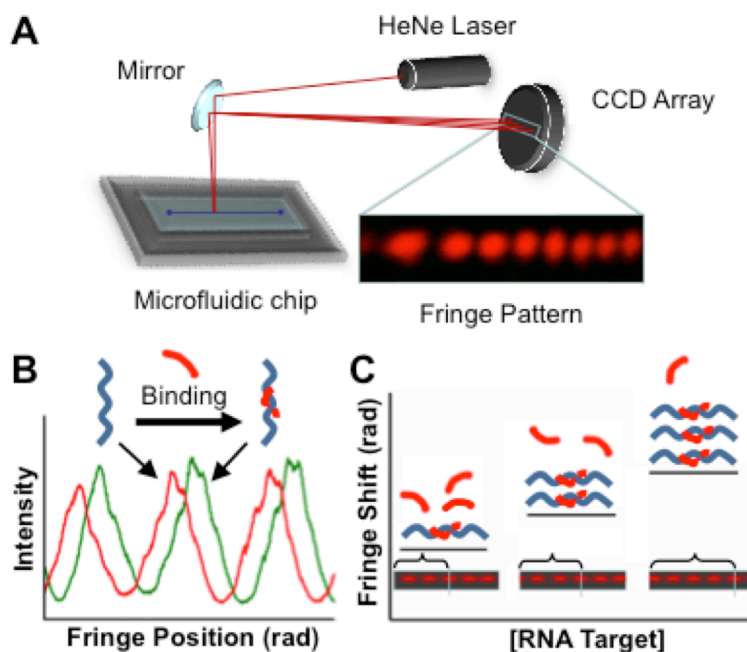


Figure 16. Depiction of the optical train and mechanism of signal generation for RNA detection using backscattering interferometry (BSI). A) Schematic of BSI optical train. B) Digital representation of interference fringes. C) Representation of signal generation as probes bind RNA targets.

quantifying RNA biomarkers.

Nucleic acid probes of various lengths and chemical compositions can be designed to complement any sequence of a target nucleic acid. Therefore, the design space of nucleic acid probes is extremely large compared to other types of probes, such as antibody-antigen or even aptamer-ligand interactions, which require specific and constrained tertiary structures for target recognition. Additionally, commercial synthesis of oligonucleotides is widely available and is able to produce virtually any sequence of natural or chemically modified nucleotides. Compared to other biomolecular probes (e.g., antibodies), nucleic acids also have relatively modest chemical complexity and are uniformly charged. These properties reduce variations in RI that may result from the interactions of the probes with the solvent, making them ideal probes for biomarker detection using BSI. Furthermore, nucleic acids are not “sticky” like proteins, reducing artificial signals from non-specific interactions, such as binding to the channel wall.

An important property of BSI in the context of biomarker detection is its large dynamic range. The optical properties of the interferometer are such that the fringes continue to shift (i.e., produce a signal) as long as a change in RI occurs and that the RI of the fluid differs from that of the microfluidic chip. Consequently, the dynamic range of BSI can be expanded as long as there are analytes available to bind and change the RI. BSI sensitivity can therefore be dramatically enhanced without reaching signal saturation. This property is in contrast to detection assays that are dependent on light intensity, in which photometers can become saturated with extreme amplification methodologies. Oligonucleotide probes that are designed to produce the maximum change in RI upon binding the RNA target will, therefore, provide maximum BSI signal and optimize sensitivity. In this chapter, I report the utility of

BSI for label-free detection of a specific viral RNA biomarker sequence in solution. The focus of these experiments is on the respiratory syncytial virus (RSV) nucleocapsid (N) gene RNA, a biomarker with which our laboratories have had considerable experience (7,70,71). A systematic evaluation of a subset of oligonucleotide probe design parameters was conducted to determine interactions and characteristics of nucleic acid probes that enhance the sensitivity of BSI for detecting this RNA biomarker.

Materials and Methods

Preparation of the synthetic RNA targets

The RNA target used in these studies is a synthetic ~1300 nucleotide positive-sense RNA molecule of the RSV strain A₂ N gene. The RNA was prepared as previously described (7). Briefly, a pGBKT7 vector containing the RSV N gene insert was amplified in *Escherichia coli* strain DH5 α , purified using a Qiagen Plasmid Midi Kit, linearized with the *Bss*HIII restriction enzyme, reverse transcribed using the Ambion T7MEGAscript transcription kit, and treated with DNase I. The integrity and length of the RNA product was confirmed using denaturing agarose gel electrophoresis. Aliquots of the RNA were stored at a concentration of ~80 nM in Tris-EDTA buffer at -80 °C until they were used. The RNA mismatch targets used in these studies were commercially synthesized at a 50 nmole scale and desalted by Sigma-Aldrich. The sequences of the full length RNA target and the mismatch targets used in these studies are provided in Supplemental Figure 1 in Appendix A.

Synthesis of the oligonucleotide probes

The DNA oligonucleotide probes used in these studies were commercially synthesized at a 200 nmole scale by Sigma-Aldrich and purified using reverse phase cartridge purification. Locked nucleic acid (LNA) oligonucleotide probes were synthesized at a 250 nmole scale by Exiqon and purified with high performance liquid chromatography. Each lyophilized oligonucleotide was resuspended to a concentration of ~100 μ M in molecular grade water (Fisher) and stored at -20 °C until they were used. The sequence of each oligonucleotide probe used in these studies is provided in Table 1.

Backscattering interferometry

Details of the BSI instrumental configuration have been described in detail previously (63). In brief, a 5 mW helium neon laser ($\lambda = 635$ nm) is directed onto a borosilicate glass microfluidic chip etched with a near-semicircular channel that is about 210 μ m wide and 100 μ m deep. The coherent, collimated light source reflects and refracts within the channel, creating a fringe pattern that is detected with a linear CCD array. The fringes shift spatially with respect to the RI of the solution, and the position of a select group of fringes is analyzed with an in-house LabView-based fast Fourier transform analysis program (72).

Unless otherwise noted, all assays were performed in an end-point format where a fixed concentration of probe (100 nM) was incubated with increasing concentrations (0 - 36.5 nM) of target RNA in Tris-buffered saline. Samples were mixed with a pipette and incubated at room temperature for 2.5 hours to ensure that the binding equilibrium was reached. One microliter of each sample was sequentially injected into the microfluidic channel and the signal was recorded for 30 seconds. To correct for bulk RI changes, a series of blank

Table 1. List of the probe sequences used in BSI studies.

	Probe name*	Probe length (nucleotides)	Sequence (5' – 3')	
varying DNA probe length	RSVN(242-256)	15	AAATACTCAGAGATG	
	RSVN(242-263)	22	AAATACTCAGAGATGCGGGATA	
	RSVN(242-285)	44	AAATACTCAGAGATGCGGGATATCATGTAAAA-GCAAATGGAGTA	
	RSVN(242-329)	88	AAATACTCAGAGATGCGGGATATCATGTAAAA-GCAAATGGAGTAGATGTAACAACACATCGT-CAAGACATTAATGGAAAAGAAATGAA	
4 consecutive DNA probes	RSVN(242-263)	22	AAATACTCAGAGATGCGGGATA	
	RSVN(264-285)	22	TCATGTAAAAGCAAATGGAGTA	
	RSVN(286-307)	22	GATGTAACAACACATCGTCAAG	
	RSVN(308-329)	22	ACATTAATGGAAAAGAAATGAA	
9 distributed DNA probes	4 distributed DNA probes	RSVN(242-263)	22	AAATACTCAGAGATGCGGGATA
		RSVN(425-444)	20	TGGGAGAGGTAGCTCCAGAA
		RSVN(603-622)	20	ACCCAAGGACATAGCCAACA
		RSVN(755-774)	20	GTGCAGGGCAAGTGATGTTA
	RSVN(4-29)	26	GCTCTTAGCAAAGTCAAGTTGAATGA	
	RSVN(193-214)	22	ATAGGTATGTTATATGCGATGT	
	RSVN(531-551)	21	TGGTCTTACAGCCGTGATTAG	
	RSVN(843-872)	30	GGAACAAGTTGTTGAGGTTTATGAATATGC	
	RSVN(957-983)	27	CTTCTCCAGTGATGATTAGGCAATGC	
	4 distributed LNA probes	RSVN(242-263)L	22	AA+ATA+CTC+AGA+GAT+GCG+GGA+TA
RSVN(425-444)L		20	TG+GGA+GAG+GTA+GCT+CCA+GAA	
RSVN(603-622)L		20	AC+CCA+AGG+ACA+TAG+CCA+ACA	
RSVN(755-774)L		20	GT+GCA+GGG+CAA+GTG+ATG+TTA	
Other DNA probes	RSVN(800-821)	22	TTAAAAATATTATGTTAGGACA	
	RSVN(1070-1091)	22	TCAAAGAAAATGGTGTGATTAA	
	RSVN(242-263)SCRAM	22	AAATAAAGGTATCCGGTCGAA	
	RSVN(264-285)SCRAM	22	AGATGAGAGAATAGTTTCCAAA	

*The probe name includes the position of the complementary sequence of the respiratory syncytial virus (RSV) nucleocapsid (N) gene in reference to the start codon. Locked nucleic acid (LNA) sequences are denoted with plus signs (+) preceding the modified nucleotides.

measurements were taken from samples containing increasing concentrations of RNA target in the absence of probe. These values were then subtracted from the sample signal. The RI shift, measured in radians, was then plotted against the concentration of the target to produce a binding response curve. The slope of the binding response curve, in radians (rad) per nanomolar, was used as a measure of sensitivity. The lower limit of detection (LOD) was calculated using the following equation:

$$\text{LOD} = 3 \times \sigma / \text{slope}$$

where σ is the average of three standard deviation measurements at each RNA target concentration tested and the slope is the best-fit trendline of the linear range of the binding curve ($y = ax + b$).

Quantification of net nucleic acid hybridization

The relative amount of nucleic acid hybridization was quantified using a SYBR Green assay. Samples were prepared in triplicate with 1 nM of the synthetic RSV N gene RNA, 10 nM of the probe or probes, and a 1:9000 dilution of SYBR Green I (Life Technologies). Samples for the blank measurements were prepared in triplicate without RNA or without the DNA probes. For the LNA:RNA and DNA:RNA hybridization comparison, samples were prepared in triplicate using 60 nM LNA or DNA, 20 nM RNA complement of the same length, and a 1:9000 dilution of SYBR Green I (Life Technologies). A standard curve of double stranded DNA of the same sequence and length was used to approximate the percent hybridization in the LNA:RNA and DNA:RNA samples. Prior to the addition of SYBR Green I, each sample was heated to 90 °C for 5 minutes and cooled slowly to room temperature over the course of 1 hour. Fluorescence measurements were recorded using a BioTek Synergy H4 Hybrid 96-well plate reader using an excitation wavelength of 497 nm and a detection wavelength of 520 nm. The values were normalized by subtracting signal of the samples from the background signal generated in the RNA-alone or the DNA-alone blank samples.

Preparation of and evaluation of surrogate nasal wash samples

HEp-2 cell lysates were prepared in a manner previously described (7). Briefly, cells were cultured to a confluent monolayer in a cell culture flask, harvested, and resuspended in a cell lysis/RNA preservation solution (4 M guanidinium thiocyanate, 25 mM sodium citrate [pH 7.0] 0.5% N-lauroylsarcosine [Sarkosyl], 0.1 M 2-mercaptoethanol), and stored at -80 °C. The surrogate nasal wash samples were prepared by diluting the cell lysates into phosphate buffered saline at 1×10^5 , 5×10^4 , 1×10^4 , and 0 cells/mL concentrations and spiking each with the synthetic ~1300 nucleotide RSV N gene RNA biomarker at a final concentration of ~16 nM.

For evaluation of the RNA target in the surrogate nasal wash samples using BSI, the samples were split into two halves. One half of each sample was used for total RNA extraction, and the other half was left unextracted. Total RNA extraction was performed using a self-contained continuous tubing extraction cassette as previously described (7). Briefly, each sample was added to an RNA binding solution containing silica-coated magnetic beads. The beads were mixed with the sample for 5 minutes and then drawn through a series of RNA extraction solutions. Total RNA was eluted into water, and evaluation of the synthetic ~1300 nucleotide RSV N gene RNA biomarker was performed using quantitative reverse-transcription polymerase chain reaction (qRT-PCR) and BSI. Each sample was extracted and evaluated in triplicate. qRT-PCR was performed as described previously (7).

RNA folding analysis

The folding state of the synthetic RSV N-gene RNA was predicted using the RNA Folding Form of the *mfold* software package available online (<http://mfold.rna.albany.edu/?q=mfold/RNA-Folding-Form>). The full-length sequence of the target (1331 nucleotides, sequence available in Supplemental Figure 1 in Appendix A) was used as the input, and the default settings were used. The five structures predicted to have the lowest energy were used to identify the folding state at the probe binding sequences. The number of consecutive unpaired bases for each of these sequences were averaged from the five predicted structures and plotted against the slope of the linear range of the BSI response curve. The five lowest energy *mfold* RNA folding structures are provided in Supplemental Figure 2 in Appendix A.

Nucleic acid secondary structure determination

Circular dichroism (CD) spectra were collected using an Aviv CD spectrometer model 215 (Aviv Biomedical, Inc.). To compare the LNA:RNA, DNA:RNA, and DNA:DNA hybrids, solutions were prepared in 40 μ L volumes containing 30 μ M of DNA, RNA, and/or LNA strands in Tris-buffered saline. Prior to collecting CD spectra, each sample was heated to 90 °C for 5 minutes and cooled slowly to room temperature over the course of 1 hour. For the A-form to B-form transition study, a solution of 80% 2,2,2-Trifluoroethanol (TFE) containing 385 μ M Tris-HCl, 38.5 EDTA, 5 mM NaCl, and 12 μ M of each DNA strand was prepared. Prior to adding the TFE, the solution was heated to 90 °C for 5 minutes and cooled slowly to room temperature over the course of 1 hour. TFE was added stepwise accompanied by immediate mixing to avoid DNA precipitation while transitioning to A-form DNA. The

concentration of TFE was diluted to 77.5%, 75%, 72.5%, and 70% to by adding the appropriate volumes of a solution containing 385 μ M Tris-HCl, 38.5 EDTA, 5 mM NaCl, and 12 μ M of each DNA strand. At each TFE concentration, 60 μ L of the sample was removed and CD and BSI measurements were immediately performed. Blank measurements were collected from solutions prepared at each TFE concentration and containing 385 μ M Tris-HCl, 38.5 EDTA, and 5 mM NaCl, with no DNA. All CD spectra were collected from 320 nm to 200 nm wavelengths at 25.0 °C in a 1.0 mm pathlength quartz cuvette using a 0.5 nm wavelength step, a 1.0 nm bandwidth, and a 1 second averaging time. Spectra were averaged from at least 3 separate scans, smoothed, and normalized using CD-215 software version 2.90 provided by the manufacturer.

Results

Enhanced BSI sensitivity using 22-mer probes

The design space of oligonucleotide probes targeting the ~1300 nucleotide RSV N gene RNA biomarker sequence is extremely large. Oligonucleotides of virtually any length and sequence complementary to the target could be used, and a variety of chemically modified nucleotides could be substituted for natural nucleotides. Because an exhaustive study of all the potential probe designs is not feasible, I conducted a systematic evaluation of a subset of oligonucleotide probe design parameters. The first probe investigated was RSVN(242-263), a 22-mer DNA probe with a sequence chosen based on previous success as a primer for PCR studies aimed at amplifying RSV N gene cDNA. BSI measurements using the RSVN(242-263) 22-mer probe produced a linear response proportional to the concentration of the RSV N gene RNA with a LOD of 3.73 nM target RNA (Figure 17A and

Table 2). As a negative control, a scrambled sequence of the same 22-mer was evaluated under the same conditions and yielded negligible signal. Postulating that probe length would correlate with BSI signal, probes RSVN(242-256), RSVN(242-285), and RSVN(242-329) were tested, which are 15, 44, and 88 nucleotides in length, respectively, and start from the same position in the target RNA as the 22-mer probe. Each of these probe lengths resulted in slightly less signal and poorer detection limits than the 22-mer probe. To relate the BSI signal to a net increase in base pairs, the relative hybridization of these probes to the RNA target was determined using a SYBR Green assay (Figure 17B). The signal generated from the

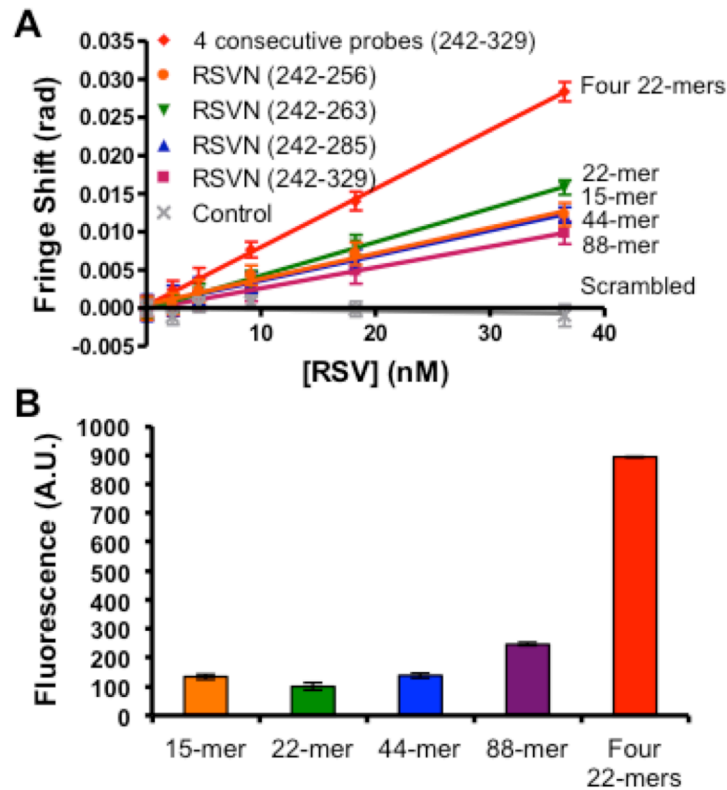


Figure 17. Comparison of the BSI binding response and net hybridization upon adding the 15-mer, 22-mer, 44-mer, 88-mer, or four consecutive 22-mer DNA probes to the RNA target. A) The probe length that produces optimal BSI signal is 22 nucleotides. Four short 22-mer DNA probes have improved signal over one 88-mer spanning the same target sequence. A scrambled negative control sequence produced negligible signal. B) Net hybridization of the four consecutive 22-mers is significantly greater than any of the four probe lengths.

intercalation of SYBR Green dye in the 15-mer, 44-mer, and 88-mer probe:target hybrids was slightly greater than that of the 22-mer probe:target hybrid. Interestingly, we discovered that by dividing the 88-mer probe into four contiguous 22-mer probes, the slope of the BSI response was significantly increased, resulting in a LOD of 2.04 nM target RNA, or $\sim 4.1 \times 10^5$ molecules. This enhancement in sensitivity was reflected by the increase in the net hybridization of the four consecutive 22-mers compared to the 15-mer, 22-mer, 44-mer, and 88-mer probes (Figure 17 and Table 2). These results indicate that of the probes tested, the optimal length is 22 nucleotides for BSI detection and that the BSI signal can be enhanced using multiple probes of that length.

Table 2. Summary of the slopes of the binding curves and limits of detection for each probe combination.

Probe	Slope (x 10⁻⁵)	LOD (nM)
RSVN(242-263)	44	3.73
RSVN(242-256)	30	26.7
RSVN(242-285)	33	5.16
RSVN(242-329)	27	8.96
Four consecutive DNA probes	77	2.04
Four distributed DNA probes	250	2.54
Nine distributed DNA probes	627	0.624
RSVN(264-285)	246	5.78
RSVN(286-307)	25	68.4
RSVN(308-329)	359	4.52
RSVN(1070-1091)	84	15.0
RSVN(800-821)	52	35.6
RSVN(755-774)	27	146
RSVN(242-263)L	175	2.15
Four distributed	349	1.05

Enhanced BSI sensitivity using multiple distributed probes

Next we investigated the influence on assay sensitivity of distributing the probes along the ~1300 nucleotide RNA target sequence. Because the four consecutive probes were designed to bind contiguous sequences of the target RNA, it was hypothesized that the conformation of the target RNA secondary structure prevented the probes from fully hybridizing and that distributed sequences would improve signal. By distributing the four probes along the length of the target RNA, the slope of response was improved more than 3-fold over the 4 contiguous sequences (Figure 18A and Table 2). Furthermore, increasing the total number of probes to nine further improved sensitivity, providing a LOD of 624 pM, or 1.5×10^5 molecules target RNA. Accordingly, studies evaluating the net hybridization of the single probe versus the four and nine probe combinations revealed increased hybridization with the increased number of probes (Figure 18C), further validating that BSI signal is at least partially the result of a net change in hybridization.

To further demonstrate that the increased signal from the nine-probe cocktail was a

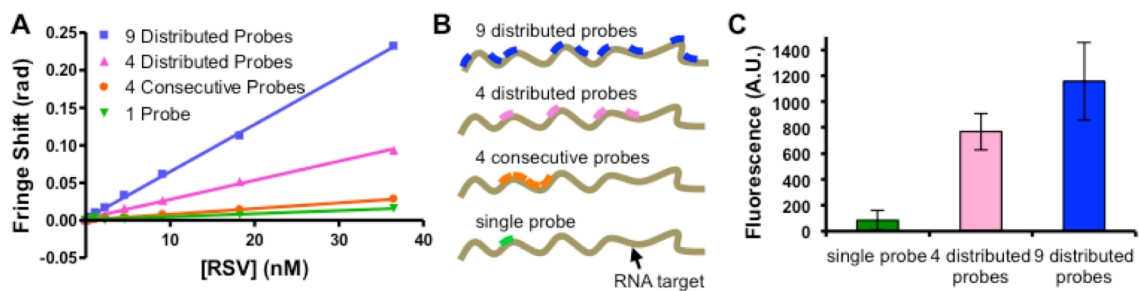


Figure 18. Comparison of the BSI binding response and net hybridization of various numbers and distributions of probes incubated with the RNA target. A) Increasing the number and distribution of distinct probes improves sensitivity. B) Illustration of the relative positions of the DNA probes along the RNA target. C) Hybridization studies confirm that increased number of probes bound correlates with increased binding signal.

result of an increase in the number of available binding sites, as opposed to the effect of having a higher concentration of probes present, a saturation binding isotherm was constructed for both the single probe and the nine-probe cocktail. For this assay, the concentration of the *target RNA* was held constant while the probe concentration was varied from 0 - 100 nM. The signal at saturation (B_{\max}) for the single probe was 0.087 radians, whereas the signal for the nine distributed probes was 0.25 radians, a 2.9-fold overall increase in signal (Figure 19). This result indicates that the sensitivity improvement observed in the nine-probe system is the result of an increased number of available binding sites; therefore, a greater number of binding events can occur before target saturation is reached. This may not be surprising as BSI signal magnitude is directly related to the number of binding events (63). These data are consistent with these previous observations and indicate that the greatest BSI sensitivity over a large dynamic range is achieved by maximizing the number of available target RNA binding sites.

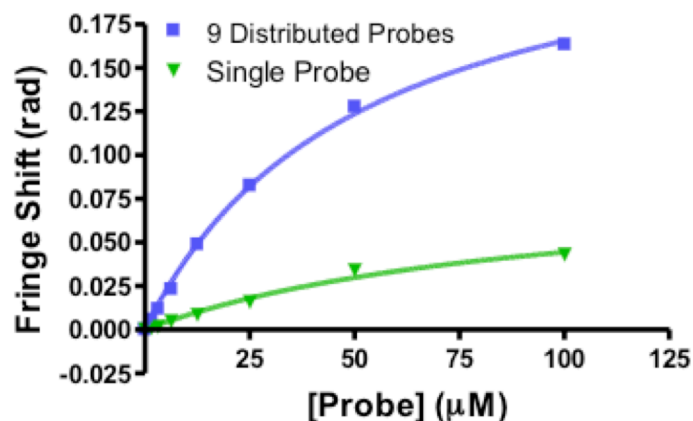


Figure 19. Saturation curves of target RNA incubated with increasing concentrations of either a single 22-mer probe or a mixture of nine distributed probes. The mixture of nine probes saturates at a higher level than the single probe.

Target specificity is maintained in RNA samples extracted from complex matrices

To evaluate the specificity of BSI using the 22-mer RSVN(242-263) DNA, six 22-mer RNA targets containing 0, 1, 3, 5, 7, and 10 mismatched nucleotides distributed throughout the sequence were tested in an end-point assay format (Figure 20A). With increasing mismatched nucleotides in the target sequence, BSI signal dropped off significantly, resulting in essentially no signal using the RNA target containing 10 mismatched bases in the sequence. The signal produced using the RNA target sequences containing 1, 3, and 5 mismatches was statistically equal to that of the 0 mismatch target. To determine if this tolerance for mismatched nucleotides in the target sequence produced false signal in complex samples, we tested BSI for detecting our synthetic ~1300 nucleotide RNA target spiked into surrogate nasal wash samples containing increasing background concentrations of HEP-2 cell lysate (Figure 20B). In unextracted samples, i.e., samples of RNA spiked into cell lysate background, BSI signal diminished with increasing cell lysate concentration, resulting in no distinguishable signal in the highest concentration of cell lysate

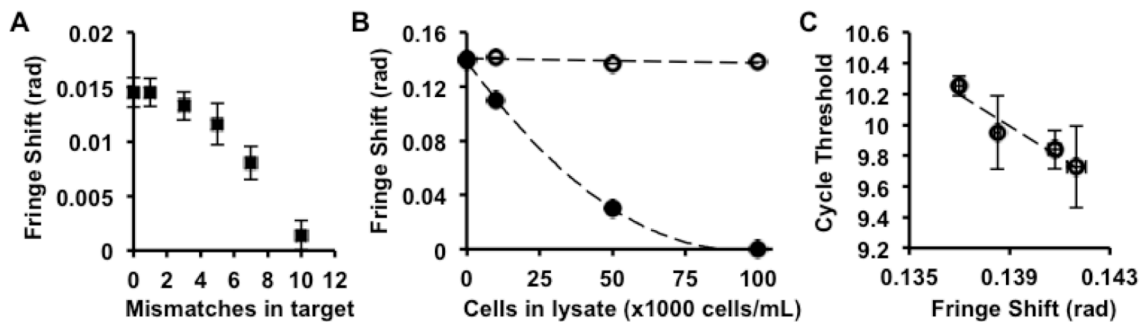


Figure 20. Evaluations of BSI specificity for mismatched targets or RNA targets in complex samples using a single 22-mer probe. A) BSI signal drops off moderately when probing for RNA targets with increasing numbers of mismatched nucleotides. B) BSI signal is consistent when probing for the ~1300 nucleotide RNA biomarker in a sample of total RNA extracted from HEP-2 cell lysates of increasing concentrations (open circles), whereas BSI signal diminishes in unextracted samples of increasing background concentration (closed circles). C) qRT-PCR cycle threshold values for the extracted samples correlate with the BSI fringe shift values.

evaluated. In extracted samples, i.e., samples of total RNA isolated from the cell lysate background, the signal produced was consistent despite the increase in the total background RNA that would be extracted from the samples. Notably, cycle threshold values of qRT-PCR analysis of the extracted RNA samples correlated very well with the fringe shift values of BSI (Figure 20C). Taken together, these data suggest that BSI detection of RNA is tolerant of a few mismatched nucleotides in the target sequence, yet specificity is retained in total RNA extracts from complex cell lysate samples.

RNA target folding affects BSI binding signal

During the process of testing a variety of oligonucleotide probe sequences, I observed that probes of similar length (i.e., 20 - 22 nucleotides) and nucleotide content, but composed of different nucleotide sequences, yielded significantly disparate BSI binding responses. Because BSI sensitivity is produced in part by changes in conformation (62), I surmised that the probes were not only interacting at the primary sequence level of the target RNA (i.e., base pairing), but that probe binding signal was also impacted by the complex folding state of the RNA target. To investigate the effects of RNA target folding on BSI response, *mfold* software was used to predict secondary structure motifs in the regions complementary to the probes that would account for the variation in probe binding. Specifically, the software was used to identify regions of the RNA target that are predicated to be open loops, or sequences that would be available to bind a complementary oligonucleotide probe. Although *mfold* cannot predict RNA folding with absolute certainty, with the exception of two probes tested, I found a positive correlation between the number of unpaired nucleotides in the open loop regions of the predicted structure of the RNA target and the BSI signal produced by the probe

complementary to that sequence (Figure 21). In line with probe design software for microarray oligonucleotide sequences (58), probes designed to bind RNA target sequences predicted to be single-stranded would result in the greatest net change in hybridization and produce the greatest change in BSI signal. Probes RSVN(264-285) and RSVN(308-329), however, produced a much greater signal that does not appear to fit this model. One possible explanation for the large signal of these probes compared the other probes is that tertiary structure rearrangements or allosteric changes in the RNA target may be occurring upon probe binding. Our laboratories have observed similar binding-order related signal enhancements in other systems, particularly the thrombin-binding aptamers (66). These observations cannot be fully explained due to limitations in the current model but are under investigation.

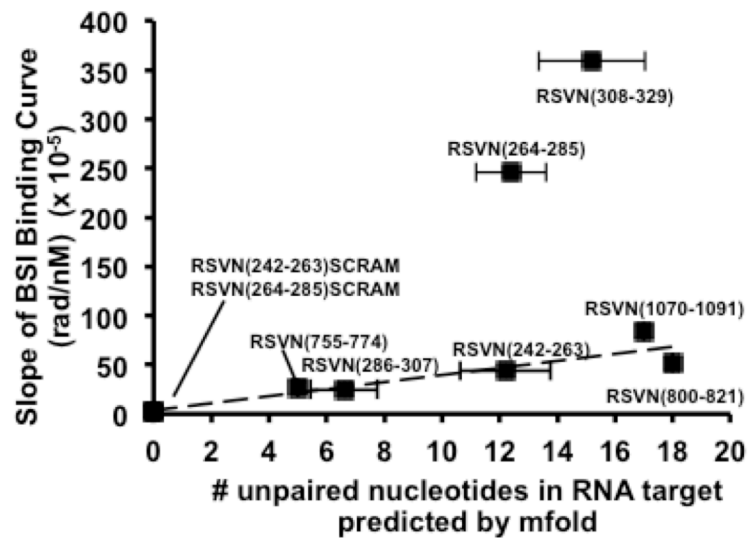


Figure 21. DNA probes designed to bind different regions of the RNA target generate a range of binding responses. With the exception of two probes, binding response correlates positively with the number of nucleotides predicted to be unpaired in the RNA target ($R^2 = 0.86$). x -axis values are averages of predicted unpaired nucleotides in the five lowest energy folding structures of *mfold* \pm standard error.

Enhanced BSI sensitivity using LNA probes

With some knowledge of the probe length and spacing parameters that yield good signal in BSI for optimized hybridization, I explored locked nucleic acids (LNAs), a category of oligonucleotides with unique structure and binding characteristics. LNA oligonucleotides have much greater binding affinities for their targets when compared to DNA or RNA of similar length and sequence (73). The first LNA probe I used, RSV(242-263)L, was the same sequence and length as the 22-mer DNA probe used in our initial experiments, except that every third nucleotide in the sequence contains a methylene group bridging the 2' oxygen and the 4' carbon of the ribose ring, "locking" the sugar into the 3'-*endo* conformation. With these simple structural modifications, a 4-fold improvement in sensitivity was achieved over the DNA probes, resulting in a LOD of 2.15 nM of target RNA (Figure 22A and Table 2). Using a mixture of four *distributed* LNA probes, identical in sequence and length to the four distributed DNA probes, a LOD of 1.05 nM target RNA was achieved. These results compare favorably to the 1.5-fold improvement in LOD observed when increasing the number of DNA probes from one to four (Table 2). Interestingly, this improvement in signal and sensitivity was not attributed to an increase in the net hybridization of the probe to the RNA target. Although the increased affinity of LNA for the RNA target would generally shift the binding equilibrium toward the bound state, both LNA and DNA probes hybridize to approximately the same number of RNA targets (Figure 22B). This result is likely because the LNA and DNA probes are added to the RNA target in such excess that, despite the increased affinity of LNA for the target RNA, the total number of LNA and DNA probes bound to the RNA target was nearly equivalent. Because there is not a significant increase in net hybridization when using LNA probes, I concluded that hybridization alone did not

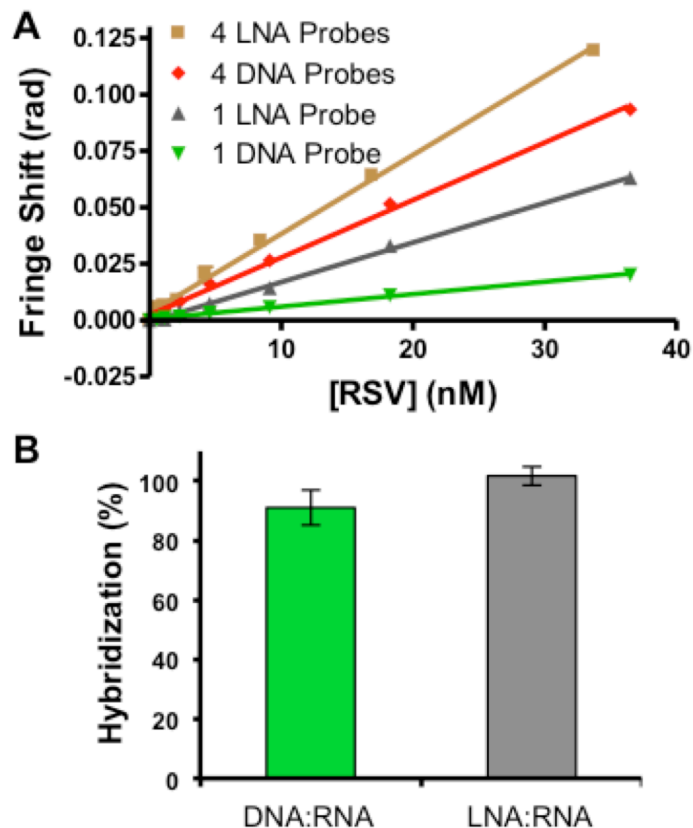


Figure 22. Comparison of the BSI binding response and net hybridization of LNA and DNA probes of the same sequence and length incubated with target RNA. A) LNA probes improve the BSI signal. B) DNA:RNA hybrids and LNA:RNA hybrids produce virtually the same net hybridization.

account for the 4-fold improvement in BSI signal using the LNA probe. Therefore, I explored the possibility that the improvement in sensitivity was the result of the unique structural characteristics of LNA:RNA hybrid.

Induced A-form secondary structure improves BSI sensitivity

LNA:RNA hybrids primarily form A-form secondary helical structures, whereas DNA:RNA hybrids consist of a mixture of A-form and B-form character (74). Since the net hybridization measured for DNA versus LNA probes binding the RNA target was

approximately equivalent but the BSI signal of the LNA probes was significantly greater than that of the DNA probes (Figure 22B and A, respectively), I hypothesized that the induced A-form helical character of the LNA:RNA hybrid was responsible for the greater RI change upon formation compared to the DNA:RNA hybridization. Accordingly, we evaluated nucleic acid hybrids of the same length and sequence that exhibit a range of secondary structures using CD and BSI. To reduce the background noise from the unbound regions of the ~1300 RNA target, the RNA and DNA complements used in these studies are the same length as the LNA and DNA probes (22 nucleotides). Based on the CD spectra, I verified that the LNA:RNA hybrid resulted in a characteristic A-form secondary structure, the DNA:RNA hybrid resulted in a secondary structure consisting of a mixture of A- and B-form, and the DNA:DNA duplex resulted in a characteristic B-form secondary structure (Figure 23A). These same hybrids were then evaluated using BSI. The LNA:RNA interaction produced the largest RI shift (1.53×10^{-2} rad/nM), followed by the DNA:RNA interaction (5.48×10^{-3} rad/nM), and the DNA:DNA interaction produced the smallest RI shift (3.75×10^{-3} rad/nM) (Figure 23B). These data indicate that the BSI signal or slope reflects the extent to which the hybridized product displays A-form secondary structure. These observations are consistent with the hypothesis that BSI signal can be maximized using oligonucleotide probes that induce the greatest net change in the nucleic acid secondary structure.

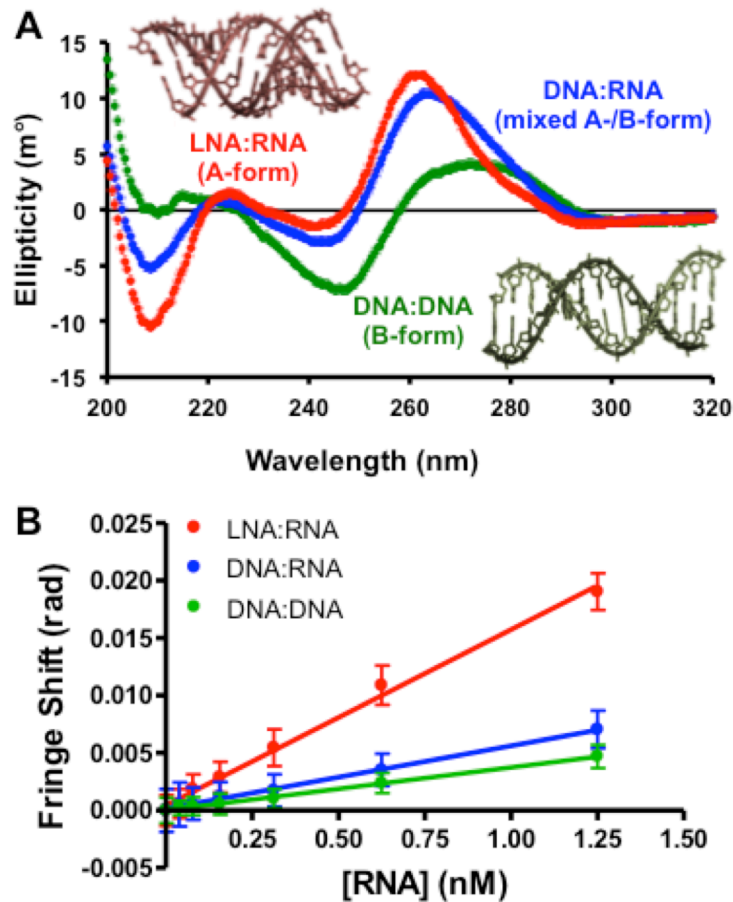


Figure 23. Relative degree of A-form nucleic acid character of the DNA:DNA, DNA:RNA, and LNA:RNA hybrids corresponds with increased BSI signal. A) The circular dichroism (CD) spectrum of the DNA:DNA duplex (green) corresponds to B-form secondary helical structure with a maximum near 280 nm, a deep minimum near 250 nm. LNA:RNA hybrid (red) produces a spectra corresponding to A-form secondary structure with a maximum near 270 nm and a shallow minimum near 245 nm. The DNA:RNA hybrid produces a spectra that is intermediate of A-form and B-form. B) BSI binding curves of LNA:RNA, DNA:RNA, and DNA:DNA.

To further validate that the formation of A-form secondary structure is responsible for the observed increase in BSI signal, as opposed to the differences in the primary structures of the nucleotide subunits, we performed BSI measurements on a DNA:DNA duplex matching the sequence of the RSVN(242-263) probe at various stages of a trifluoroethanol (TFE)-induced B-form to A-form transition. Incubation with high concentrations of TFE is a well-

established method for converting B-form secondary structure in DNA:DNA duplexes to A-form (75,76). TFE was titrated into a solution containing a DNA:DNA duplex and the secondary structure transition was confirmed by CD analysis (Figure 24A). BSI signal magnitude increased as the DNA:DNA duplex adopted a more A-form character as monitored by the ellipticity at 270 nm. These data validate the BSI signal enhancing effect of induced alterations to the helical geometry of the nucleic acid hybrid (Figure 24B).

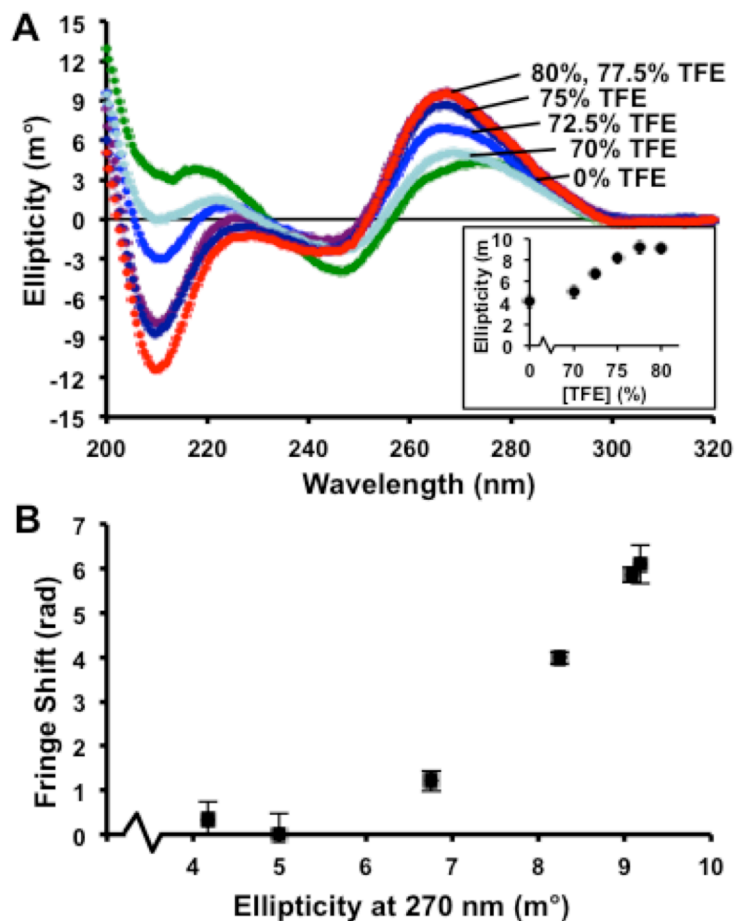


Figure 24. Relative degree of A-form character corresponds to increased BSI signal. A) Circular dichroism (CD) spectra of the DNA duplex demonstrate a shift from A-form to B-form structure with decreasing concentrations of trifluoroethanol (TFE). Inset: A-form to B-form transition monitored at 270 nm. B) Ellipticity at 270 nm correlates positively with the shift in the refractive index (RI) as detected by BSI.

Discussion and Conclusions

In this study, our laboratories demonstrated the use of BSI for the detection of a respiratory syncytial virus N gene RNA biomarker in solution using unlabeled nucleic acid probes. These studies have shown that induced secondary structure formation is a major contributing factor to signal generation for detecting RNA with oligonucleotide probes by BSI. Several factors are important in obtaining a maximum signal to noise ratio. The number of binding events are an important factor, yet as our laboratories have previously shown with protein binding systems (63), the nature of the binding event (i.e., the resulting structure) also plays a critical role in BSI signal magnitude. The first and most obvious source of secondary structure formation is the net helical duplex formation that occurs when a nucleic acid probe hybridizes to the RNA target. we found that the sensitivity of the assay is greatest when multiple, short probes are employed, distributed along the length of the RNA target (Figure 18 and Table 2), which results in the maximum number of binding events (Figure 18C). In comparison to a single 22-mer DNA probe which detects RNA target concentration at a sensitivity of 4.4×10^{-4} radians/nM (LOD = 3.73 nM); four DNA probes produce a 5.7-fold increase in sensitivity, or 2.50×10^{-3} radians/nM (LOD = 2.54 nM); and nine DNA probes produce a 14.3-fold increase in sensitivity, or 6.27×10^{-3} radians/nM (LOD = 624 pM) (Table 2). As one would expect, the increase in signal is directly proportional to the number of probes available to bind the RNA target.

Experiments aimed at studying the effects of probe length demonstrated that BSI signal magnitude was greatest using a probe length of 22 nucleotides (Figure 17). Interestingly, though they contain the same number of base pairs, four contiguous 22-mer probes yield an appreciably larger signal than a single 88-mer probe. We postulate that steric hindrance resulting from the native structure of the ~1300 nucleotide RNA target prevents

the longer probe from binding as effectively as the four shorter probes. Additionally, in a multi-probe assay, it may be the case that some probes bind at a higher kinetic rate than others, altering the conformation of the target RNA and thus creating more favorable binding conditions for subsequent probes. We also found that while four short, adjacent probes create more binding signal than one long probe, sensitivity is improved even further by distributing the probes along the length of the target. This may be explained by the potential for probes that target sequences immediately adjacent to prevent the other probes from binding because of the induced secondary structure and rigidity of the probe-bound sequences.

BSI was demonstrated to be effective in detecting the synthetic ~1300 RNA target from total RNA extracted from a surrogate nasal wash samples of increasing complexity (Figure 20B and C). This result demonstrates the specificity of BSI for detecting target RNA as the target only made up a portion of the total RNA extracted from the sample. In unextracted samples, however, BSI signal diminished with increasing background cell lysate concentration. I hypothesize that the complex bimolecular content present in unextracted cell lysate samples has a signal-suppressing effect on BSI. Despite the successful detection of a specific RNA target from a background of total RNA extract, BSI displayed moderate specificity using a series of mismatched RNA targets (Figure 20A). As the focus of this initial work has been centered on improving sensitivity, there is much unknown about factors involved in the optimization of specificity in BSI. Future work on developing probes optimized for specificity will be needed to improve mismatch specificity.

It was determined that individual probes of similar nucleotide content and length did not produce a similar level of BSI signal. I found that the discrepancy in BSI signal produced from the various probe sequences can be partially explained with RNA folding predictions of

the RNA target. For most RNA sequences, secondary structures are significantly more stable than tertiary structures and, therefore, are more likely to contribute to the native structure of the RNA target (77). Consequently, only the secondary structure of the RNA target was evaluated in these studies. Using *mfold* software to predict the folding state of the RNA target, I found that probes targeting sequences predicted to have mostly unpaired nucleotides (i.e., open loops) generally produced more signal than probes targeting sequences predicted to be mostly double stranded. Two probes, however, produced exceptionally high signal compared to probes targeting regions of similar predicted secondary structure. Alterations in the tertiary structure of the RNA target induced by probe binding may explain the comparatively large signal changes produced by these probes. Future studies will be aimed at investigating the role of tertiary structure in BSI signal generation.

I also found that the integration of “locked” nucleotides into the DNA probe nearly quadruples the sensitivity of BSI (Figure 22 and Table 2). LNA has been widely used for nucleic acid probing applications (78-80). It has been reported that LNA has exceptional binding affinity for complementary RNA or DNA targets while maintaining or even improving sequence specificity (73). Because BSI detects changes in the RI that are induced by the binding of two molecules, the signal enhancement produced by LNA oligonucleotides could potentially have thermodynamic, structural, and/or solvation explanations. Perhaps the most important characteristic of LNA oligonucleotides is the high thermal stability when duplexed with RNA. Melt temperatures of LNA:RNA hybrids can increase by ~ 5 °C per locked nucleotide incorporated into the sequence (78). Because of this high affinity for RNA, a higher proportion of LNA oligonucleotides should bind complementary targets compared to DNA of identical sequence and length. However, the amount of DNA and LNA probe

used in these studies is in great excess relative to the number of available targets, which is intended to drive binding toward probe saturation. The hybridization studies confirmed that the relative amount of bound LNA probes is nearly the same as DNA probes at equilibrium (Figure 22), indicating that the thermodynamic explanation is probably not the greatest contributor to the BSI signal enhancement.

The RI of a solution changes when solutes undergo changes in structural conformation. When binding RNA, a single LNA nucleotide can perturb the surrounding DNA nucleotides to adopt the *C3'-endo* conformation. Consequently, LNA:RNA hybrids form homogeneous A-form helical secondary structures, whereas DNA:RNA hybrids generally form a heterogeneous mix of both A-form and B-form (74). Our secondary structural analysis of the nucleic acid hybrids using circular dichroism confirmed that the LNA:RNA hybrids formed A-form helical structure, whereas the DNA:RNA hybrid forms a mixture of A-form and B-form helical structures (Figure 23A). As another point of reference, I studied a DNA:DNA duplex with distinct B-form character as confirmed by CD. The increased sensitivity of BSI for detecting A-form hybrids, compared to the A-form and B-form mixed hybrid or the B-form duplex, indicates a structural basis for RI perturbation (Figure 23B). This was further validated through the measurements conducted on the TFE-induced A-form character of the DNA:DNA duplex, which resulted in increased BSI signal (Figure 24).

In addition to structural changes, the exchange of the water molecules that hydrate the soluble molecules upon binding is also thought to influence the RI, which would have direct implications for BSI signal generation. It has been predicted based on NMR structure measurements of LNA:RNA hybrids that the number of water molecules interacting with the

minor groove may be increased compared to DNA:RNA hybrids (81). The structure of an A-form hybrid may produce a larger BSI signal than B-form due to this exchange of waters of hydration from the solvent to the molecules, accounting in part for the improved BSI sensitivity when using the LNA probe. Continued efforts are aimed at identifying the role of waters of hydration on the shift of RI that occurs when an oligonucleotide probe hybridizes to an RNA target.

The results of these studies outline a set of optimal characteristics of nucleic acid probes for BSI detection of a viral RNA biomarker. It was determined that multiple nucleic acid probes, 22 nucleotides in length, designed to target regions distributed across the RNA target resulted in the greatest BSI signal. These studies also indicate that the folding of the RNA target as well as the formation of the secondary structure geometry also contribute substantially to BSI sensitivity for RNA detection. There is evidence that *mfold* software can be used to identify regions of unpaired nucleotides in RNA targets that are likely to produce high signal upon binding. Additional studies aimed at determining tertiary structure contributors to signal enhancement along with the secondary structure predictions of *mfold* could be useful for the rational design of oligonucleotide probes for BSI detection. Additionally, it was determined that the induction of altered helical geometry of nucleic acids upon probe binding significantly improves BSI signal. I found that this can be achieved using LNA probes or a high background concentration of TFE, which promote formation of A-form structure in nucleic acids. Future work will focus on strategies to further enhance BSI signal, which could pave the way for a clinically relevant BSI assay for the detection of viral RNA in patient samples.

Acknowledgements

The purchase of materials and reagents and funding for those that contributed to this project was supported by the Bill & Melinda Gates Foundation through the Grand Challenges in Global Health initiative in diagnostics, a Vanderbilt University Discovery Grant, and National Science Foundation Grant [CHE 0848788]. I thank the National Science Foundation Graduate Research Fellowship Program (DGE 0909667) for personal support during the time I worked on this project.

The work presented in this chapter could not have been completed without the efforts of several individuals. The development of BSI as an analytical technique is credited to Darryl Bornhop. The initial concept of using BSI to detect nucleic acids is credited to Darryl Bornhop and David Wright. Rick Haselton and David Wright contributed brilliant technical insights into the interpretation and significance of nucleic acid structure secondary structure alterations on BSI signal. Much of the data and presented in this chapter was collected by Ian Olmsted. Ian also contributed significantly to writing of the manuscript that is the basis for this chapter.

Chapter V

QUADRUPLEX PRIMING AMPLIFICATION FOR THE DETECTION OF mRNA FROM SURROGATE PATIENT SAMPLES

Abstract

Simple and rapid methods for detecting mRNA biomarkers from patient samples are valuable in settings with limited access to laboratory resources. In this chapter, we describe the development and evaluation of a self-contained assay to extract and quantify mRNA biomarkers from complex samples using a novel nucleic acid-based molecular sensor called quadruplex priming amplification (QPA) (25). QPA is a simple and robust isothermal nucleic acid amplification method that exploits the stability of the G-quadruplex nucleotide structure to drive spontaneous strand melting from a specific DNA template sequence. Quantification of mRNA was enabled by integrating QPA with a magnetic bead-based extraction method using an mRNA-QPA interface reagent. The assay was found to maintain >90% of the maximum signal over a 4 °C range of operational temperatures (64 - 68 °C). The overall efficiency of mRNA extraction and delivery into the QPA reaction from a surrogate patient sample was ~45%. QPA had a dynamic range spanning four orders of magnitude, with a limit of detection of ~20 pM template molecules using a highly controlled heating and optical system and a limit of detection of ~250 pM using a less optimal water bath and plate reader. These results demonstrate that this integrated approach has potential as a simple and effective mRNA biomarker extraction and detection assay for use in resource-limited settings. At the

end of this chapter, I outline the barriers and challenges that must be overcome to implement QPA as a readout in a complete diagnostic device.

Introduction

Many methods are used to extract and detect mRNA biomarkers found in patient samples for diagnosing pathogenic infections. These methods often involve multiple steps to perform and commonly require expensive laboratory equipment or trained technicians. For example, reverse transcriptase-polymerase chain reaction (RT-PCR) is commonly used to identify RNA disease biomarkers from patient samples but requires complex and time-consuming sample purification and preparation strategies that are inaccessible to individuals in settings with limited resources because of training, electricity, or financial constraints (13,14). Simple rapid diagnostic tests based on lateral flow sample processing and antibody binding are commonly used in limited resource settings, but despite being easy to use, they are not effective in many cases for two primary reasons: non-target molecules present in patient samples often interfere with detection, and target biomarkers are often present at low abundance (7,14,16,17). Therefore, better methods for purifying and detecting biomarkers of disease in patient samples are needed in settings with limited access to laboratory resources and trained personnel.

The four-stranded G-quadruplex nucleotide structure has been exploited as a platform for a variety of novel nucleic acid detection assays because of its unique stability and folding characteristics. The quadruplex structure is thermodynamically more stable than duplex DNA (28,82) and has been developed to detect short nucleic acid sequences, such as microRNAs, that are inaccessible by traditional PCR (83). In general, these assays are designed to promote the

formation of G-quadruplex structures by complementary base pairing with the target nucleic acids and use colorimetric or fluorescence means to monitor the formation of the quadruplex structures. Many groups have taken advantage of the peroxidase-like activity of the G-quadruplex/hemin complex to produce a colorimetric dye in the presence of a target nucleic acid (83-85). Some of these peroxidase-like amplification assays have been reported to achieve extremely low detection limits (86,87), yet outside of carefully controlled laboratory conditions, the assays are limited by the highly unstable peroxide reagents and the degradation of the exposed hemin complex (88). Other groups have monitored the formation of the G-quadruplex structures using quadruplex-specific intercalating dyes (89-91) or Förster resonance energy transfer (FRET) pairs (92). Some of these methods have been demonstrated to detect nucleic acids in the mid-pM range (91,92), yet only when performed in simple sample matrices (i.e., buffer) under optimal conditions or over the course of many hours.

Quadruplex priming amplification (QPA) is an isothermal amplification reaction that is also based on the thermodynamic stability of the G-quadruplex structure. QPA has been demonstrated to function as a robust molecular switch, producing fluorescence in the presence of template oligonucleotides with high sensitivity and specificity (28,29,93). A schematic of the reaction is shown in Figure 25A. The reaction functions much like polymerase chain reaction, but does not require costly and complex thermal cycling. The reaction begins when a 13-nucleotide QPA primer precursor to the 15-nucleotide G-quadruplex sequence anneals to a complementary template molecule. After annealing, a polymerase enzyme extends the 3' end of the QPA primer with the guanine nucleotides required to complete the G-quadruplex sequence. Because the stability of the G-quadruplex

structure is greater than that of the duplex DNA, thermodynamic factors drive the spontaneous self-dissociation of the duplex (28). Once the G-quadruplex forms, the template is released and is free to anneal to another primer and start the next cycle of amplification. The G-quadruplex products of the QPA reaction are detected using the incorporated fluorescent nucleotide, 6-methyl isoxanthopterin (6-MI) (depicted in Figure 25B), a guanosine analog used for studying nucleic acid structures (94). The 6-MI dye functions as a readout for the QPA assay as it fluoresces intensely when the oligonucleotide is folded into a G-quadruplex structure but is suppressed in the single- and double-stranded states. This occurs because 6-MI fluorescence is quenched when π - π stacked with surrounding nucleotides, whereas in the parallel G-quadruplex structure, 6-MI forms the chain-reversal

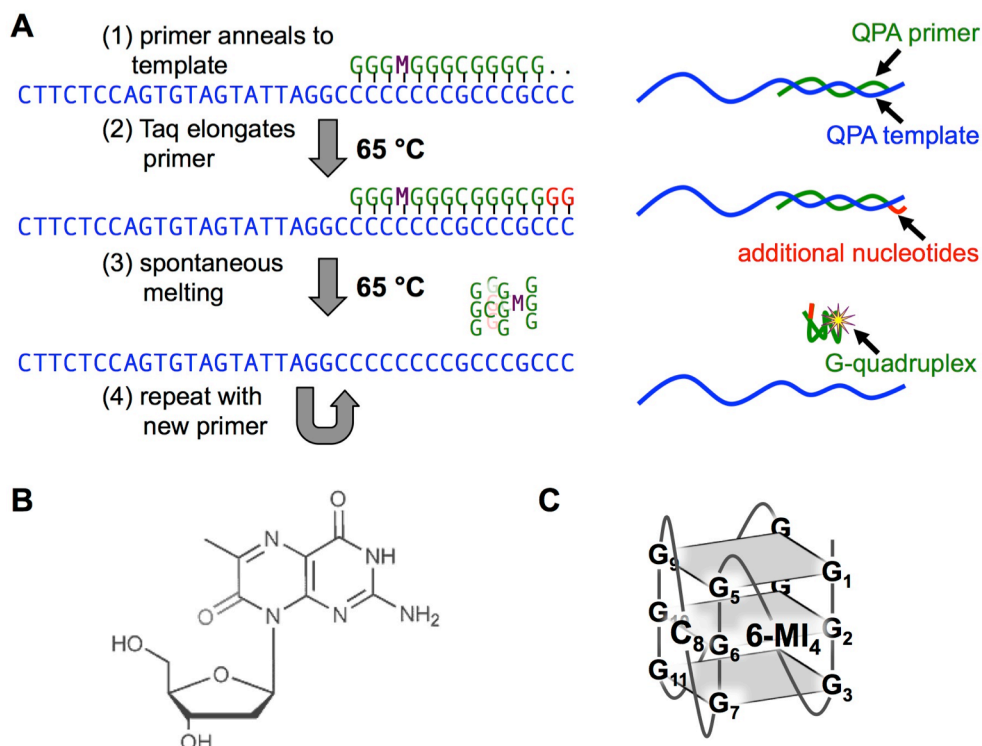


Figure 25. A) Schematic of the isothermal quadruplex priming amplification (QPA) method. The guanosine analog 6-methyl isoxanthopterin (6-MI) is denoted with the letter M. The QPA template sequence (blue) is abbreviated for simplicity. B) Chemical structure of the 6-MI dye used in QPA. C) Illustration of the parallel G-quadruplex product of QPA.

loop between guanine-quartets and protrudes into the solvent, unquenched by the surrounding nucleotides (Figure 25C) (29).

Although QPA has been found to be an effective nucleic acid amplification method, the challenge as it relates to biomarker detection is that QPA is limited to the amplification of a single unique template oligonucleotide sequence complementary to the G-quadruplex sequence and not biomarker target sequences. In these studies, I develop an mRNA-QPA interface reagent, which contains the 15-nucleotide template sequence linked to a 22-nucleotide probing sequence complementary to the mRNA biomarker. This interface reagent enables indirect QPA detection of mRNA biomarkers by associating mRNA biomarker targets with the templates.

The implementation of the interface reagent is facilitated using our previously described self-contained extraction format (7,16,17,27). This self-contained format for biomarker extraction has been used to process RNA, DNA, and protein biomarkers from complex samples to improve RT-PCR, PCR, and lateral flow detection, respectively (7,16,17). In this format, sample processing is carried out in small diameter tubing by pulling functional magnetic beads bound to target biomarkers through processing solutions that are separated by surface tension valves. Surface tension valves (i.e., air or oil separators) keep the solutions within the tubing stationary while permitting the transport of magnetic beads across the interface (27). The advantages of the self-contained format are that it facilitates complex sample processing steps with the use of simple magnetic bead manipulation using a permanent magnet, enables the assay to be performed without the use of pipettes or other laboratory equipment, and protects the assay contents from environmental contaminants.

I have integrated this self-contained format to enable the detection of mRNA from surrogate patient sample matrices by QPA. The complete assay functions by extracting mRNA biomarkers from a complex sample on the surface of a magnetic bead, binding the magnetic bead-captured mRNA biomarkers with QPA template sequences using an mRNA-QPA interface reagent, and delivering the bead/mRNA/interface reagent complex into a final QPA reaction solution for detection (Figure 26). The interface reagent determines specificity of the assay; if the specific mRNA biomarkers are present, the interface reagents are delivered to the QPA reaction for amplification. In this chapter, I describe the development and evaluation of the three critical components that make this integrated assay possible: i) self-contained extraction of mRNA using magnetic beads, ii) conversion of mRNA biomarkers to QPA templates using the mRNA-QPA interface reagent, and iii) optimization of the sensitivity and dynamic range of QPA.

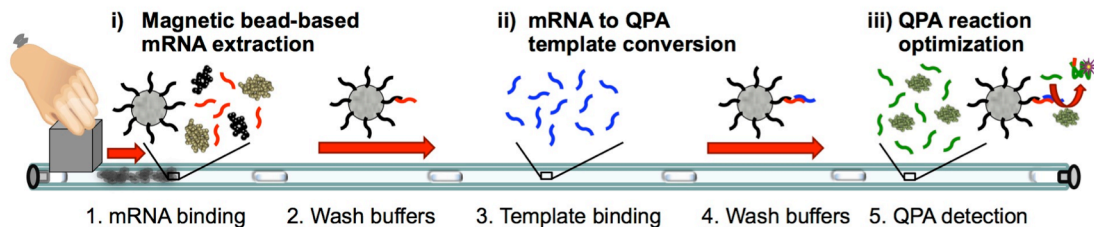


Figure 26. Schematic representation of the integrated self-contained mRNA extraction and QPA amplification assay. The three critical components for integration (i – iii) and the assay processing steps (1 – 5) are identified.

Experimental Section

Oligonucleotide synthesis

The oligonucleotides used in these studies include QPA primers, mRNA-QPA interface reagents, and a synthetic mRNA biomarker (Table 3). The QPA primer oligonucleotides containing the 6-MI dye were synthesized at a 200 nmole scale by Fidelity Systems, Inc. and purified by desalting. The mRNA-QPA interface reagents and the synthetic mRNA biomarker oligonucleotide were synthesized by Integrated DNA Technologies at 250 nmole scale and purified using high performance liquid chromatography. Although virtually any mRNA sequence could be used as a demonstration of feasibility, the sequence used in these studies is based on a 38 nucleotide sequence from the respiratory syncytial virus nucleocapsid gene mRNA. The synthetic 22-nucleotide adenine tail was added to this sequence to enable extraction using oligo-dT beads. Upon arrival, the oligonucleotides were

Table 3. Oligonucleotide sequences used in the QPA studies.

Oligonucleotide name	Function	Length (nt)	Sequence (5' – 3')
G4BK_primer_6MI@4	QPA primer (G-quadruplex precursor)	13	GGG(6-MI)GGGCGGGCG*
G4BK_+primer_6MI@4	Complete G-quadruplex (positive control)	15	GGG(6-MI)GGGCGGGCGGG*
G4BK_temp_RSV22	mRNA-QPA interface reagent (unlabeled)	37	CCCGCCCGCCCCCCTTCTCCAGTGTAGTAT TAGGC
G4BK_temp_RSV22 +5 w/Cy5	Interface reagent with spacer (Cy5 labeled)	42	(Cy5)CCCGCCCGCCCCCGGAGTCTTCTCCA GTGTAGTATTAGGC
RSVN_939-978_mRNA w/HEX	Synthetic mRNA biomarker (HEX labeled)	60	(HEX)GCCUAAUACUACACUGGAGAAGUGAGG AAAUUGAGUCAAAAAAAAAAAAAAAAAAAAAA

*6-MI (6-methyl isoxanthopterin) is a fluorescent guanosine analog

resuspended to a concentration of ~100 mM in molecular grade water (cat. no. BP2819-4, Fisher Scientific) and stored at -20 °C until use.

Circular dichroism of QPA oligonucleotides

An Aviv circular dichroism (CD) spectrometer (mod. no. 215, Aviv Biomedical, Inc.) was used to collect CD spectra of the single-stranded and quadruplex DNA molecules. Oligonucleotides were prepared at a 100 μ M base concentration in QPA buffer (10 mM Tris HCl, pH 8.7, 2 mM MgCl₂, 25 mM KCl, 25 mM CsCl). Each sample was heated in 1 mL tubes to 90 °C for 5 minutes and cooled slowly over the course of 1 hour to room temperature by controlling the heat block temperature. The samples were analyzed using a 1 cm path length CD cell. The spectra were collected at 25 °C from 320 nm to 200 nm using a 1 nm step, a 1.0 nm bandwidth, and a 2 second averaging time. At least three spectra from each sample collected, averaged, and smoothed using the using CD-215 software version 2.90 provided by the manufacturer. The spectra were normalized by subtracting the CD spectrum generated from a blank sample (QPA buffer only) collected under the same conditions.

6-methyl isoxanthopterin (6-MI) fluorescence measurements

Solutions of QPA primer or G-quadruplex oligonucleotides were prepared in triplicate at 10 nM, 50 nM, 100 nM, 500 nM, and 1 μ M concentrations. Each solution was heated to 90 °C for 5 min and cooled over the course of 1 hour to room temperature. One hundred microliters of each solution was added to a well of a black Costar round bottom 96-well plate. Fluorescence measurements were collected in triplicate using a BioTek Synergy

H4 Hybrid 96-well plate reader using an excitation wavelength of 340 nm and a detection wavelength of 430 nm.

Optimizing the quadruplex priming amplification reaction

Unless otherwise noted, QPA reactions were carried out in a 100 μ L volume containing QPA buffer (10 mM Tris HCl, pH 8.7, 2 mM MgCl₂, 25 mM KCl, 25 mM CsCl), 2.5 μ M QPA primer (G4BK_primer_6MI@4), 0.15 units/ μ L AmpliTaq DNA Polymerase (cat. no. P15533, Roche), 0.5 mM dGTP (cat. no. R0161, Thermo Scientific), and 10% w/v Trehalose (cat. no. 90210-50G, Sigma Aldrich). Each reaction solution was split into three thin-walled PCR tubes (cat. no. 981005, Qiagen), with 25 μ L in each tube. The reaction ran at 65 °C in the Rotor-Gene Q 6plex thermal cycler (cat. no. 9001720, Qiagen) and real-time fluorescence measurements were collected every three minutes using an excitation wavelength of 365 nm and a detection wavelength of 460 nm for detecting the 6-methyl isoxanthopterin dye in the G-quadruplex product. QPA reactions with 0 nM, 0.05 nM, 0.1 nM, 0.5 nM, and 1 nM mRNA-QPA interface reagent (QPA template) concentrations were run in triplicate and in parallel and were used as a standard curve. The lower limit of detection was calculated using the following formula: $LOD = 3\sigma / m$, where σ is the average of three standard deviation measurements of the QPA signal from each interface reagent concentration and m is the slope as calculated by the best-fit trendline of the linear range of the standard curve.

Preparation of the self-contained processor

Prior to processing a sample, the solutions of the self-contained processor were preloaded by serially injecting the solutions in reverse order through one end of 1.6 mm ID Tygon R-3603 tubing (Saint-Gobain). Unless otherwise noted, the processing solutions and volumes used in the self-contained processor were adapted from the Life Technologies Dynabeads Oligo (dT)₂₅ (cat. no. 61005) product manual. The final processing solution was loaded into the tubing first by injecting 100 μ L of 10 mM Tris-HCl buffer (pH 8.0) for studies to determine biomarker and mRNA-QPA interface reagent yield or 100 μ L of QPA reaction solution for studies on QPA detection. To separate this solution from the next one, a surface tension valve, or air bubble spacer, was formed by slightly tilting the tubing until the solution moved \sim 1 cm away from the end of the tubing. This procedure was followed after injecting each of the following solutions. Three post-template wash solutions were then loaded by injecting 100 μ L of wash buffer B (10 mM Tris-HCl, pH 8.0 150 mM LiCl, 1 mM EDTA) into the tube three times. One hundred microliters of template binding solution was then added by injecting 100 μ L of wash buffer B containing 75 nM mRNA-QPA interface reagent (G4BK_temp_RSV22+5 w/Cy5), unless otherwise noted. Another series of wash chambers were then added: 250 μ L of wash buffer B, and two solutions of wash buffer A (10 mM Tris-HCl, pH 8.0, 150 mM LiCl, 1 mM EDTA, 0.1% LiDS). The end of the tubing opposite of the loading end was then sealed using a small plug. At this point the preloaded processor was ready for sample loading and processing.

Procedure for self-contained processing of mRNA

The procedure for processing the sample included preparing and injecting the binding solution into the processor tubing followed by pulling the magnetic beads through the processing solutions. The binding solution was prepared with 1 mg Dynabeads Oligo (dT)₂₅ (cat. no. 61005, Life Technologies) resuspended in 225 µL binding/lysis buffer (100 mM Tris-HCl, pH 8.0, 500 mM LiCl, 10 mM EDTA, 1% LiDS). The sample matrices that were used include 100 mM Tris-HCl (pH 8.0), ~2.5 ng/µL yeast total RNA extract (cat. no. AM7118, Life Technologies), or HEp-2 cell lysate containing 10⁵ cells/mL (preparation of this matrix is described in ref. (7)), each spiked with 30 pmol synthetic mRNA (RSVN_939-978_mRNA w/HEX). For each sample, 25 µL of the matrix was added to the binding solution and mixed for 10 minutes on a laboratory rotator. The plug was then removed from the processor tubing, the 250 µL binding solution was added to tubing, and the plug was replaced. The magnetic beads were then gathered within the binding solution using a 2.54 cm neodymium cube magnet (SKU no. M1CU, Apex Magnets). The beads were then carefully pulled through the air separator and into the first wash solution. The beads were dispersed within the wash solution for ~5 seconds, gathered, and then pulled into the subsequent solution. These steps were repeated for each of the wash buffer solutions. Once the beads were pulled into the template binding chamber, they were dispersed throughout the chamber, and the processing tube was placed in the dark for 30 minutes, unless otherwise noted. Afterwards, the beads were pulled through the three 100 µL wash buffer B chambers as described above. Finally, the beads were pulled into the final solution for oligonucleotide content analysis or for quantitation by QPA.

For content analysis, the elution solution containing the beads was placed on a heating block for 10 minutes at 85 °C, the supernatant was removed from the beads, and the 40 μ L of the supernatant was added to a well of a black Costar round bottom 96-well plate. Fluorescence measurements were collected in triplicate using a BioTek Synergy H4 Hybrid 96-well plate reader with an excitation wavelength of 535 nm and a detection wavelength of 565 nm for the mRNA biomarker (RSVN_939-978 mRNA w/HEX) and with an excitation wavelength of 646 nm and a detection wavelength of 670 nm for the mRNA-QPA interface reagent (G4BK_temp_RSV22+5 w/Cy5), and measurements were compared to standard curves. For quantitation by QPA, the Tygon tube was placed in a water bath for 5 minutes at 85 °C and 45 minutes at 65 °C and endpoint fluorescence measurements were collected in triplicate using an excitation wavelength of 365 nm and a detection wavelength of 460 nm for detecting the 6-methyl isoxanthopterin dye in the G-quadruplex product. QPA reactions with 0 nM, 0.05 nM, 0.1 nM, 0.5 nM, and 1 nM mRNA-QPA interface reagent concentrations were run in parallel and used as a standard curve.

The overall effective delivery yield of mRNA-QPA interface reagents in the final solution was calculated as a percentage relative to the concentration of spiked mRNA biomarkers present in the initial binding solution, and is based on the standard curve of interface reagents. This measurement reflects the efficiency of mRNA extraction and subsequent binding of the interface reagent.

Results And Discussion

6-methyl isoxanthopterin-labeled G-quadruplex as a molecular sensor

Our first objective was to establish the 6-MI-labeled G-quadruplex sequence as an effective molecular sensor under the conditions of our assay. QPA signal depends on a significant difference in fluorescence intensity between the single-stranded state of the 6-MI-labeled QPA primer (G4BK_primer_6MI@4) and the G-quadruplex product (G4BK_+primer_6MI@4). I compared the relative fluorescence intensity of increasing concentrations of the two oligonucleotides. The results show that the G-quadruplex product had a ~25-fold fluorescence enhancement over the QPA primer, which established it as an effective molecular sensor (Figure 27A).

To validate that this fluorescence enhancement correlated with a G-quadruplex structure, circular dichroism was performed on the oligonucleotide samples. The single-stranded mRNA-QPA interface reagent oligonucleotide was also analyzed as a control. The circular dichroism spectrum of the G-quadruplex product had a minimum at 241 nm, strong maxima at 210 and 262 nm, and a slight maximum at 300 nm (Figure 27B). These results are characteristic of a parallel quadruplex nucleotide structure (29,76). The single-stranded QPA primer, on the other hand, had a spectrum consistent with oligonucleotides with high GC content, with a maximum at 264 nm and a minimum at 238 nm. The single-stranded interface reagent had a spectrum with a maximum at 276 and a minimum at 243 nm, characteristic of single-stranded oligonucleotides.

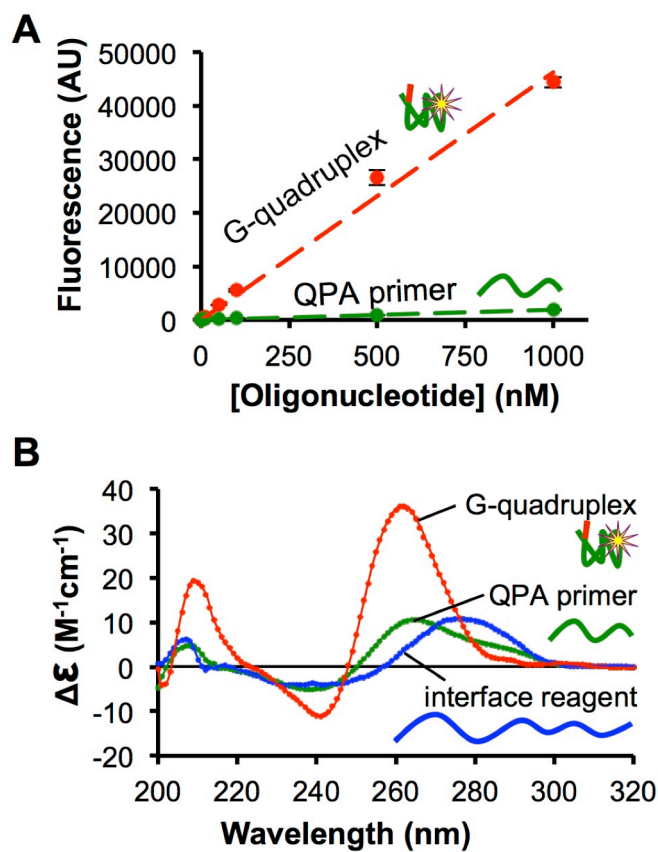


Figure 27. The 6-MI-labeled G-quadruplex is an effective molecular sensor. A) 6-MI has a ~ 25 -fold fluorescence enhancement in the G-quadruplex product compared to the single-stranded QPA primer (mean $\pm \sigma$, $n = 3$). B) Circular dichroism (CD) spectra of the components of the QPA reaction. The CD spectrum of the elongated QPA primer is consistent with a parallel G-quadruplex structure (red), while the spectra of the QPA primer precursor is consistent with single-stranded DNA.

Together, these data indicate that 6-MI is effectively quenched in the single-stranded state and that the fluorescence is enhanced ~ 25 -fold when the two nucleotides are added to complete the sequence necessary to form the G-quadruplex. This signal-to-noise ratio under these ideal conditions is exceptional compared to the 3- to 10-fold ratios reported for other G-quadruplex-based amplification assays (83,86,89-92). These results validate 6-MI-labeled G-quadruplex as a potential molecular sensor.

Optimizing and evaluating QPA for sensitivity

The next step was to optimize and evaluate the sensitivity and dynamic range of QPA (integration component iii from Figure 26). Because QPA is a linear amplification method, the most effective measure of efficiency is the slope of the response curve (i.e., the change in fluorescence signal per unit time). In these studies, a variety of conditions were tested using Qiagen's Rotor-Gene Q real-time PCR instrument to monitor the change in fluorescence in real-time. The optimal temperature was determined by running the QPA reaction at six different temperatures from 61 °C to 71 °C using a set of baseline reaction conditions (QPA buffer, 2.5 µM QPA primer, 0.05 units/µL Taq polymerase, 0.5 mM dGTP, 0% trehalose, 1 nM mRNA-QPA interface reagent). While the optimal reaction temperature was determined to be 65 - 66 °C, QPA was found to maintain >90% of the maximum signal from approximately 64 to 68 °C. (Figure 28A). Using the baseline reaction conditions and a 65 °C reaction temperature, a range of primer concentrations from 0 to 10 µM were then tested. Optimal signal was produced using a 5 µM primer concentration (Figure 28B). At 5 µM concentration, however, the background signal from the QPA primers disproportionately increased, which increased the signal-to-noise ratio and decreased the dynamic range. Therefore, a 2.5 µM primer concentration was determined as optimal. Next, a range of Taq polymerase concentrations from 0 to 0.5 units/µL was tested. Taq polymerase concentration had a significant impact on the signal produced, resulting in a signal ~3-fold greater at 0.25 units/µL compared to the 0.05 units/µL baseline concentration (Figure 28C). Because of the cost of the commercial Taq polymerase, 0.15 units/µL was determined to be the most economical concentration as it falls within ~20% of the optimal signal yet uses 40% less enzyme. The effect of adding trehalose sugar was also evaluated. Trehalose sugar has

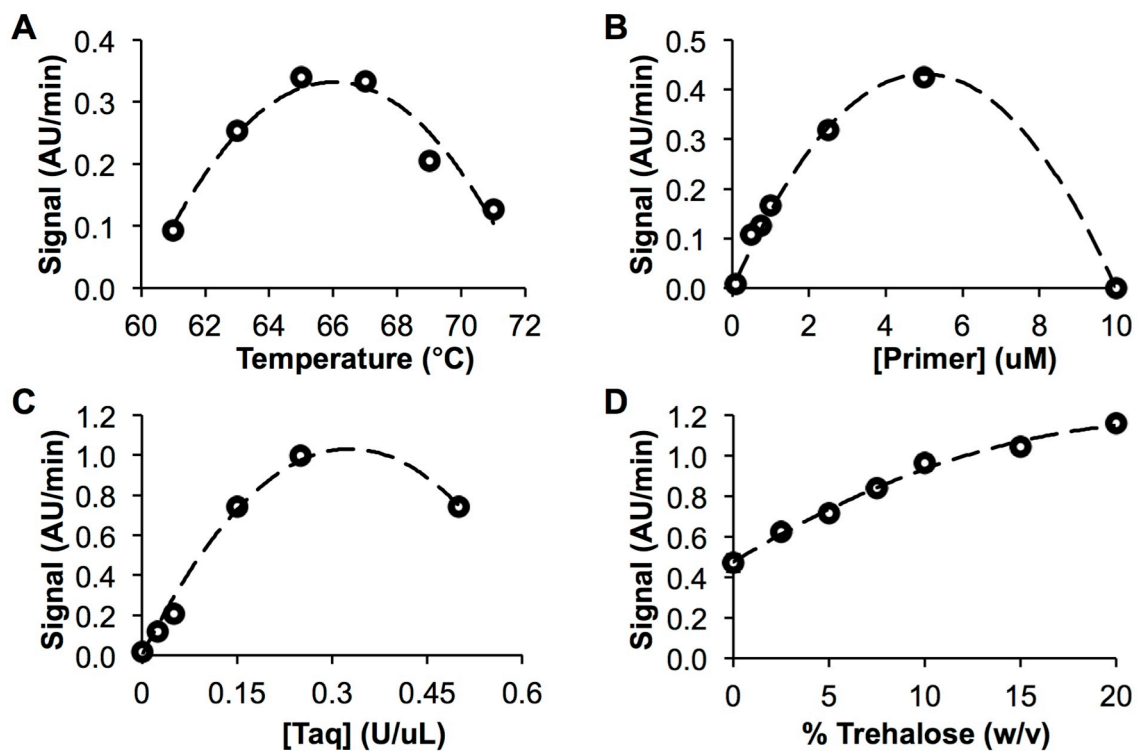


Figure 28. The optimal QPA signal was determined by testing a range of temperatures (A), QPA primer concentrations (B), Taq polymerase concentrations (C), and trehalose concentrations (D) (mean \pm σ , n = 3).

historically been used to stabilize enzymatic reagents for lyophilization and long-term storage (95,96). Furthermore, one group reported that the addition of trehalose sugar to Taq polymerase chain reaction increases the efficiency of amplification of GC-rich templates by reducing the DNA melt temperature and thermally stabilizing the Taq polymerase enzyme (97). Consistent with these findings, the signal generated from the QPA reaction, which amplifies templates that are composed exclusively of GC nucleotides, increased linearly from 0% to 10% trehalose, effectively doubling the signal of the reaction (Figure 28D). Concentrations greater than 10% trehalose had less effect on signal; therefore, a 10% trehalose concentration was determined to be optimal. Overall, a 3- to 4-fold increase in signal was achieved over the course of these optimization studies.

Using the optimized reaction conditions, the limit of detection and dynamic range of the QPA reaction was determined. A series of mRNA-QPA interface reagent concentrations were added to the QPA reaction, and the Rotor-Gene Q instrument monitored the change in fluorescence over a period of 45 minutes at 65 °C. The data that was collected produced a series of linear response curves with slopes proportional to the concentration of interface reagents present in the reaction (Figure 29A). The slopes of these response curves were plotted against their respective interface reagent concentrations to generate a standard curve for quantification (Figure 29B). Based on these data obtained under optimal conditions, the

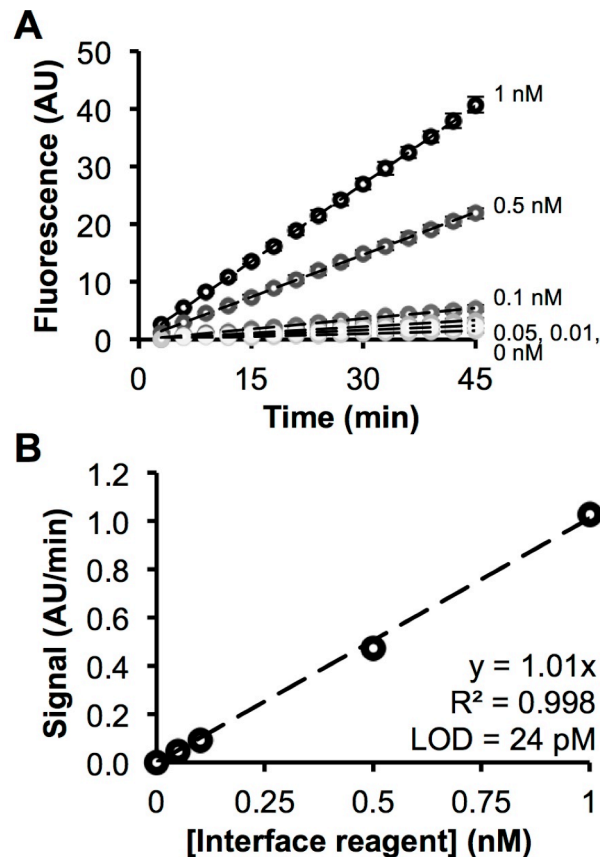


Figure 29. Isothermal QPA is a linear and quantitative amplification method as measured in real-time using a Rotor-Gene Q PCR instrument. A) QPA signal results in linear increase of fluorescence for each interface reagent concentration during the course of the reaction (mean \pm σ , n = 3). B) The increase in fluorescence over time is directly proportional to the concentration of interface reagents present in the reaction. This linear response results in a limit of detection of 24 pM interface reagents (mean \pm σ , n = 3).

limit of detection was determined to be 24 pM mRNA-QPA interface reagents. Using a greater range of interface reagent concentrations, it was determined that the dynamic range spans nearly 4 orders of magnitude (~20 pM to ~100 nM) (Figure 30). These data demonstrate that the QPA reaction effectively quantifies interface reagents at low sensitivity and across a relatively wide range of concentrations.

mRNA-QPA interface reagent enables mRNA detection by QPA

To be useful as a readout for a diagnostic test, QPA templates must be associated with an mRNA biomarker characteristic of a particular disease. I developed an mRNA-QPA interface reagent for associating mRNA biomarkers with QPA templates to enable QPA detection of these mRNA targets (research focus ii from Figure 26). This mRNA-QPA interface reagent is key for introducing sequence specificity in the presence of bulk mRNA on the surface of the oligo-dT functionalized beads; only if the specific mRNA biomarker is present will the template sequence of the mRNA-QPA interface reagent be delivered to the QPA reaction.

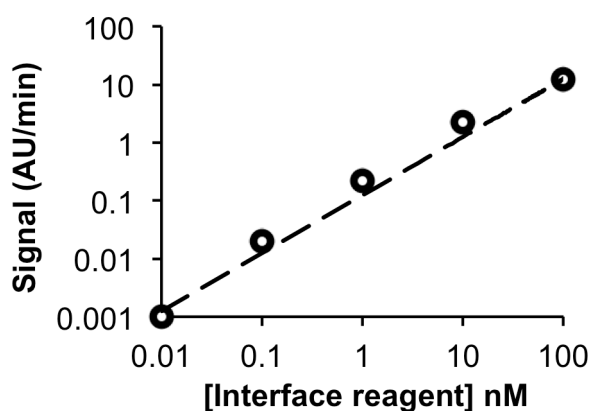


Figure 30. The increase in fluorescence over time is directly proportional to the concentration of interface reagents present in the QPA reaction. This linear response has a dynamic range that spans nearly 4 orders of magnitude. Note: log scale on x- and y- axes (mean \pm s. n = 3).

The interface reagent contains a 22-nucleotide probing region complementary to an mRNA biomarker, a 5-nucleotide spacer, and the 15-nucleotide template sequence for QPA. The complete integrated assay involves isolating mRNA biomarkers from complex samples using oligo-dT functionalized magnetic particles, and then probing for the mRNA biomarkers with the mRNA-QPA interface reagent. The QPA reaction is then used to indirectly quantify the mRNA by amplifying from the template portion of the mRNA-QPA interface reagent. A schematic representation of the physical layout of the assay is depicted in Figure 26. Each step of the assay takes place inside of 1.6 mm ID Tygon tubing by simply pulling the magnetic particles through processing solutions separated by surface tension valves, until the last step, where QPA spontaneously initiates amplification upon the delivery of the interface reagents.

To determine the efficiency of the mRNA extraction assay in the presence of background biomolecules (integration component i from Figure 26), mRNA biomarkers were extracted from solutions containing Tris-HCl buffer (pH 8.0), ~2.5 ng/ μ L non-target yeast total RNA (~100-fold more RNA than the mRNA biomarker), or a surrogate nasal wash sample containing HEp-2 cell lysate. Each of the samples was spiked with 30 pmol mRNA biomarker. Although virtually any mRNA sequence could be used as a demonstration of feasibility, the sequence used in these studies is based on a 38 nucleotide sequence from the respiratory syncytial virus (RSV) nucleocapsid gene mRNA to which a 22-nucleotide poly-A tail was added. Extraction of the mRNA was then carried out by pulling the beads through the wash buffers and into a Tris-HCl buffer (pH 8.0) elution solution. The concentration of the labeled mRNA biomarkers in the final solution was determined using fluorescence spectroscopy. Extraction yields from the sample matrices was ~35% of the starting amount of

mRNA biomarker, and there was no statistical difference among the three sample types (Figure 31A). Notably, the biomarkers are concentrated 2.5-fold through the extraction process (the initial binding solution is 250 μ L and the final elution solution is 100 μ L); therefore, the effective biomarker enrichment is nearly 90%. These results indicate that the

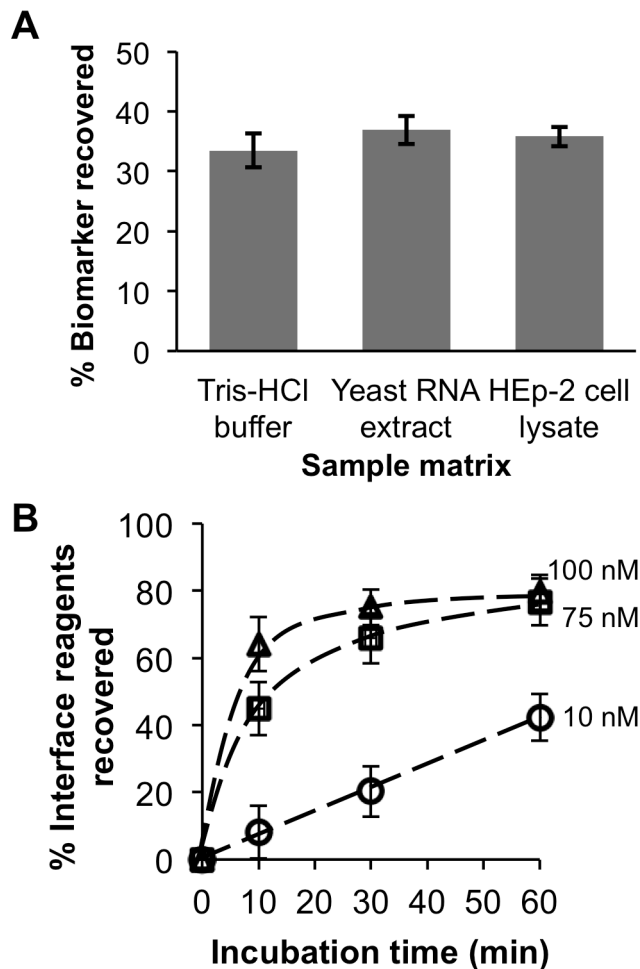


Figure 31. The self-contained format is effective for extracting mRNA biomarkers from complex samples and associating biomarkers with mRNA-QPA interface reagents. (A) Extraction of the synthetic mRNA biomarker sequence is effective in the self-contained format using oligo dT-functionalized magnetic beads. mRNA was extracted from solutions of increasing complexity: Tris-HCl buffer at pH 8.0, yeast RNA extract at 100-fold the amount of target mRNA, or Hep-2 cell lysate at 105 cells/mL (mean \pm σ , n = 3). (B) The number of interface reagents recovered (i.e., the number of interface reagents associated with mRNA biomarkers) increases with incubation time and interface reagent concentration in the template binding solution (circles = 10 nM, squares = 75 nM, and triangles = 100 nM) (mean \pm σ , n = 3).

mRNA extraction method is robust and compatible with sample matrices of increasing complexity.

The efficiency of mRNA-QPA interface reagent binding to mRNA biomarker was evaluated next (integration component ii from Figure 26) by testing 10 to 100 nM interface reagent concentrations and 10 to 60 minute incubation times in the template binding solution. The amount of interface reagents eluted into Tris-HCl buffer was measured using fluorescence spectroscopy and expressed relative to the amount of biomarker recovered in the same solution. The data show that the amount of interface reagent recovered increased with template concentration and with incubation time, resulting in a maximum interface reagent yield of nearly 80% of the amount of recovered mRNA biomarkers using a 100 nM interface reagent concentration and a 60 minute incubation time (Figure 31B). An interface reagent concentration of 75 nM was chosen, however, to limit the amount of interface reagent that would be nonspecifically pulled through with solution carryover, and an incubation time of 30 minutes was chosen to decrease the overall assay time. Under these conditions, the mRNA-QPA interface reagent yield was 66% of the amount of the recovered mRNA biomarkers.

These data demonstrate that this self-contained assay based on oligo-dT functionalized magnetic beads and surface tension valves effectively associates mRNA-QPA interface reagents with mRNA biomarkers preparatory to running isothermal QPA. The overall effective delivery of interface reagents to the final solution, relative to the concentration of mRNA biomarkers present in the initial binding solution, is ~60%. Although this effective yield is sufficient for a demonstration of feasibility, there may be instances where it may need to be increased. As demonstrated in previous biomarker extraction and concentration

studies (17), by simply decreasing the elution solution volume, the final interface reagent concentration can be increased.

Self-contained mRNA extraction and detection

To determine the efficacy of QPA within the self-contained tube format, QPA performance was evaluated at 30, 45, 60, 75, and 90 minute time points after incubating the tubes at 65 °C in a circulating water bath. In this format, real-time monitoring of the QPA reaction was not feasible, so endpoint fluorescence measurements were collected after the tubes were pulled from the water bath. The data show that limits of detection between ~300 and ~250 pM mRNA-QPA interface reagents were achieved when incubated in the tube for 45, 60, and 75 minutes (Figure 32A, solid squares). At the 30 and 90 minute time points, the limits of detection of the in-tube QPA assay were worse, at ~1 nM. These data demonstrate that 30 minutes is not long enough to get consistent signal and that at 90 minutes signal begins to plateau. A 45-minute incubation time was used for subsequent assays, as it was the earliest time point that resulted in a reasonable limit of detection (300 nM). These limits of detection are greater than one order of magnitude worse than the QPA reaction monitored in real-time using the Rotor-Gene Q PCR instrument (see Figure 29B). To determine if this was an effect of the less precise heating method or the endpoint measurement method, endpoint measurements of the QPA reaction were also collected using the Rotor-Gene Q instrument. Under the precise thermal control of the Rotor-Gene Q instrument, the limit of detection at 30 minutes was 1.4 nM mRNA-QPA interface reagents and decreased steadily with increasing incubation times, approaching a lower limit of ~400 pM mRNA-QPA interface reagents at 90 minutes (Figure 32A, open circles). These data demonstrate that the QPA

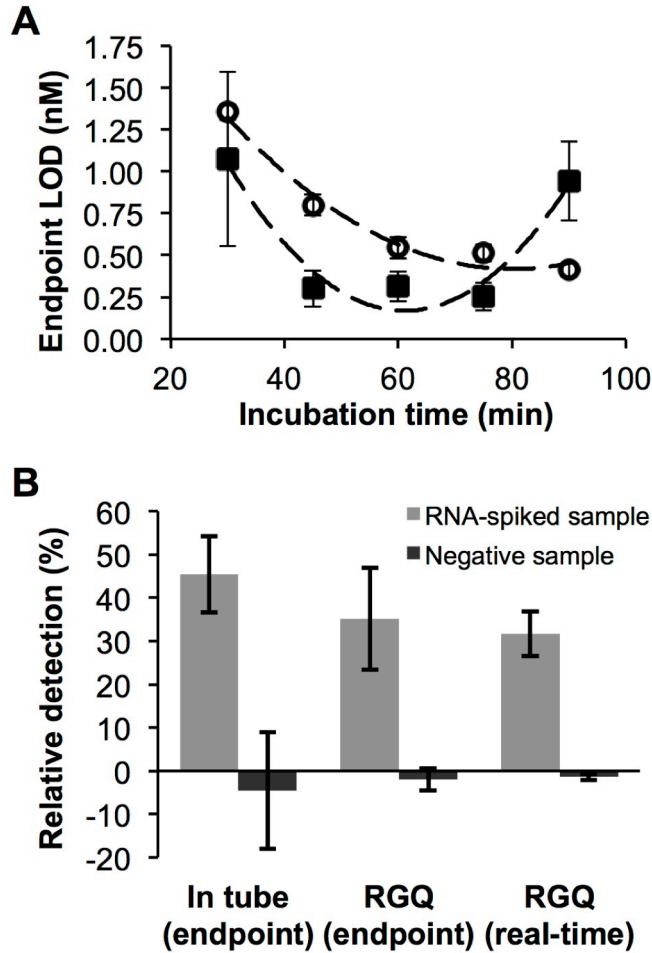


Figure 32. Isothermal QPA performs well when heated within the self-contained format in a water bath. A) The limits of detection based on endpoint fluorescence measurements at a range of incubation time points of the in-tube QPA reaction heated by water bath (solid squares) compared to QPA reaction heated in the Rotor-Gene Q (open circles) (mean \pm σ , n = 3). B) Detection of the synthetic mRNA biomarker from RNA-spiked (gray bars) and unspiked (black bars) surrogate nasal wash samples after self-contained extraction and QPA template binding. Three QPA reaction conditions are compared after a 45-minute incubation: i) Water bath heated within a tube, endpoint measured (left bars); ii) Rotor-Gene Q heated, endpoint measured (middle bars); and iii) Rotor-Gene Q heated, measured in real-time (right bars). QPA signal is expressed as a percentage of the total possible signal given a starting mRNA concentration of 1.2 nM (mean \pm σ , n = 3).

reaction performs well while being heated in a water bath within the self-contained format, achieving limits of detection on par with the more precise, thermally controlled Rotor-Gene Q instrument. Because of these observations, I hypothesize that real-time monitoring of the

in-tube QPA reaction will achieve the limits of detection of the real-time Rotor-Gene Q instrument. Current efforts are focused on developing an instrument format for heating and reading fluorescence of the QPA reaction performed within the self-contained format.

The performance of the integrated self-contained mRNA extraction and QPA detection assay was evaluated next. The assay was performed using surrogate patient samples positive for the synthetic mRNA biomarker (30 pmol mRNA spiked into HEP-2 lysates) and negative for the mRNA biomarker (unspiked). After loading the sample containing the magnetic beads, the entire assay was performed within the assay tube, including mRNA extraction, mRNA-QPA interface reagent binding, and QPA amplification. The QPA reaction solution was removed after a 45-minute incubation time and the contents were endpoint detected using a benchtop plate reader. This method resulted in the detection of $\sim 45 \pm 8.9\%$ of mRNA-QPA interface reagents relative to the mRNA content in the RNA-spiked sample and $-4.5 \pm 13\%$ in the negative sample (Figure 32B, left gray bar and left black bar, respectively). For comparison, the same samples were tested using the Rotor-Gene Q instrument for the QPA incubation and detection step, while the mRNA extraction and template binding steps remained in the self-contained format. The results from the Rotor-Gene Q instrument was comparable to the in-tube method, detecting $35 \pm 12\%$ mRNA-QPA interface reagents relative to the mRNA content in the RNA-spiked sample and $-2.0 \pm 2.5\%$ in the negative sample when measured at the 45 minute endpoint. Using real-time monitoring of QPA outside of the tubing, the quantification of the mRNA-QPA interface reagent was $32 \pm 5.1\%$ relative to the mRNA content in the RNA-spiked sample and $-1.5 \pm 0.7\%$ in the negative samples (Figure 32B). These data show that monitoring the QPA reaction in real-time

produces much more consistent results, while endpoint measurements of QPA result in a substantial amount of error.

These data demonstrate that isothermal QPA performs well when heated in a simple water bath and detected using a plate reader, achieving a limit of detection of ~250 pM mRNA-QPA interface reagents bound to mRNA. Furthermore, I found the complete self-contained mRNA extraction and QPA detection assay to be specific, detecting between ~35 and ~45% of the potential interface reagents relative to the initial concentration of synthetic mRNA biomarkers in the biomarker-spiked surrogate nasal wash samples, while detecting virtually no signal in the negative control samples, despite containing a high background of non-target mRNA molecules from the HEp-2 cell lysates. Based on a 45% relative detection of mRNA biomarkers, the effective limit of detection of the complete integrated assay is ~560 pM mRNA biomarkers from a surrogate patient sample. These data also reveal that real-time monitoring of the change in fluorescence over the course of the reaction (i.e., the slope fluorescence response curve) produces more consistent results than endpoint analysis of the samples (compare the error in Figure 29B to Figure 32A). This is likely because variation in the baseline or starting fluorescence of individual samples does not affect the slope of the fluorescence response curve, yet influences values of the endpoint analysis. Therefore, methods to monitor real-time fluorescence of the QPA reaction are necessary to achieve the optimal sensitivity and specificity in the self-contained mRNA extraction and QPA detection assay.

Conclusions

In this chapter, I described the integration of self-contained mRNA biomarker extraction and isothermal detection based on QPA. The simple assay effectively isolates mRNA biomarkers from complex samples, binds the mRNA biomarkers with mRNA-QPA interface reagents, and deposits them into a final solution for isothermal QPA detection. Our results indicate that this system has a number of advantages for use as an mRNA biomarker detection assay. First, the assay is able to detect relatively short RNA molecules, which is not possible using traditional RT-PCR. The biomarker target I tested is 60 nucleotides long; however, it is theoretically reasonable that targets as short as 35 nucleotides could be detected using this assay while still maintaining reasonable specificity (i.e., 15 nucleotides complementary to the capture sequence on the bead with 15 nucleotides complementary to the mRNA-QPA interface reagent, plus 5 nucleotides in between to prevent steric constraints). Second, the QPA assay is simple and robust. The molecular mechanism does not require a complex series of interactions and events to function, but is carried out at a single temperature with a single primer and polymerase enzyme. Also, the reaction is tolerant of ± 2 °C change in operational temperature while maintaining reaction efficiency within 90% of the optimal efficiency. Another advantage of the QPA assay is that it is quantitative over four orders of magnitude and has a lower limit of detection of ~ 250 pM using an endpoint analysis or ~ 20 pM using real-time analysis. Furthermore, the complete mRNA extraction and detection assay is self-contained and requires relatively few steps for the end user to complete. The tubing can be preloaded with the assay reagents, so that performing the assay simply consists of injecting the patient sample into the tube, pulling the magnetic beads through the assay solutions, incubating the tube in a water bath, and reading the fluorescence

against a standard curve. The total time duration from sample-in to answer-out is ~90 minutes. These advantages may also benefit others that are developing simple detection methods for amplifying targets from complex samples.

The integrated mRNA extraction and amplification assay is a practical platform for the development of a diagnostic device suitable for settings that lack laboratory resources and trained personnel. The assay format is particularly suitable for automated sample processing, because of the flexibility of the physical tube format and simplicity of the magnetic bead transport. The development of an automated device for reducing the number of steps that are completed by the end user is the focus of our current efforts. Furthermore, because many mRNA biomarkers of disease are found in patient samples at lower concentrations than the mid-pM range, the sensitivity of the assay must be improved to be deployed as a diagnostic device. To enhance the sensitivity, an exponential form of the QPA reaction is currently under investigation and has shown promise of improving the limit of detection of the assay by several orders of magnitude. The ability to test a patient sample for multiple biomarkers at once would also be a valuable component of a diagnostic device in limited resource settings. Because QPA detects mRNA-QPA interface reagents associated with the mRNA biomarkers, as opposed to the mRNA biomarkers themselves, QPA has the potential to be used as a standardized amplification interface, where the QPA reaction is used as a singular readout for a variety of biomarkers. This could be done by tagging molecular recognition elements (i.e., antibody, aptamer, etc.) with the QPA template sequence for detecting proteins, cells, and other classes of biomarkers in a manner analogous to the mRNA extraction, only using the respective magnetic capture beads instead of the oligo-dT beads. I expect that the culmination of these focused efforts, in addition to the data presented in this chapter, will

result in the development of a simple and rapid diagnostic device for a variety of diseases with the potential to be implemented in limited resource settings.

Acknowledgments

The purchase of materials and reagents and funding for those that contributed to this project was supported by the Bill & Melinda Gates Foundation through the Grand Challenges in Global Health initiative in diagnostics, a Vanderbilt University Discovery Grant, and National Science Foundation Grant [CHE 0848788]. I thank the National Science Foundation Graduate Research Fellowship Program (DGE 0909667) for personal support during the time I worked on this project. I also recognize the National Science Foundation REU in Chemical Biology at Vanderbilt University [NSF CHE-1156922], which provided support for a wonderful undergraduate researcher, Lana Thomas.

The work presented in this chapter could not have been completed without the efforts of several individuals. The development of QPA as a molecular sensor is credited to Besik Kankia from The Ohio State University. I am also grateful for Adam Taylor, David Gvarjaladze, and Levan Lomidze from The Ohio State University for their preliminary work on the optimization of QPA as a molecular sensor. The initial concept of using the self-contained format to enable QPA detection of mRNA is credited to Rick Haselton and David Wright. Lana Thomas is credited for producing the preliminary mRNA extraction results that laid the foundation for this project. Much of the data and presented in this chapter was collected by Abraham Wang and Alison Caprioli.

Chapter VI

TOWARD THE DEVELOPMENT OF A COMPLETE DIAGNOSTIC DEVICE

Abstract

Although each of the methods, insights, or components discussed in the preceding chapters has the potential to make diagnostic tests more accessible to end users, the integration of them into an automated diagnostic device would have great value. Therefore, this final chapter ties together the concepts that are described in chapters II through V and presents a plan for the development of a complete diagnostic device. First, our preliminary design for an automated sample processor is described. This automated processor is formatted to interface with our self-contained format by rotating a disk containing the tubing wrapped around its circumference passed a fixed permanent magnet to pull the magnetic beads through the processing solutions. A plan for developing this automated sample processor into a complete diagnostic device is described, which includes steps that could be taken to create a device that performs sample-in-to-answer-out detection of nucleic acids. The proposed device will be able to perform nucleic acid extraction on the surface of magnetic beads, amplification by PCR and thermal cycling, and detection in real-time using integrated fluorescence optics. A plan for standardizing the readout to PCR for multiple biomarker types, including proteins and cells, is also described. The completion of the steps described in this plan has the potential to lead to the development of a complete diagnostic device with the potential to be implemented in limited resource settings.

Introduction

The development of a complete diagnostic device will be a research thrust of our laboratories in the years to come. The intent of this chapter is to describe the state of the technologies developed during my graduate tenure and to outline the next steps that I perceive are required to implement these technologies in a meaningful way at the point-of-care. This chapter serves as a note to those that follow and is written as a guide of sorts for developing a complete diagnostic device.

Progress made toward a complete diagnostic device

The studies presented in this dissertation have attempted to overcome specific technical obstacles in the field of point-of-care diagnostics. I have demonstrated that our self-contained format based on surface tension valves is an effective platform for nucleic acid biomarker extraction, amplification, and detection, with fewer steps than is required in conventional laboratory settings (7). This format enables simple patient sample processing and biomarker detection for untrained personnel, has the flexibility to be interfaced with a variety of upstream and downstream processes, and maintains independence from pipetting, centrifugation, and other complex or expensive laboratory-based procedures. To function as a complete diagnostic device, I hope to integrate sample loading, processing, and biomarker amplification and detection into a single, standalone instrument. Toward this goal, our current efforts are focused on developing an automated processor to draw the magnetic beads through the self-contained tubing and a simple approach to introduce the patient sample into the tubing.

Development of an automated processor

As described throughout this dissertation, preparation of the patient sample was achieved by manually moving a small magnet along the edge of the tube to gather magnetic beads and move them into the next processing chamber. Our laboratories have designed a prototype automated sample processor based on our self-contained format that rotates sample processing cassettes past fixed permanent magnets (Figure 33A). Sample processing

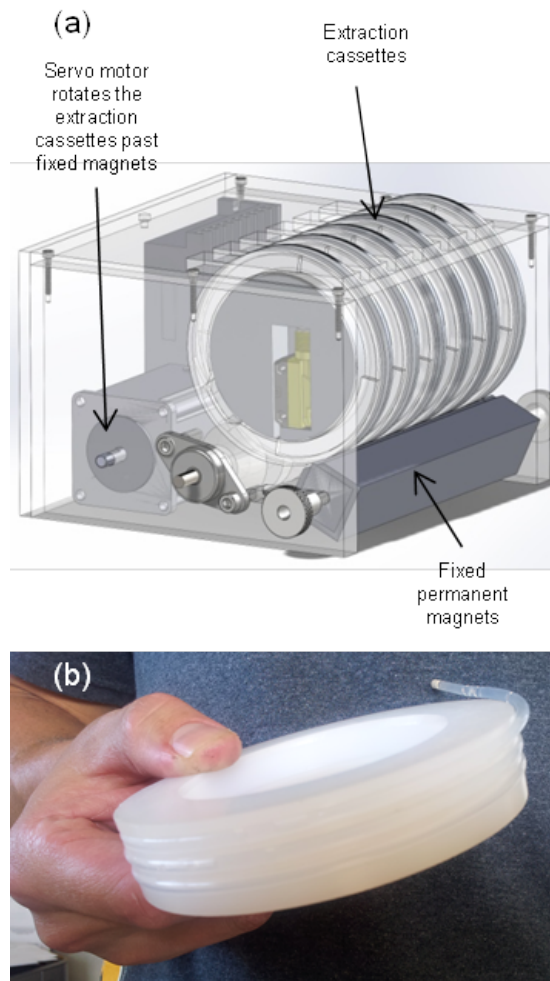


Figure 33. Depiction of the prototype automated sample processor based on our self-contained format. A) The extraction cassette processor relies on a stepper motor to rotate individual cassettes past fixed permanent magnets for magnetic bead processing. B) The extraction tubing is wrapped around the outside of individual cassettes.

cassettes are plastic disks with the required length of preloaded tubing wrapped around its outer edge. The design aligns the tubing directly over the magnet for magnetic bead processing (Figure 33B). The rollers are rotated by a stepper motor at two speeds: a slow speed to gather magnetic beads and pull them slowly forward through each solution and a fast speed to spread the beads in each chamber and allow them to mix with each individual wash solution. This roller operation is independent of both chamber and surface tension valve length, and allows the flexibility to extract different biomarker types using the same continuously operating program. The continuous roller operation gives the processor multiplex capabilities and allows each individual cassette to be placed on the processor and removed independently of other cassettes.

Design of a simple patient sample loader

One approach to sample loading is to draw the patient sample into a transfer pipette containing lyophilized magnetic beads and binding reagents and buffers within the bulb end of the pipette. In this simple method, the beads are rehydrated with the sample and the biomarkers are captured on the surface of the magnetic beads by simply shaking the bulb. In this design, the entire transfer pipette contents were then injected into the extraction cassette, effectively shifting the processing solutions down the tube. Shifting the processing solutions changes chamber location and makes alignment with detectors more difficult. Therefore, I have designed a simple variation on this approach, which does not shift the pre-arrayed solutions. The design is illustrated in Figure 34. The first step is to draw the patient sample into the bulb of the transfer pipette and simply shake the bulb to dissolve the beads and the other freeze-dried reagents. The second step is to apply the tip of the transfer pipette to an

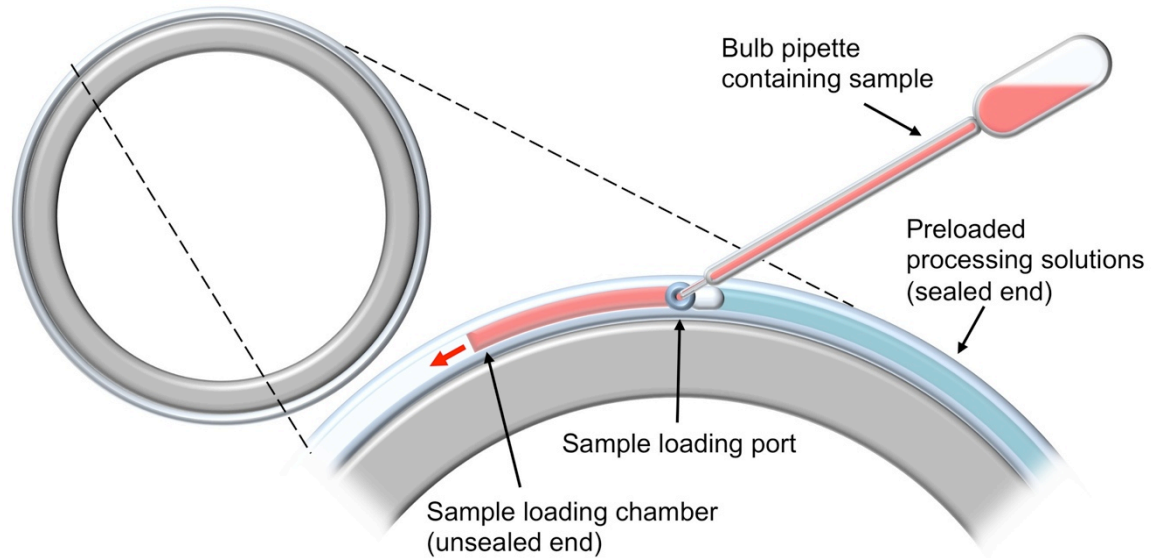


Figure 34. Illustration of the basic sample introduction method.

injection hole in the side of the tubing wrapped around the ring cassette. When the bulb is squeezed the liquid contents and the magnet beads travel down an unsealed region (left in the illustration) and fill the contents of a previously open section of tubing. The blue region (right in the illustration) contains the processing solutions, which do not move during the injection because the far end of this section of tubing is plugged. After the patient sample has been loaded into the tubing, the cartridge is placed on the processor and in subsequent passes over the fixed magnet the magnetic beads are drawn into the next processing chamber in the blue section. Residual patient sample is retained inside of the tubing and is disposed of with the ring cartridge.

Next steps for the development of a complete diagnostic device

Despite the success our laboratories have had in developing components of a diagnostic device, hurdles still exist that prevent these technologies from being implemented at the point-of-care. These hurdles include integrating sample loading, processing, and

biomarker amplification and detection and developing a standard amplification interface for multiple biomarker types. These barriers can be resolved through concerted efforts in device engineering and chemical investigation.

Integrated sample loading, processing, and biomarker amplification and detection

To develop a complete diagnostic device, one plan is to integrate sample loading, sample preparation, biomarker amplification and detection into a single instrument. When viewed as a complete diagnostic system, integration will provide the following principle advantages: 1) integrated sample loader simplifies patient sample loading and reduces operator training; 2) cartridges are self-contained, inexpensive, and potentially disposable; 3) when cartridges are placed on the processor, processing proceeds automatically; and 4) multiple cartridges are processed independently and on a continuous basis. In the following sections, I describe plans to incorporate and evaluate an instrument with these additional features.

The components needed to develop a diagnostic device from our self-contained patient sample preparation technology include (A) a simple patient sample loader, (B) a means of heating and cooling the samples, and (C) an integrated optical detection strategy. These components are conceptually illustrated within the context of the automated device in Figure 35. The complete diagnostic is envisioned to function in the following way. A sample loader containing lyophilized magnetic biomarker capture beads and binding reagents is removed from the cartridge rim and used to draw up a patient sample (Figure 35A). The sample loader is reinserted into the cartridge rim and the cartridge is placed on the sample

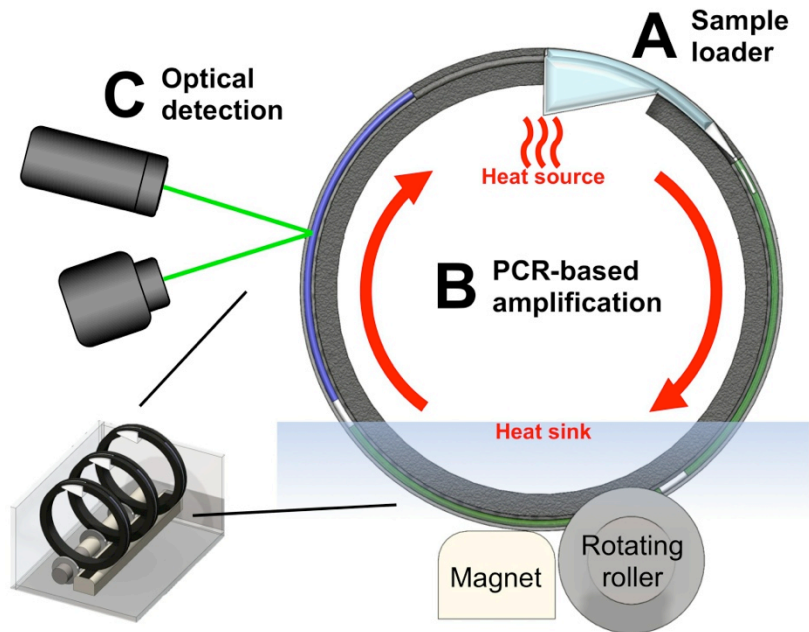


Figure 35. Conceptual summary of the major integration components, including A) patient sample loading, B) biomarker amplification, and C) optical detection of results.

processor. The remaining steps of the assay are carried out automatically as the processor rotates the cartridge.

As the studies presented in this dissertation have shown, a fixed magnet contained within the processor can be used to pull biomarker capture beads through pre-arrayed solutions contained within the tubing to remove contaminants from a patient sample and concentrate them. Amplification can then be achieved by standard PCR or isothermal PCR reagents in the amplification solution and by rotating the cartridge through areas of heating and cooling within the box (Figure 35B). Isothermal reactions have one particularly attractive advantage over traditional PCR in that they operate at a fixed temperature above the highest environmental ambient temperature, which is expected to be at most 45°C. Temperature control of reactions can be achieved simply by surrounding the rotating cartridges with a simple containment box and heating the air inside of this volume to the temperature required

to maintain the target temperatures typical of isothermal reactions (approximately 65°C). An alternative approach that could also be considered is the use of a thermally controlled water bath. Both of these approaches might cheaply enable isothermal reactions but would seem unlikely to be feasible solutions for higher temperature PCR reactions. Microwave radiation or infrared light would also appear to be feasible approaches to heat water-based reaction solutions. Thermal control for traditional PCR requires the ability to cool the PCR reaction mixture to a target temperature, which is critical for optimum assay performance. One simple design is to incorporate a fan to draw ambient air into the box. Alternatively, a cooled water bath could be used in which the cartridge passes through during each rotation. Amplification is detected optically through the transparent tubing wall (Figure 35C).

To incorporate fluorescence into the automated device format, I plan to produce a design that would incorporate a complete dual channel fluorescence subsystem from Qiagen (Figure 36). This device appears to have the characteristics needed for measuring the fluorescence of the sample solution through the tube wall. As shown in the diagram, the yellow region shown at the bottom of their product brochure image would be replaced by the rotating tube section containing the fluorescing solution. The system uses a series of short pulses to illuminate the sample and thus should have the capabilities to read the moving tubing as it passes slowly in front of the detector. Because the presence of magnetic beads may interfere with optical sensing, beads will need to pass through an elution/amplification segment where biomarkers are released and then the magnetic beads are pulled into a bead graveyard downstream of the amplification region. In this tube layout design, the biomarkers elute in the amplification reagent segment and the beads, without biomarkers, are drawn into a final water segment and therefore will not be present in the amplification region. In

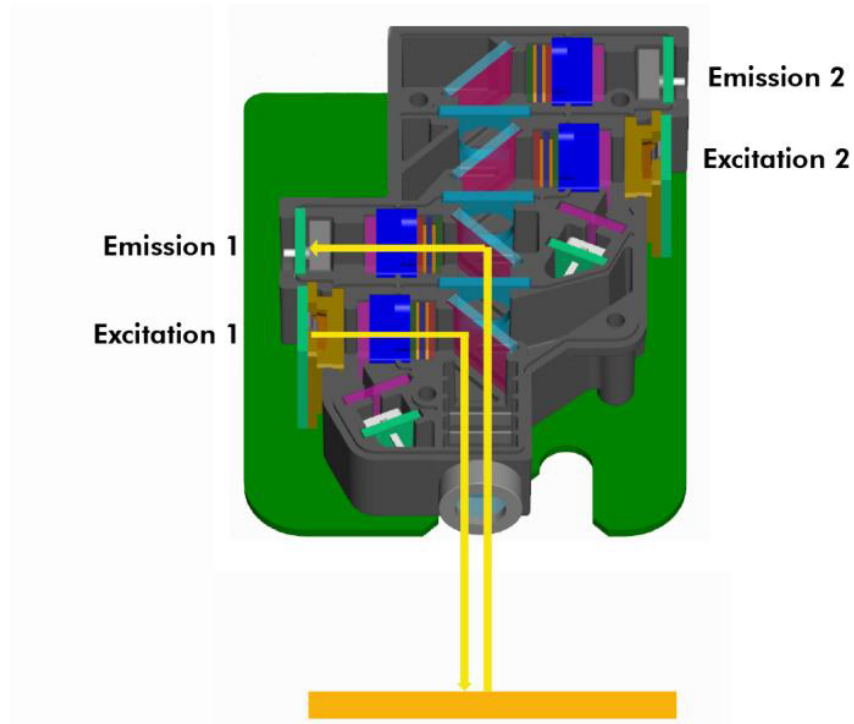


Figure 36. Depiction of the Qiagen fluorescence detection system (ESElog fluorescence detector).

traditional intercalating methods the intercalating dye is also present in the amplification reaction mix and thus this segment will be illuminated by the dye excitation wavelength during the cartridge rotation. The physical hardware to detect the increase in emission of a rotating section of tubing will be based on the proven designs contained in the commercially available Qiagen Rotor-Gene Q real-time PCR machine.

Development of a standard amplification interface for detecting multiple biomarker types

Another important feature of a simple diagnostic device would be a single readout for a variety of biomarker targets. Based on the proven amplification properties of PCR and the

potential for isothermal methods, one approach would be to convert target biomarkers into a predetermined set of DNA sequences as inputs into a standardized PCR or isothermal reaction. Our laboratories have designed a means to convert mRNA, protein, cell surface biomarkers, or other biomarkers of interest to a single DNA sequence for this standardized amplification and detection method. If successful, this molecular translation or conversion will narrow the amplification and detection focus to PCR or isothermal amplification, thus simplifying the overall design of the diagnostic instrument. Furthermore, this interface standard will enable straightforward integration of any future molecular recognition technology with an output conforming to this standardized amplification and detection method.

The rationale for considering this approach is that the use of PCR for the detection of nucleic acid biomarkers has become the benchmark for sensitivity and specificity in molecular diagnostics. However, many biomarker targets that most directly correlate with infection and disease are not nucleic acids, but proteins, whole cells, or other small molecules. The detection of these types of biomarkers requires various amplification and detection readouts. Therefore, the development of a universal method to standardize amplification and detection of diverse biological and molecular targets would greatly simplify the design of a standalone device that incorporates detection of multiple classes of biomarkers.

The approach to a standardized amplification interface that we are considering involves “digitizing” the molecular detection, i.e., linking a biomarker recognition element to a unique DNA tag (amplicon) enabling PCR amplification and subsequent detection of amplified DNA as a proxy for the biomarker. The concept of digitizing a molecular

recognition event into the A, T, C, and G readout for PCR detection has been previously established with immuno-PCR, an approach that uses monoclonal antibodies linked to DNA tags. Though the sensitivity achieved with immuno-PCR was unprecedented for protein detection (attomolar detection limits for proteins) (98), the approach has not been widely implemented in clinical diagnostics because its sensitivity is limited by the specificity of antibodies. Other methods have been developed to improve the specificity of the biomarker recognition element. For example, a proximity ligation approach improves specificity by using two antibodies to bind distinct epitopes of the same protein biomarker so that DNA amplification occurs only when the two tags are in close proximity. However, the difficulty of finding two antibodies that bind close enough together for the reaction to function on a relevant protein biomarker surface has impeded its adoption as a clinical diagnostic tool. Other DNA-tagged biomarker recognition elements, such as aptamers, have also been used to convert a molecular recognition event into a PCR signal with similar results to the traditional immuno-PCR (i.e., sensitivity of the assay is limited by the specificity of the recognition element). This standardized biomarker-amplification interface approach will help to solve the specificity issues associated with immuno-PCR techniques, as our self-contained extraction processor will be used to remove non-target interferents.

This approach for standardizing biomarker detection to PCR requires two components to integrate with our magnetic bead-based biomarker extraction system: biomarker recognition elements tagged with DNA and an amplification system for the DNA tags. A demonstration of the conversion of biomarker recognition events to PCR using could be done using validated reagents from our laboratories, including DNA tagged hybridization probes

for viral mRNA, DNA-tagged Ni(II)NTA for the malarial protein HRP-II, and DNA tagged-CD4 monoclonal antibody for whole CD4+ cells (Figure 37).

The plan to achieve this objective is aimed at developing the chemical components for a functional standardized amplification interface. It will be necessary to identify the optimal chemical methods for associating unique DNA tags with specific biomarker recognition elements and test isothermal and standard PCR methods to amplify and detect the DNA amplicons associated with captured biomarkers. The basic approach is illustrated in Figure 37. As this figure illustrates, three different types of biomarkers (mRNA, proteins, and cells) are captured onto the surface of magnetic beads (left side). If biomarkers are present on the surface of the magnetic beads they are transported into the next segment of the tubing, which contains the amplification interface components (right side). Interaction of these

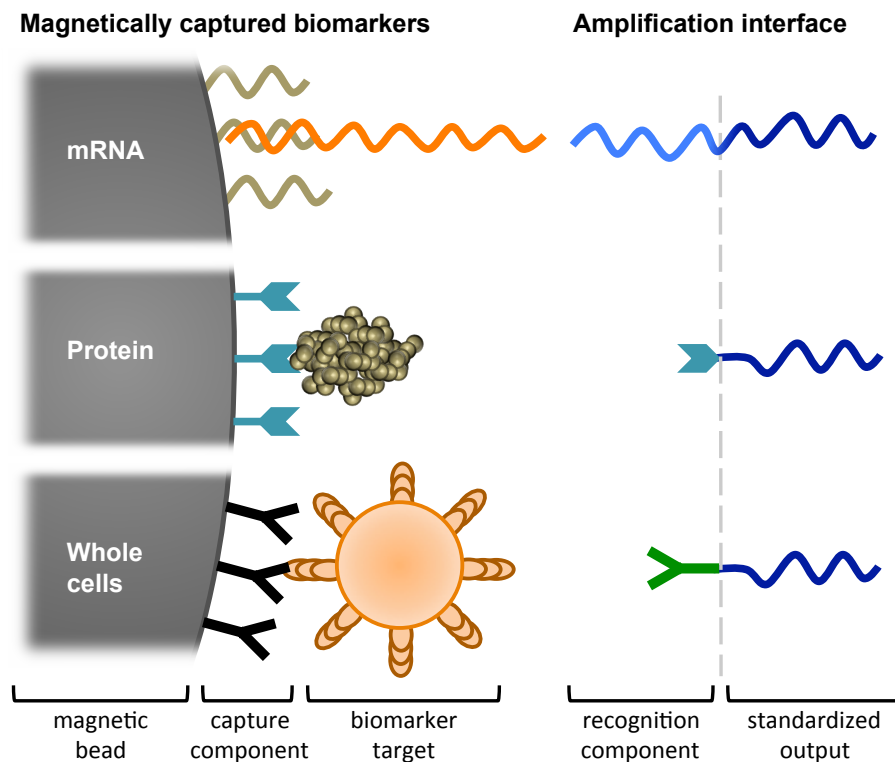


Figure 37. Molecular interface components (right side) required to convert mRNA, protein, or cell surface biomarkers (left side) to standardized DNA output (dark blue lines to the right of the vertical dotted-line).

interface components then associates a single common DNA tag for amplification by a standardized PCR or isothermal reaction. Our self-contained processor is particularly suitable for this application for three reasons: 1) it enables the capture and presentation of biomarker targets on the surface of magnetic beads, preparatory to binding and isolating DNA-tagged molecular recognition agents and depositing them into a PCR reaction; 2) it improves biomarker recognition specificity by reducing the number of non-target biomolecules present in the assay solutions; and 3) it is compatible with standard PCR and various isothermal PCR amplification methods.

REFERENCES

1. (2013) World Health Organization. *Global Health Observatory Data Repository*, www.who.int/gho/data/.
2. Bisno, A.L. (2001) Acute pharyngitis. *New England Journal of Medicine*, **344**, 205-211.
3. Thompson, W.W., Weintraub, E., Dhankhar, P., Cheng, P.Y., Brammer, L., Meltzer, M.I., Bresee, J.S. and Shay, D.K. (2009) Estimates of US influenza-associated deaths made using four different methods. *Influenza and Other Respiratory Viruses*, **3**, 37-49.
4. Strimbu, K. and Tavel, J.A. (2010) What are biomarkers? *Current Opinion in HIV and AIDS*, **5**, 463.
5. Aronson, J. (2005) Biomarkers and surrogate endpoints. *British Journal of Clinical Pharmacology*, **59**, 491-494.
6. Bae, H.-G., Nitsche, A., Teichmann, A., Biel, S.S. and Niedrig, M. (2003) Detection of yellow fever virus: a comparison of quantitative real-time PCR and plaque assay. *Journal of Virological Methods*, **110**, 185-191.
7. Bordelon, H., Adams, N.M., Klemm, A.S., Russ, P.K., Williams, J.V., Talbot, H.K., Wright, D.W. and Haselton, F.R. (2011) Development of a low-resource RNA extraction cassette based on surface tension valves. *ACS Applied Materials & Interfaces*, **3**, 2161-2168.
8. Schützle, H., Weigl, J., Puppe, W., Forster, J. and Berner, R. (2008) Diagnostic performance of a rapid antigen test for RSV in comparison with a 19-valent multiplex RT-PCR ELISA in children with acute respiratory tract infections. *European Journal of Pediatrics*, **167**, 745-749.
9. Talbot, H.K., Shepherd, B.E., Crowe, J.E., Jr., Griffin, M.R., Edwards, K.M., Podsiad, A.B., Tollefson, S.J., Wright, P.F. and Williams, J.V. (2009) The pediatric burden of human coronaviruses evaluated for twenty years. *Pediatric Infectious Disease Journal*, **28**, 682-687.
10. Williams, J.V., Tollefson, S.J., Nair, S. and Chonmaitree, T. (2006) Association of human metapneumovirus with acute otitis media. *International Journal Pediatric Otorhinolaryngology*, **70**, 1189-1193.
11. Beuselinck, K., van Ranst, M. and van Eldere, J. (2005) Automated extraction of viral-pathogen RNA and DNA for high-throughput quantitative real-time PCR. *Journal of Clinical Microbiology*, **43**, 5541-5546.
12. Radstrom, P., Knutsson, R., Wolffs, P., Lovenklev, M. and Lofstrom, C. (2004) Pre-PCR processing. *Molecular Biotechnology*, **26**, 133-146.

13. Niemz, A., Ferguson, T.M. and Boyle, D.S. (2011) Point-of-care nucleic acid testing for infectious diseases. *Trends in Biotechnology*, **29**, 240-250.
14. Yager, P., Domingo, G.J. and Gerdes, J. (2008) Point-of-care diagnostics for global health. *Annual Review of Biomedical Engineering*, **10**, 38.
15. Gill, P. and Ghaemi, A. (2008) Nucleic acid isothermal amplification technologies--a review. *Nucleosides, Nucleotides and Nucleic Acids*, **27**, 224-243.
16. Davis, K.M., Swartz, J.D., Haselton, F.R. and Wright, D.W. (2012) Low-resource method for extracting the malarial biomarker histidine-rich protein II to enhance diagnostic test performance. *Analytical Chemistry*, **84**, 6136-6142.
17. Bordelon, H., Russ, P.K., Wright, D.W. and Haselton, F.R. (2013) A magnetic bead-based method for concentrating DNA from human urine for downstream detection. *PLoS ONE*, **8**, e68369.
18. Olsvik, O., Popovic, T., Skjerve, E., Cudjoe, K.S., Hornes, E., Ugelstad, J. and Uhlén, M. (1994) Magnetic separation techniques in diagnostic microbiology. *Clinical Microbiology Reviews*, **7**, 43 - 54.
19. Tewari, D., Zellers, C., Acland, H. and Pedersen, J.C. (2007) Automated extraction of avian influenza virus for rapid detection using real-time RT-PCR. *Journal of Clinical Virology*, **40**, 142-145.
20. Stemmer, C., Beau-Faller, M., Pencreac'h, E., Guerin, E., Schneider, A., Jaqmin, D., Quoix, E., Gaub, M.-P. and Oudet, P. (2003) Use of magnetic beads for plasma cell-free DNA extraction: toward automation of plasma DNA analysis for molecular diagnostics. *Clinical Chemistry*, **49**, 1953-1955.
21. Siddiqui, H., Nederbragt, A.J. and Jakobsen, K.S. (2009) A solid-phase method for preparing human DNA from urine for diagnostic purposes. *Clinical Biochemistry*, **42**, 1128-1135.
22. Panning, M., Kramme, S., Petersen, N. and Drosten, C. (2007) High throughput screening for spores and vegetative forms of pathogenic *B. anthracis* by an internally controlled real-time PCR assay with automated DNA preparation. *Medical Microbiology and Immunology*, **196**, 41-50.
23. Jacobsen, C. (1995) Microscale detection of specific bacterial DNA in soil with a magnetic capture-hybridization and PCR amplification assay. *Applied and Environmental Microbiology*, **61**, 3347-3352.
24. Adams, N.M., Olmsted, I.R., Haselton, F.R., Bornhop, D.J. and Wright, D.W. (2013) The effect of hybridization-induced secondary structure alterations on RNA detection using backscattering interferometry. *Nucleic Acids Research*.

25. Adams, N.M., Wang, K.-K.A., Caprioli, A.C., Thomas, L.C., Kankia, B., Haselton, F. and Wright, D. (2014) Quadruplex priming amplification for the detection of mRNA from surrogate patient samples. *Analyst*, **139**, 1644 - 1652.
26. Casadevall, A. and Fang, F.C. (2009) Important science--it's all about the SPIN. *Infection and Immunity*, **77**, 4177-4180.
27. Adams, N.M., Creecy, A.E., Majors, C.E., Wariso, B.A., Short, P.A., Wright, D.W. and Haselton, F.R. (2013) Design criteria for developing low-resource magnetic bead assays using surface tension valves. *Biomicrofluidics*, **7**, 014104.
28. Kankia, B.I. (2011) Self-dissociative primers for nucleic acid amplification and detection based on DNA quadruplexes with intrinsic fluorescence. *Analytical Biochemistry*, **409**, 59-65.
29. Johnson, J., Okyere, R., Joseph, A., Musier-Forsyth, K. and Kankia, B. (2013) Quadruplex formation as a molecular switch to turn on intrinsically fluorescent nucleotide analogs. *Nucleic Acids Research*, **41**, 220-228.
30. Smit, M.L., Giesendorf, B.A.J., Heil, S.G., Vet, J.A.M., Trijbels, F.J.M. and Blom, H.J. (2000) Automated extraction and amplification of DNA from whole blood using a robotic workstation and an integrated thermocycler. *Biotechnology and Applied Biochemistry*, **32**, 121-125.
31. Khan, S.A. (2012) Preface to special topic: multiphase microfluidics. *Biomicrofluidics*, **6**, 021901.
32. Chen, H., Abolmatty, A. and Faghri, M. (2011) Microfluidic inverse phase ELISA via manipulation of magnetic beads. *Microfluidics and Nanofluidics*, **10**, 593-605.
33. Mitsuhiro, S., Kentaro, T., Hiroyuki, H., Hiroshi, I. and Kazuo, S. (2006) Development of an enzymatic reaction device using magnetic bead-cluster handling. *Journal of Micromechanics and Microengineering*, **16**, 1875.
34. Berry, S.M., Alarid, E.T. and Beebe, D.J. (2011) One-step purification of nucleic acid for gene expression analysis via Immiscible Filtration Assisted by Surface Tension (IFAST). *Lab on a Chip*, **11**, 1747-1753.
35. Sur, K., McFall, S.M., Yeh, E.T., Jangam, S.R., Hayden, M.A., Stroupe, S.D. and Kelso, D.M. (2010) Immiscible phase nucleic acid purification eliminates PCR inhibitors with a single pass of paramagnetic particles through a hydrophobic liquid. *The Journal of Molecular Diagnostics*, **12**, 620-628.
36. Shikida, M., Takayanagi, K., Inouchi, K., Honda, H. and Sato, K. (2006) Using wettability and interfacial tension to handle droplets of magnetic beads in a micro-chemical-analysis system. *Sensors and Actuators B: Chemical*, **113**, 563-569.

37. Gijs, M.A.M. (2004) Magnetic bead handling on-chip: new opportunities for analytical applications. *Microfluidics and Nanofluidics*, **1**, 22-40.
38. Marin, A.G., Loscertales, I.G. and Barrero, A. (2012) Surface tension effects on submerged electrosprays. *Biomicrofluidics*, **6**, 044104.
39. Kong, T., Wu, J., To, M., Wai Kwok Yeung, K., Cheung Shum, H. and Wang, L. (2012) Droplet based microfluidic fabrication of designer microparticles for encapsulation applications. *Biomicrofluidics*, **6**, 034104-034104-034109.
40. Rondeau, E. and Cooper-White, J.J. (2012) Formation of multilayered biopolymer microcapsules and microparticles in a multiphase microfluidic flow. *Biomicrofluidics*, **6**, 024125.
41. Vertti-Quintero, N., Song, Y., Manneville, P. and Baroud, C.N. (2012) Behavior of liquid plugs at bifurcations in a microfluidic tree network. *Biomicrofluidics*, **6**, 034105-034105-034110.
42. Monteiro, L., Bonnemaïson, D., Vekris, A., Petry, K.G., Bonnet, J., Vidal, R., Cabrita, J. and Megraud, F. (1997) Complex polysaccharides as PCR inhibitors in feces: *Helicobacter pylori* model. *Journal of Clinical Microbiology*, **35**, 995-998.
43. Wilson, I.G. (1997) Inhibition and facilitation of nucleic acid amplification. *Applied and Environmental Microbiology*, **63**, 3741-3751.
44. Chomczynski, P. and Sacchi, N. (1987) Single-step method of RNA isolation by acid guanidinium thiocyanate-phenol-chloroform extraction. *Analytical Biochemistry*, **162**, 156-159.
45. Avison, M.B. (2007) *Measuring gene expression*. Taylor & Francis, New York ; Abingdon [England].
46. Yamada, O., Matsumoto, T., Nakashima, M., Hagari, S., Kamahora, T., Ueyama, H., Kishi, Y., Uemura, H. and Kurimura, T. (1990) A new method for extracting DNA or RNA for polymerase chain reaction. *Journal of Virological Methods*, **27**, 203-209.
47. Chirgwin, J.M., Przybyla, A.E., MacDonald, R.J. and Rutter, W.J. (1979) Isolation of biologically active ribonucleic acid from sources enriched in ribonuclease. *Biochemistry*, **18**, 5294-5299.
48. MacDonald, R.J., Swift, G.H., Przybyla, A.E., Chirgwin, J.M., Shelby, L.B. and Allan, R.K. (1987), *Methods in Enzymology*. Academic Press, Vol. Volume 152, pp. 219-227.
49. Price, C.W., Leslie, D.C. and Landers, J.P. (2009) Nucleic acid extraction techniques and application to the microchip. *Lab Chip*, **9**, 2484-2494.

50. Chen, D.F., Mauk, M., Qiu, X.B., Liu, C.C., Kim, J.T., Ramprasad, S., Ongagna, S., Abrams, W.R., Malamud, D., Corstjens, P.L.A.M. *et al.* (2010) An integrated, self-contained microfluidic cassette for isolation, amplification, and detection of nucleic acids. *Biomed Microdevices*, **12**, 705-719.
51. Hagan, K.A., Reedy, C.R., Uchimoto, M.L., Basu, D., Engel, D.A. and Landers, J.P. An integrated, valveless system for microfluidic purification and reverse transcription-PCR amplification of RNA for detection of infectious agents. *Lab Chip*, **11**, 957-961.
52. Webb, D.P., Knauf, B., Liu, C.Q., Hutt, D. and Conway, P. (2009) Productionisation issues for commercialisation of microfluidic based devices. *Sensor Rev*, **29**, 349-354.
53. Hu, A.Z., Colella, M., Tam, J.S., Rappaport, R. and Cheng, S.M. (2003) Simultaneous detection, subgrouping, and quantitation of respiratory syncytial virus A and B by real-time PCR. *Journal of Clinical Microbiology*, **41**, 149-154.
54. Coiras, M., Perez-Brena, P., Garcia, M. and Casas, I. (2003) Simultaneous detection of influenza A, B, and C viruses, respiratory syncytial virus, and adenoviruses in clinical samples by multiplex reverse transcription nested-PCR assay. *Journal of Medical Virology*, **69**, 132-144.
55. Letant, S.E., Ortiz, J.I., Tammero, L.F.B., Birch, J.M., Derlet, R.W., Cohen, S., Manning, D. and McBride, M.T. (2007) Multiplexed reverse transcriptase PCR assay for identification of viral respiratory pathogens at the point of care. *Journal of Clinical Microbiology*, **45**, 3498-3505.
56. Stone, G.P., Wetzel, J.D., Russ, P.K., Dermody, T.S. and Haselton, F.R. (2006) Autonomous reovirus strain classification using filament-coupled antibodies. *Annals of Biomedical Engineering*, **34**, 1778-1785.
57. Jayagopal, A., Halfpenny, K.C., Perez, J.W. and Wright, D.W. (2010) Hairpin DNA-functionalized gold colloids for the imaging of mRNA in live cells. *Journal of the American Chemical Society*, **132**, 9789-9796.
58. Mehlmann, M., Dawson, E.D., Townsend, M.B., Smagala, J.A., Moore, C.L., Smith, C.B., Cox, N.J., Kuchta, R.D. and Rowlen, K.L. (2006) Robust sequence selection method used to develop the FluChip diagnostic microarray for influenza virus. *Journal of Clinical Microbiology*, **44**, 2857-2862.
59. Marras, S.A.E., Tyagi, S. and Kramer, F.R. (2006) Real-time assays with molecular beacons and other fluorescent nucleic acid hybridization probes. *Clinica Chimica Acta*, **363**, 48-60.
60. Nam, J.-M., Stoeva, S.I. and Mirkin, C.A. (2004) Bio-bar-code-based DNA detection with PCR-like sensitivity. *Journal of the American Chemical Society*, **126**, 5932-5933.

61. Zhang, J., Lang, H.P., Huber, F., Bietsch, A., Grange, W., Certa, U., McKendry, R., Guntherodt, H.J., Hegner, M. and Gerber, C. (2006) Rapid and label-free nanomechanical detection of biomarker transcripts in human RNA. *Nature Nanotechnology*, **1**, 214-220.
62. Springer, T., Piliarik, M. and Homola, J. (2010) Surface plasmon resonance sensor with dispersionless microfluidics for direct detection of nucleic acids at the low femtomole level. *Sensors and Actuators B: Chemical*, **145**, 588-591.
63. Bornhop, D.J., Latham, J.C., Kussrow, A., Markov, D.A., Jones, R.D. and Sorensen, H.S. (2007) Free-Solution, Label-Free Molecular Interactions Studied by Back-Scattering Interferometry. *Science*, **317**, 1732-1736.
64. Kussrow, A., Enders, C.S., Castro, A.R., Cox, D.L., Ballard, R.C. and Bornhop, D.J. (2010) The potential of backscattering interferometry as an in vitro clinical diagnostic tool for the serological diagnosis of infectious disease. *Analyst*, **135**, 1535-1537.
65. Kussrow, A., Enders, C.S. and Bornhop, D.J. (2011) Interferometric methods for label-free molecular interaction studies. *Analytical Chemistry*, **84**, 779-792.
66. Olmsted, I.R., Xiao, Y., Cho, M., Csordas, A.T., Sheehan, J.H., Meiler, J., Soh, H.T. and Bornhop, D.J. (2011) Measurement of aptamer-protein interactions with back-scattering interferometry. *Analytical Chemistry*, **83**, 8867-8870.
67. Latham, J.C., Markov, D.A., Sorensen, H.S. and Bornhop, D.J. (2005) Photobiotin surface chemistry improves label-free interferometric sensing of biochemical interactions. *Angewandte Chemie*, **118**, 969-972.
68. Baksh, M.M., Kussrow, A.K., Mileni, M., Finn, M. and Bornhop, D.J. (2011) Label-free quantification of membrane-ligand interactions using backscattering interferometry. *Nature Biotechnology*, **29**, 357-360.
69. Pesciotta, E.N., Bornhop, D.J. and Flowers II, R.A. (2011) Back-scattering interferometry: a versatile platform for the study of free-solution versus surface-immobilized hybridization. *Chemistry--An Asian Journal*, **6**, 70-73.
70. Perez, J.W., Vargis, E.A., Russ, P.K., Haselton, F.R. and Wright, D.W. (2011) Detection of respiratory syncytial virus using nanoparticle amplified immunopolymerase chain reaction. *Analytical Biochemistry*, **410**, 141-148.
71. Perez, J.W., Haselton, F.R. and Wright, D.W. (2009) Viral detection using DNA functionalized gold filaments. *Analyst*, **134**, 1548-1553.
72. Markov, D., Begari, D. and Bornhop, D.J. (2002) Breaking the 10⁻⁷ Barrier for RI measurements in nanoliter volumes. *Analytical Chemistry*, **74**, 5438-5441.
73. Vester, B. and Wengel, J. (2004) LNA (locked nucleic acid): high-affinity targeting of complementary RNA and DNA. *Biochemistry*, **43**, 13233-13241.

74. Petersen, M., Bondensgaard, K., Wengel, J. and Jacobsen, J.P. (2002) Locked nucleic acid (LNA) recognition of RNA:NMR solution structures of LNA:RNA hybrids. *Journal of the American Chemical Society*, **124**, 5974-5982.
75. Ivanov, V.I., Minchenkova, L.E., Minyat, E.E., Frank-Kamenetskii, M.D. and Schyolkina, A.K. (1974) The B to A transition of DNA in solution. *Journal of Molecular Biology*, **87**, 817-833.
76. Kypr, J., Kejnovska, I., Renciuik, D. and Vorlickova, M. (2009) Circular dichroism and conformational polymorphism of DNA. *Nucleic Acids Research*, **37**, 1713-1725.
77. Wiese, K.C. and Hendriks, A. (2006) Comparison of P-RnaPredict and mfold--algorithms for RNA secondary structure prediction. *Bioinformatics*, **22**, 934-942.
78. Braasch, D.A. and Corey, D.R. (2001) Locked nucleic acid (LNA): fine-tuning the recognition of DNA and RNA. *Chemistry & Biology*, **8**, 1-7.
79. Robertson, K.L. and Thach, D.C. (2009) LNA flow-FISH: A flow cytometry-fluorescence in situ hybridization method to detect messenger RNA using locked nucleic acid probes. *Analytical Biochemistry*, **390**, 109-114.
80. Tran Tan, T., Pawestri, H., My, N., Minh, H., Syahrial, H., Vu, T., van Doorn, H.R., Wertheim, H., Van Vinh, C., Quang, H. *et al.* (2010) A real-time RT-PCR for detection of clade 1 and 2 H5N1 Influenza A virus using Locked Nucleic Acid (LNA) TaqMan probes. *Virology Journal*, **7**, 46.
81. Nielsen, K.E., Rasmussen, J., Kumar, R., Wengel, J., Jacobsen, J.P. and Petersen, M. (2004) NMR studies of fully modified locked nucleic acid (LNA) hybrids: solution structure of an LNA:RNA hybrid and characterization of an LNA:DNA hybrid. *Bioconjugate Chemistry*, **15**, 449-457.
82. Rachwal, P.A., Brown, T. and Fox, K.R. (2007) Effect of G-tract length on the topology and stability of intramolecular DNA quadruplexes. *Biochemistry*, **46**, 3036-3044.
83. Nakayama, S. and Sintim, H.O. (2009) Colorimetric split G-quadruplex probes for nucleic acid sensing: improving reconstituted DNAzyme's catalytic efficiency via probe remodeling. *Journal of the American Chemical Society*, **131**, 10320-10333.
84. Xiao, Y., Pavlov, V., Niazov, T., Dishon, A., Kotler, M. and Willner, I. (2004) Catalytic beacons for the detection of DNA and telomerase activity. *Journal of the American Chemical Society*, **126**, 7430-7431.
85. Kolpashchikov, D.M. (2008) Split DNA enzyme for visual single nucleotide polymorphism typing. *Journal of the American Chemical Society*, **130**, 2934-2935.

86. Shimron, S., Wang, F., Orbach, R. and Willner, I. (2011) Amplified detection of DNA through the enzyme-free autonomous assembly of hemin/G-quadruplex DNAzyme nanowires. *Analytical Chemistry*, **84**, 1042-1048.
87. Wang, F., Freage, L., Orbach, R. and Willner, I. (2013) Autonomous replication of nucleic acids by polymerization/nicking enzyme/DNAzyme cascades for the amplified detection of DNA and the aptamer-cocaine complex. *Analytical Chemistry*.
88. Yang, X., Fang, C., Mei, H., Chang, T., Cao, Z. and Shangguan, D. (2011) Characterization of G-quadruplex/hemin peroxidase: substrate specificity and inactivation kinetics. *Chemistry-A European Journal*, **17**, 14475-14484.
89. Guo, Y., Xu, P., Hu, H., Zhou, X. and Hu, J. (2013) A label-free biosensor for DNA detection based on ligand-responsive G-quadruplex formation. *Talanta*.
90. Ren, J., Wang, J., Wang, J., Luedtke, N.W. and Wang, E. (2012) Contribution of potassium ion and split modes of G-quadruplex to the sensitivity and selectivity of label-free sensor toward DNA detection using fluorescence. *Biosensors and Bioelectronics*, **31**, 316-322.
91. Zhao, C., Wu, L., Ren, J. and Qu, X. (2011) A label-free fluorescent turn-on enzymatic amplification assay for DNA detection using ligand-responsive G-quadruplex formation. *Chemical Communications*, **47**, 5461-5463.
92. Yue, Q., Shen, T., Wang, C., Wang, L., Li, H., Xu, S., Wang, H. and Liu, J. (2012) Construction of a controllable Forster resonance energy transfer system based on G-quadruplex for DNA sensing. *Biosensors and Bioelectronics*.
93. Taylor, A., Joseph, A., Okyere, R., Gogichaishvili, S., Musier-Forsyth, K. and Kankia, B. (2012) Isothermal quadruplex priming amplification for DNA-based diagnostics. *Biophysical Chemistry*.
94. Datta, K., Johnson, N.P., Villani, G., Marcus, A.H. and von Hippel, P.H. (2012) Characterization of the 6-methyl isoxanthopterin (6-MI) base analog dimer, a spectroscopic probe for monitoring guanine base conformations at specific sites in nucleic acids. *Nucleic Acids Research*, **40**, 1191-1202.
95. Tomlinson, J., Boonham, N., Hughes, K., Griffin, R. and Barker, I. (2005) On-site DNA extraction and real-time PCR for detection of *Phytophthora ramorum* in the field. *Applied and Environmental Microbiology*, **71**, 6702-6710.
96. Klatser, P.R., Kuijper, S., van Ingen, C.W. and Kolk, A.H. (1998) Stabilized, freeze-dried PCR mix for detection of mycobacteria. *Journal of Clinical Microbiology*, **36**, 1798-1800.
97. Spiess, A.-N., Mueller, N. and Ivell, R. (2004) Trehalose is a potent PCR enhancer: lowering of DNA melting temperature and thermal stabilization of Taq polymerase by the disaccharide trehalose. *Clinical Chemistry*, **50**, 1256-1259.

98. Sano, T., Smith, C. and Cantor, C. (1992) Immuno-PCR: very sensitive antigen detection by means of specific antibody-DNA conjugates. *Science*, **258**, 120-122.

Appendix A.

Supplementary Data

Supplemental Figure 1. Target sequences used in chapter IV studies. A) Full length respiratory syncytial virus (RSV) N gene RNA sequence used in these studies (5' - 3'). Regions complementary to the probes used in these studies are underlined and colored. B) RNA target sequences containing mismatched nucleotides (5' - 3'). Mismatched nucleotides are indicated in bold font.

A CAAAAACCCCUCAAGACCCGUUUAGAGGCCCAAGGGGUUAUGCUAGUUAUGCGGCCG
CUGCAGGUCGACGGAUCCUCAAGCUCUACAUCAUUAUCUUUUGGAUUAAGCUGAUGU
UUGAUAGCCUCUAGUUCUUCUGCUGUCAAGUCUAGUACACUGUAGUUAAUCACACCAU
UUUCUUUGAGUUGUUCAGCAUAUAGCCUUGCUGCAUCAUAUAGAUAUAGUUAUCCUCGG
UGUACCUCUGUACUCUCCAUUAUGCCUAGGCCAGCAGCAUUGCCUAAUACUACACUGG
AGAAGUGAGGAAAUUGAGUCAAGAUAAUAAUGAUGCUUUUGGGUUGUCAAUAUUG
GUAGAAUCCUGCUUCACCACCCAAUUUUUGGGCAUUAUUCAUAAACCUCACAAACUUGU
CCAUUUCUGCUUGCACACUAGCAUGUCCUAAUAAUAAUUAUUAACUGAUUUUGCUAA
GACUCCCCACCGUAAACAUCACUUGCCCUGCACCAUAGGCAUUCAAAACAAUCCUGCAA
AAAUCCCUCAACUCUACUGCCACCUCUGGUAGAAGAUUGUGCUAUACCAAAAUGAACA
AAAACAUCUAUAAAGUGGGGAUGUUUUUCAACACUUCAUAGAAGCUGUUGGCUAUGU
CCUUGGGUAGUAAGCCUUUGUAACGUUUAUUAUUAUUUUUAGGACAUUAUAGCUCU
CCUAAUCACGGGUGUAAGACCA GAUCUGUCCUUGCUGCUAAUUUAGUUAUUAUUAU
GCUGCUAUACAUAUUAUUAUCAUCCACAAUCAGGAGAGUCAUGCCUGUAUUCUGGAG
CUACCUCUCCCAUUUCUUUAGCAUUUUUUUGUAGGAUUUUUCUAGAUUCUAUCUCAAU
GUUGAUUUGAAUUCAGUUGUUAAGCUUGCCAAUGUUAACACUCAAUUAUUCUUAUUCU
UUUCCAUAUUAUGUCUUGACGAUGUGUUGUUAUCAUCUACUCCAUUUGCUUUUACAUGAU
AUCCCGCAUCUCUGAGUAUUUUUAUGGUGUCUUCUCUUCUUAACCUAGACAUCGCAUUA
AAUUAUCCUUAUUAACCCAGUGAAUUUAUGAUUAGCAUCUUCUGUGAUUAAUACAUGC
CACUAACUUAUUGAUGUGUUUCUGCACAUCAAUUAGGAGUAUCAUACUACUCC
UGUGCUCCGUUGGAUGGUGUAUUUGCUGGAUGACAGAAGUUGAUCUUUGUUGAGUGUA
UCAUUAACUUGACUUUGCUAAGAGCCAUAAUGAAUUCGGCCUCCAUGGCCAUUAUGCA
GGUCCUCCUCUGAGAUCAGCUUCUGCUCCUCCAUGAUGGCGGCUCGCC

Grey: RSVN(1070-1091)

Light purple: RSVN(843-872)

Red: RSVN(755-774)

Light green: RSVN(531-551)

Pink: RSVN(308-329)

Blue: RSVN(264-285)

Orange: RSVN(242-256)

Orange/Green/Blue/Purple/Pink: RSVN(242-329)

Maroon: RSVN(4-29)

Teal: RSVN(957-983)

Brown: RSVN(800-821)

Light blue: RSVN(603-622)

Light brown: RSVN(425-444)

Purple: RSVN(286-307)

Green/Orange: RSVN(242-263)

Orange/Green/Blue: RSVN(242-285)

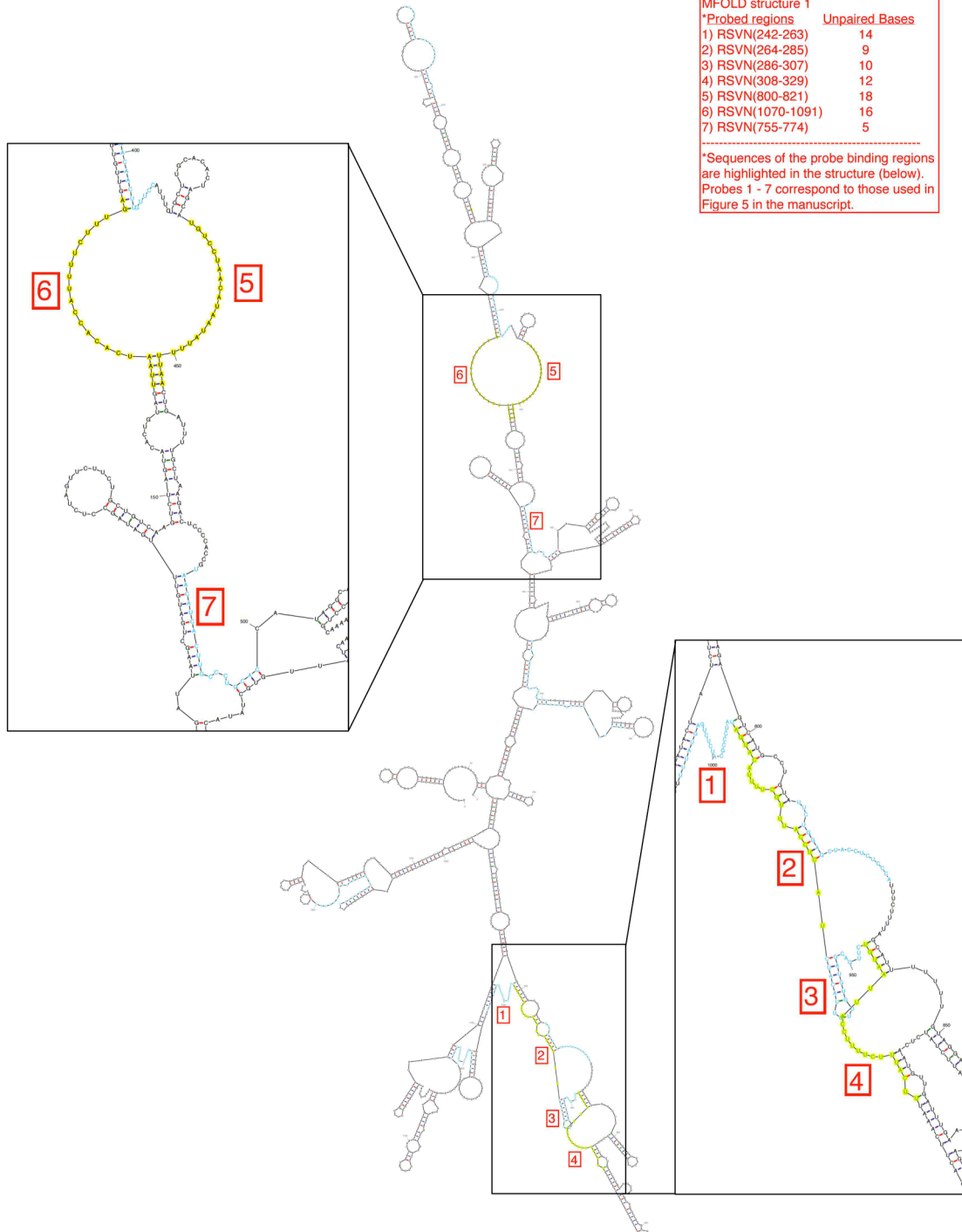
Tan: RSVN(193-214)

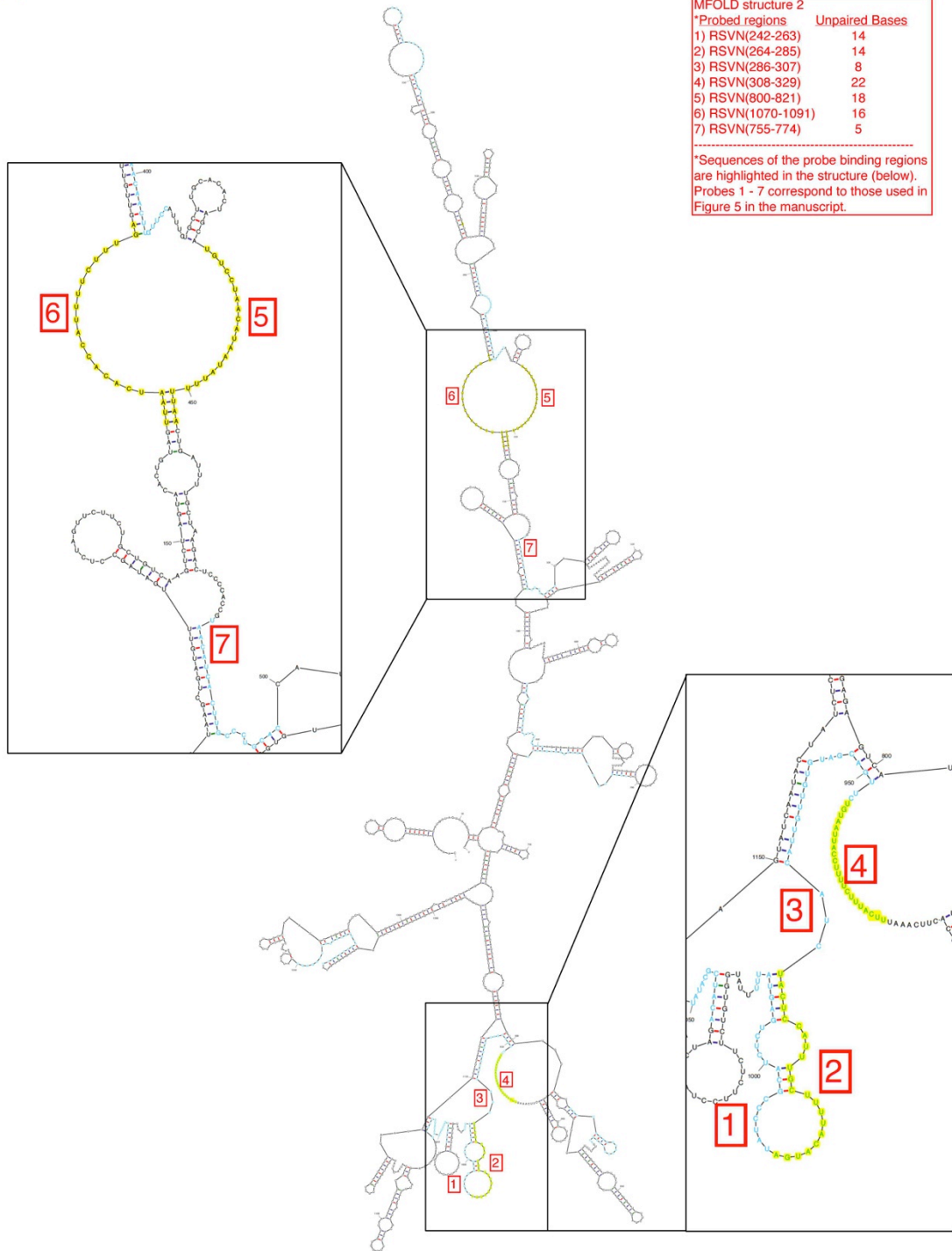
B 0 mismatches: UAUCCCGCAUCUCUGAGUAUUU
1 mismatch: UAUCCCGCAUGUCUGAGUAUUU
3 mismatches: UAUCGCGCAUGUCUGACUAUUU
5 mismatches: UAUCGCGGAUGUCAGACUAUUU

Supplemental Figure 2. The five lowest energy *mfold* folding structures predicted for the ~1300 nucleotide RSV N gene RNA sequence. The binding regions of the probes used in these studies are highlighted in yellow or blue and numbered 1 - 7. Legends in the top right of each structure list each probe evaluated and the number of unpaired bases predicted in the corresponding binding region.

Output of sir_graph (©)
mfold_util 4.6

Created Tue Aug 21 17:53:19 2012

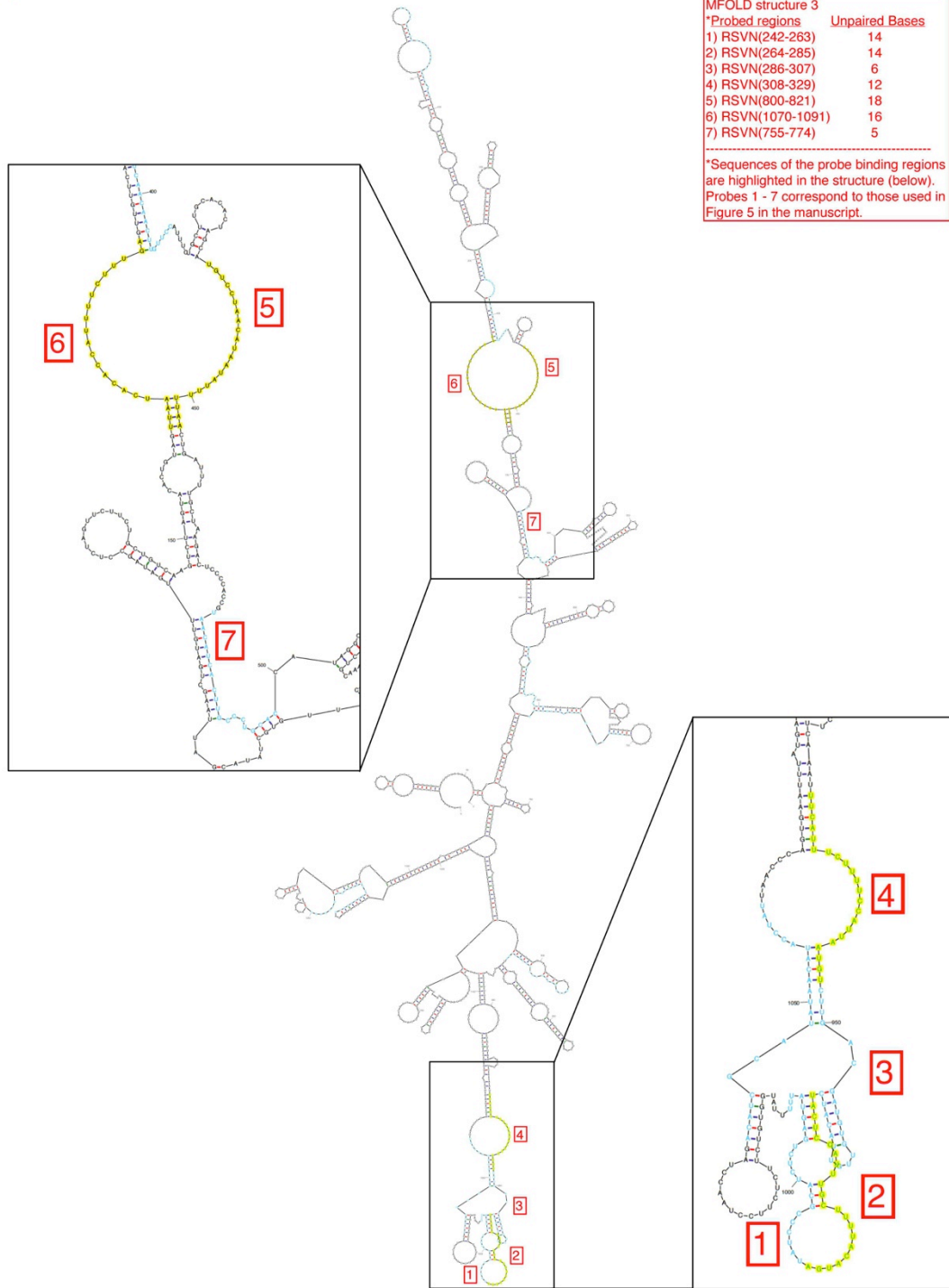




$dG = -269.73$ [Initially -326.90] RSV A2 N gene [1 - 1331]

MFOLD structure 3	
*Probed regions	Unpaired Bases
1) RSVN(242-263)	14
2) RSVN(264-285)	14
3) RSVN(286-307)	6
4) RSVN(308-329)	12
5) RSVN(800-821)	18
6) RSVN(1070-1091)	16
7) RSVN(755-774)	5

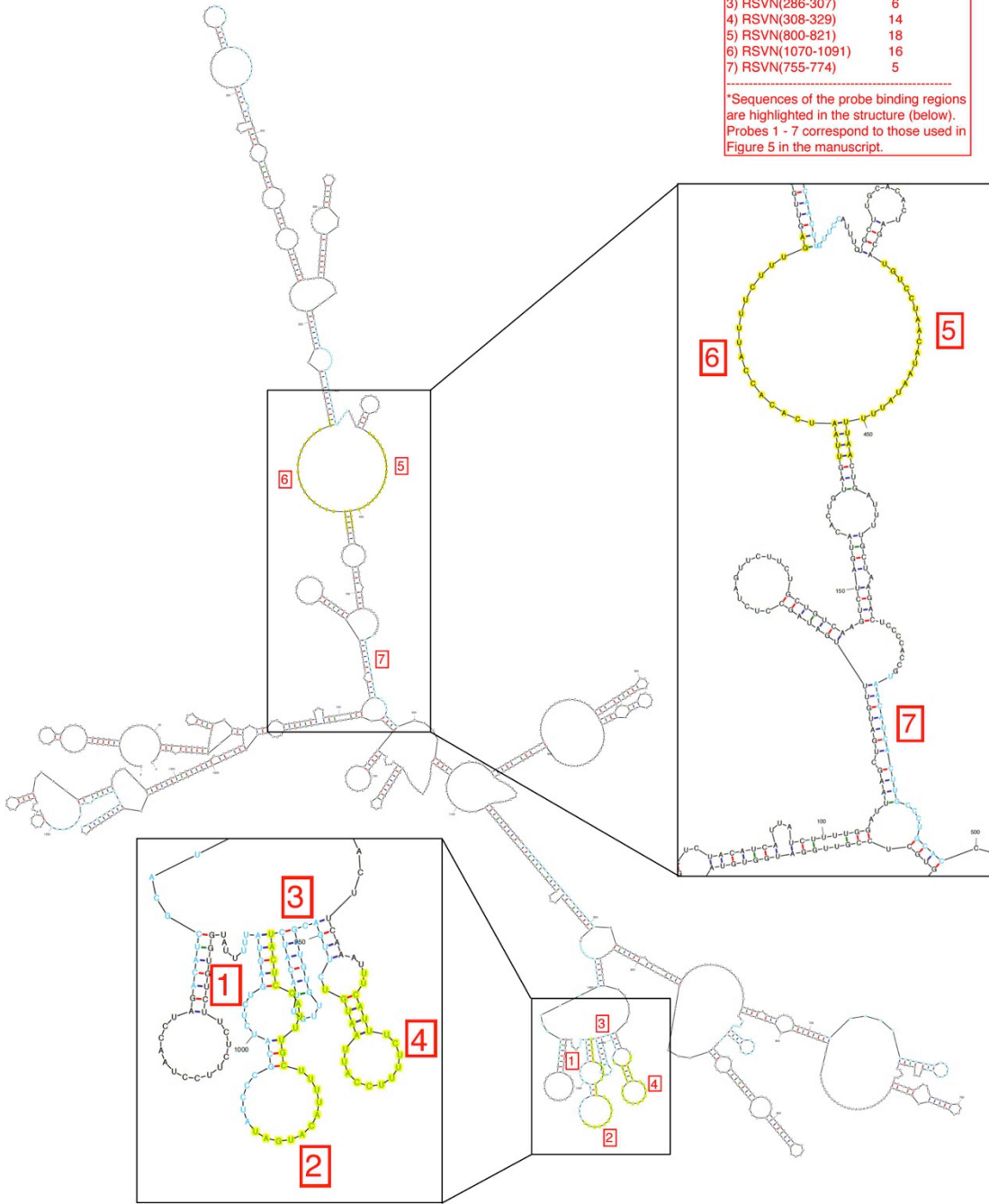
*Sequences of the probe binding regions are highlighted in the structure (below). Probes 1 - 7 correspond to those used in Figure 5 in the manuscript.



$dG = -276.80$ [Initially -325.80] RSV A2 N gene [1 - 1331]

MFOLD structure 4	
*Probed regions	Unpaired Bases
1) RSVN(242-263)	13
2) RSVN(264-285)	15
3) RSVN(286-307)	6
4) RSVN(308-329)	14
5) RSVN(800-821)	18
6) RSVN(1070-1091)	16
7) RSVN(755-774)	5

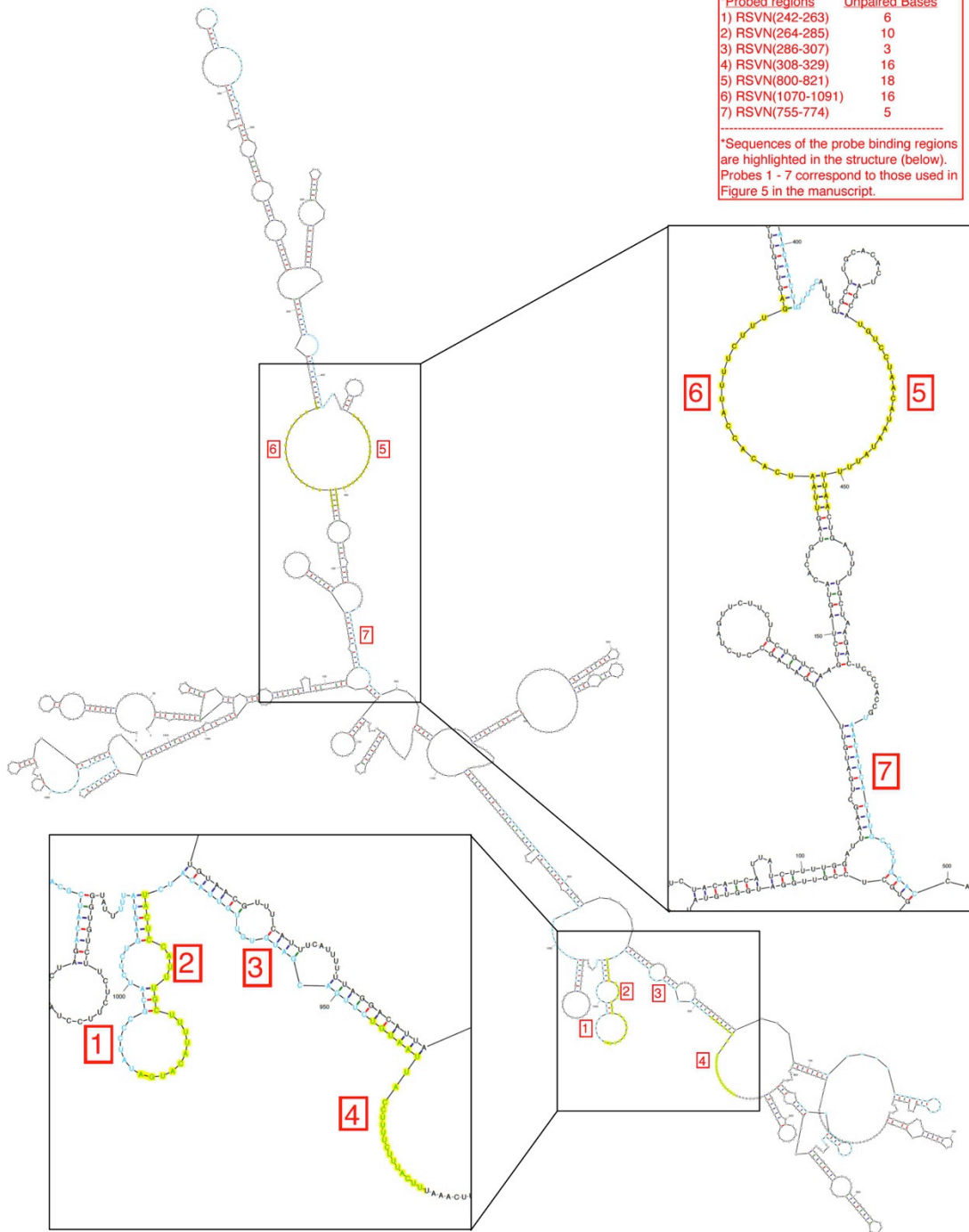
*Sequences of the probe binding regions are highlighted in the structure (below).
Probes 1 - 7 correspond to those used in Figure 5 in the manuscript.



$dG = -279.61$ [Initially -325.10] RSV A2 N gene [1 - 1331]

MFOLD structure 5	
*Probed regions	Unpaired Bases
1) RSVN(242-263)	6
2) RSVN(264-285)	10
3) RSVN(286-307)	3
4) RSVN(308-329)	16
5) RSVN(800-821)	18
6) RSVN(1070-1091)	16
7) RSVN(755-774)	5

*Sequences of the probe binding regions are highlighted in the structure (below). Probes 1 - 7 correspond to those used in Figure 5 in the manuscript.

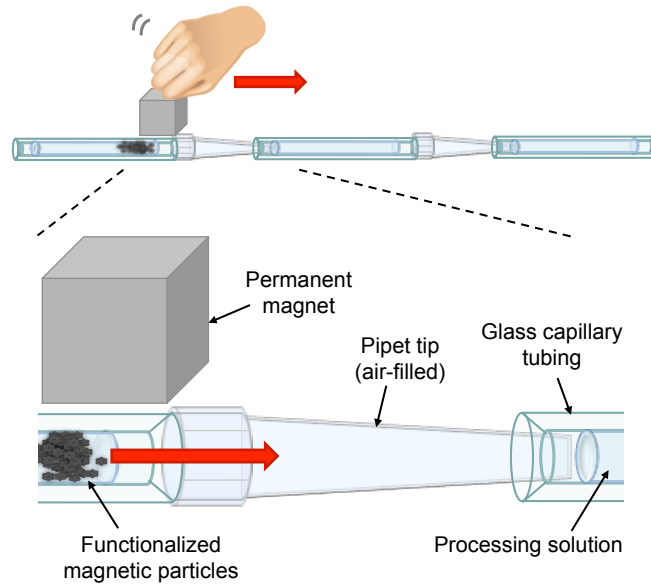


dG = -278.99 [Initially -325.00] RSV A2 N gene [1 - 1331]

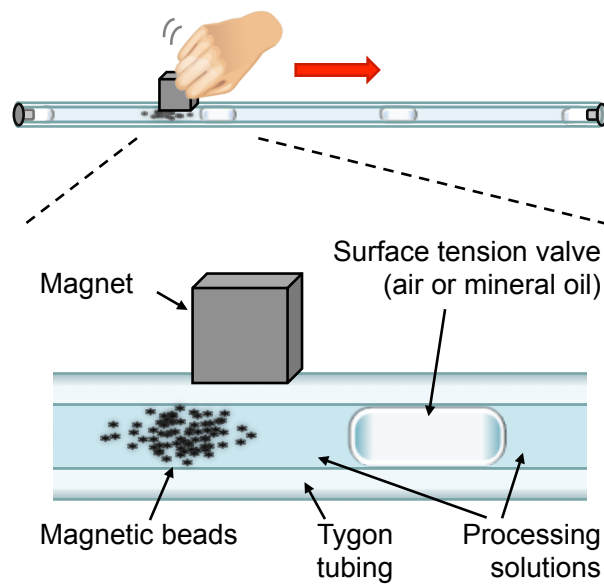
Appendix B.

Illustrations of Concepts and Designs for Biomarker Extraction and Detection

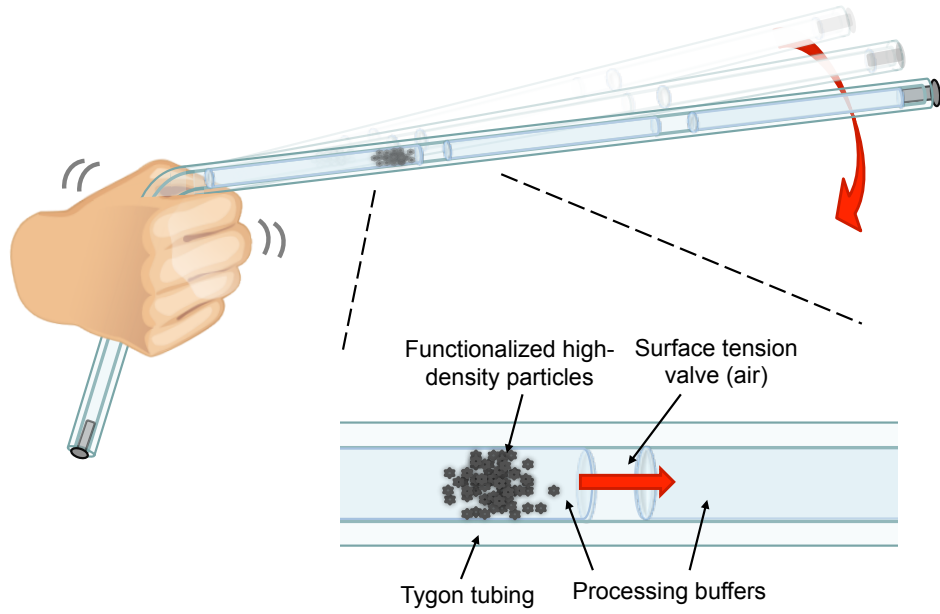
Original “Extractionator” design using pipette tips to connect solution-filled capillary tubes



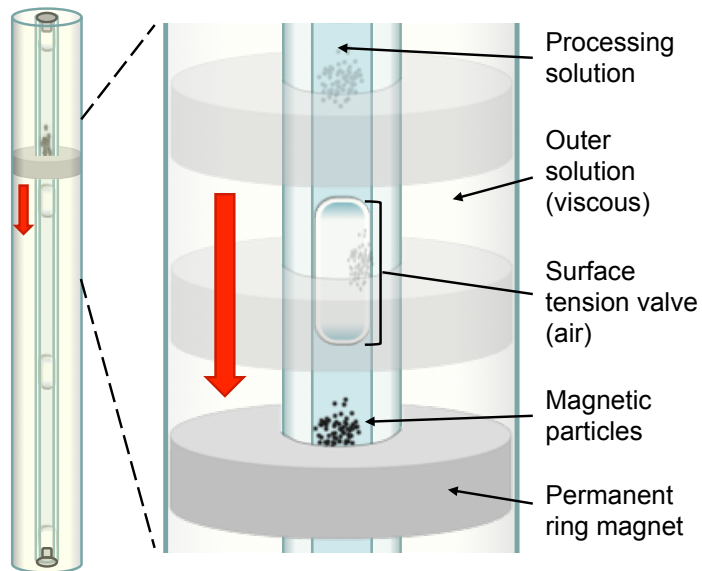
Current manual Extractionator design using a continuous length of plastic tubing



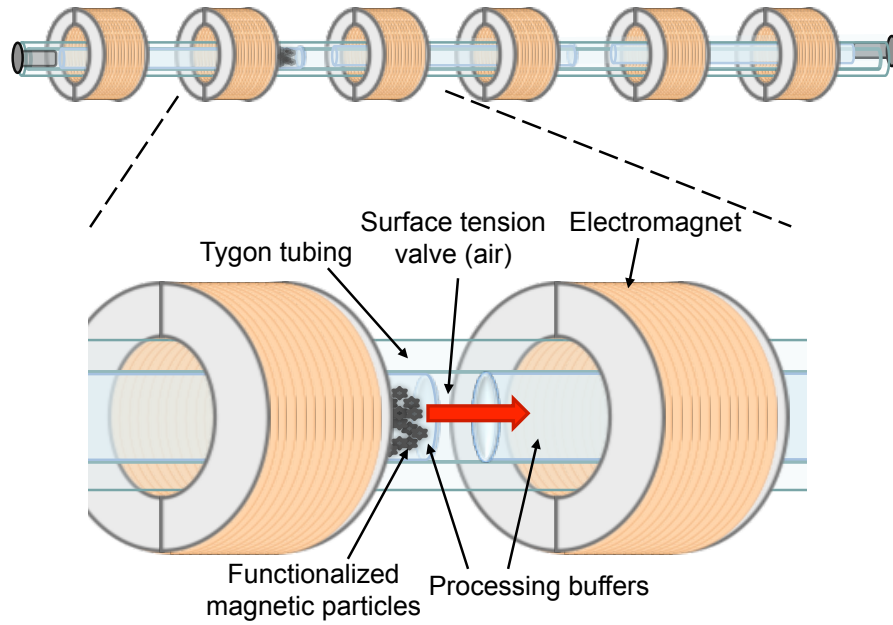
“Whip-It” Extractionator design relying on centrifugal force to transport beads through tube



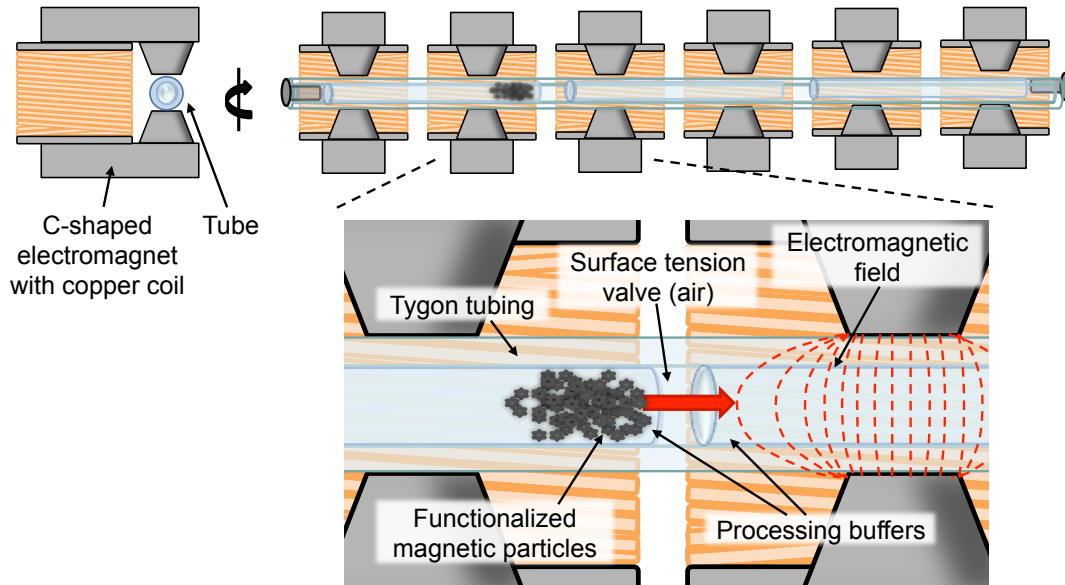
“Egg Timer” Extractionator design for hands-free magnetic transport of beads through tube



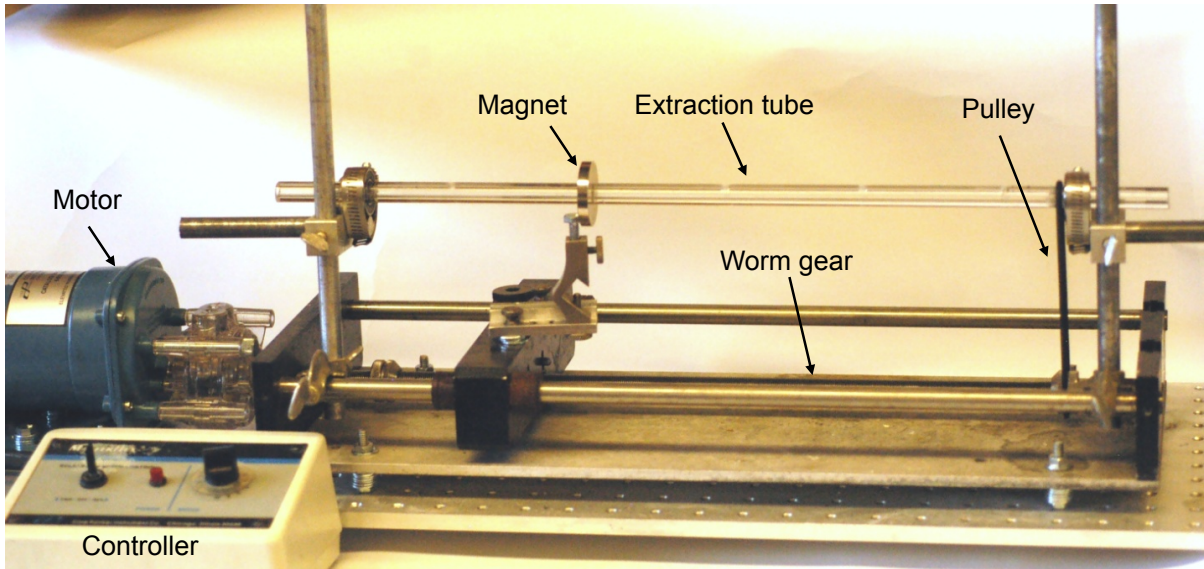
Hollow electromagnet Extractionator design for automated biomarker extraction



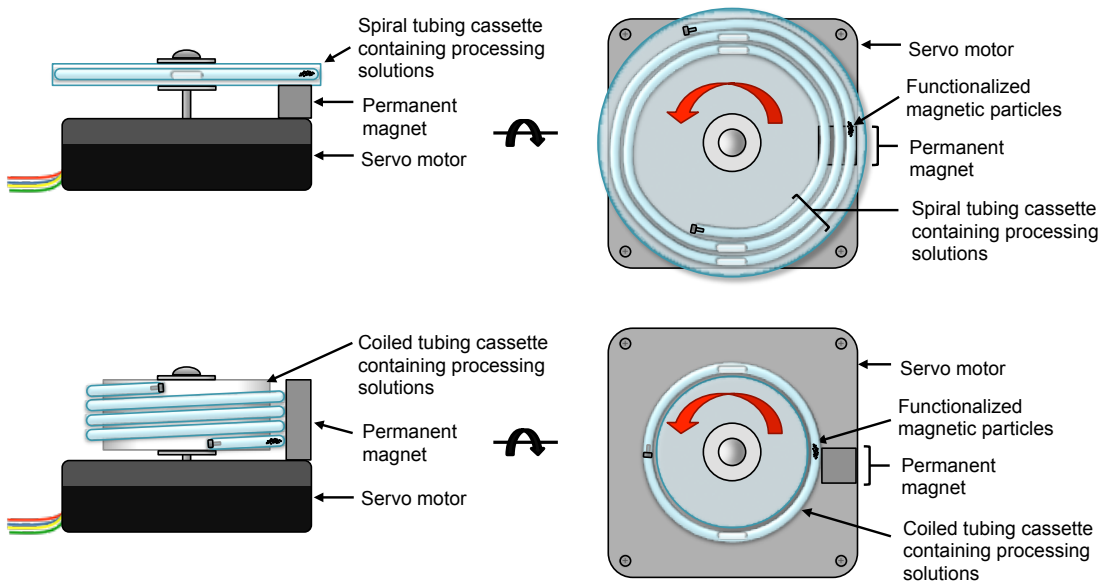
C-shaped electromagnet Extractionator design for automated extraction



“Worm gear” based automated Extractionator prototype based on a linear actuated magnet



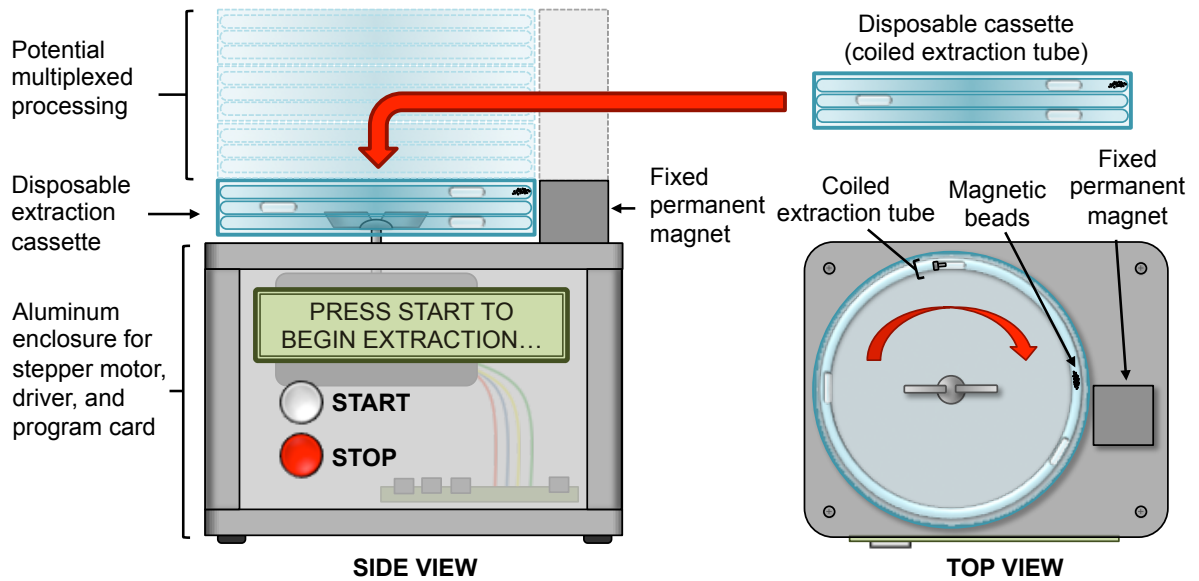
“Washing machine” style automated Extractionator design using a motor to turn coiled tube



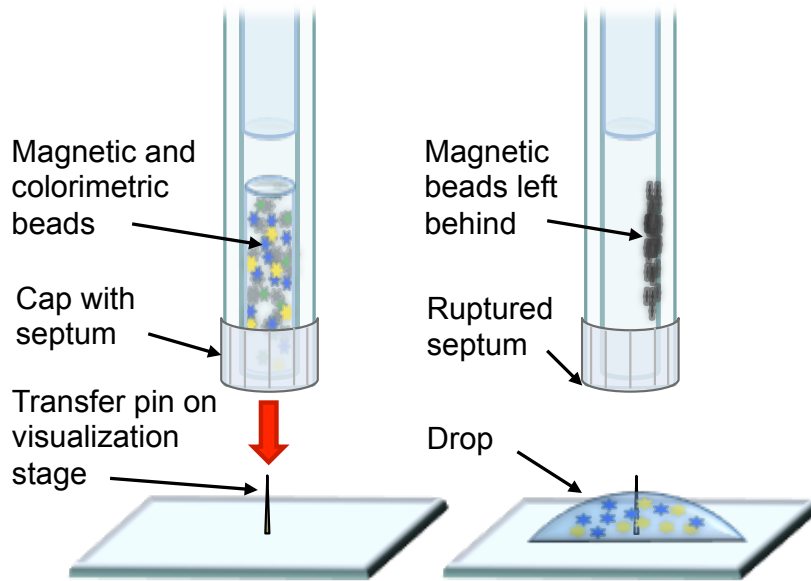
Washing machine style automated Extractionator prototype using a motor to turn coiled tube



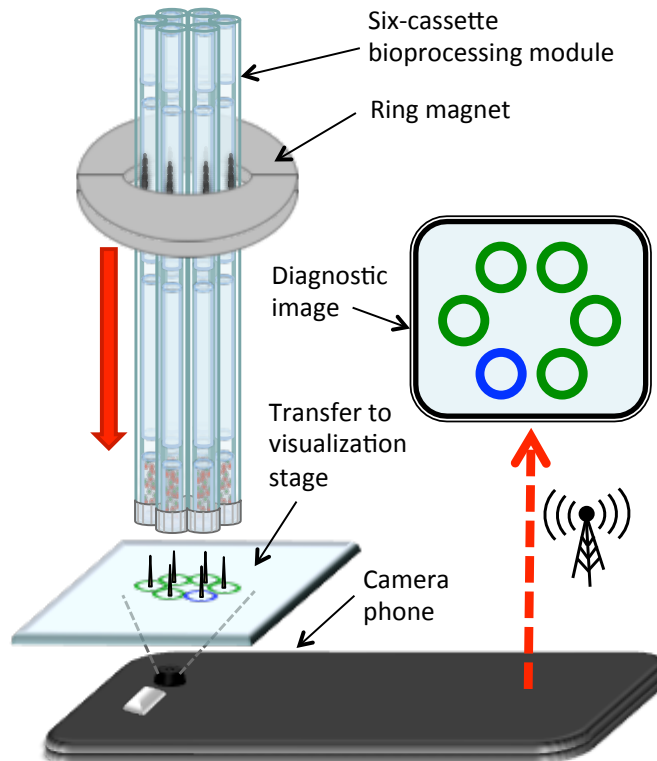
Multiplexed extraction based on the washing machine style automated Extractionator



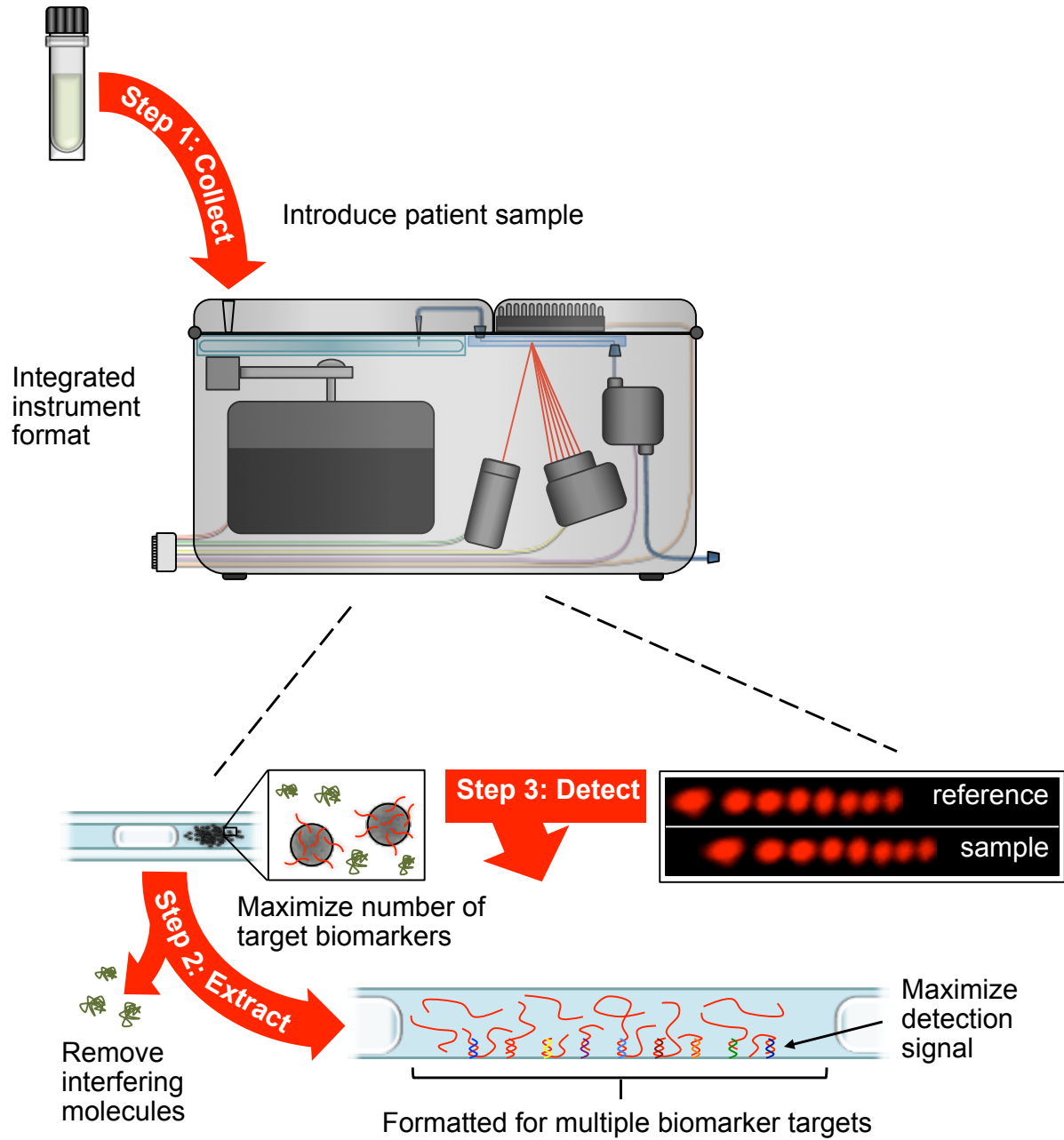
“Drop diagnostics” enabled by Extractionator-based purification and processing



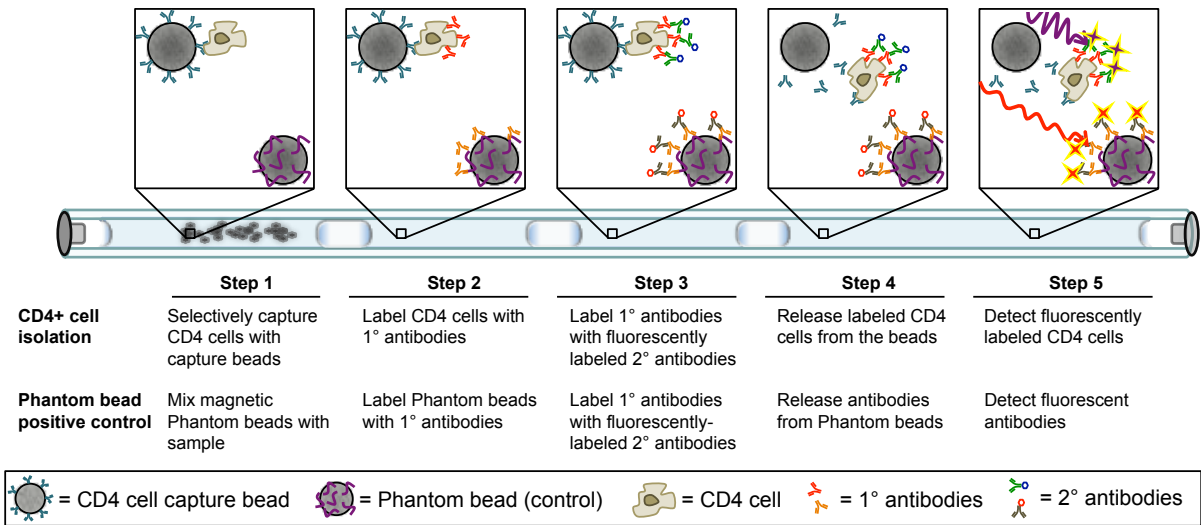
Multiplexed drop diagnostics and mobile result reporting enabled by the Extractionator



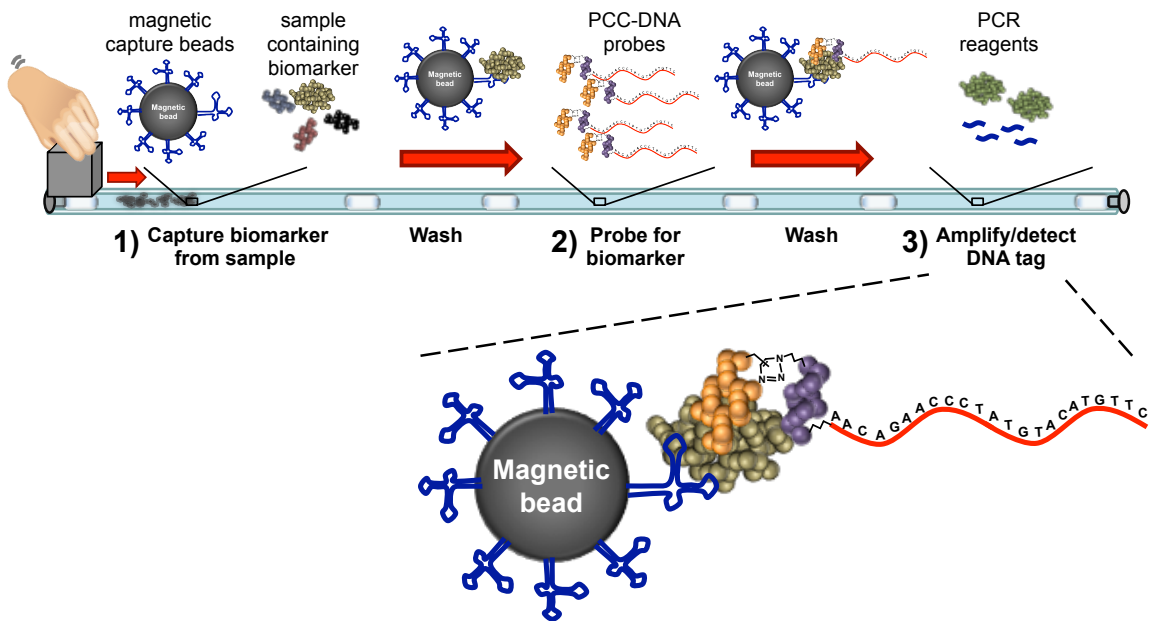
Self-contained extraction and detection device design based on the Extractorator and BSI



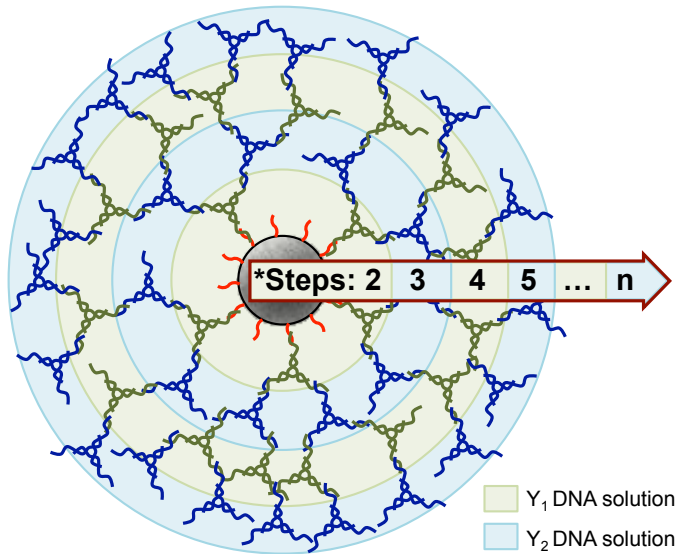
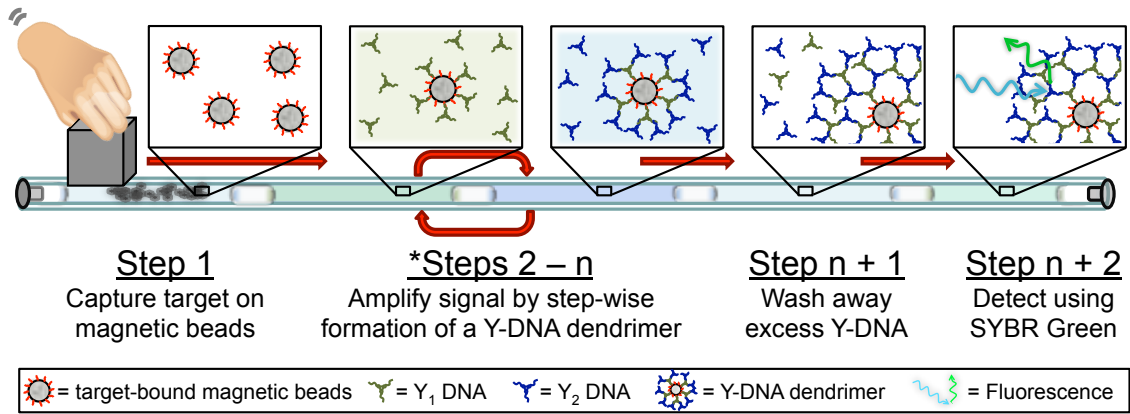
CD4+ cell extraction and “Phantom bead” based detection design using the Extractionator



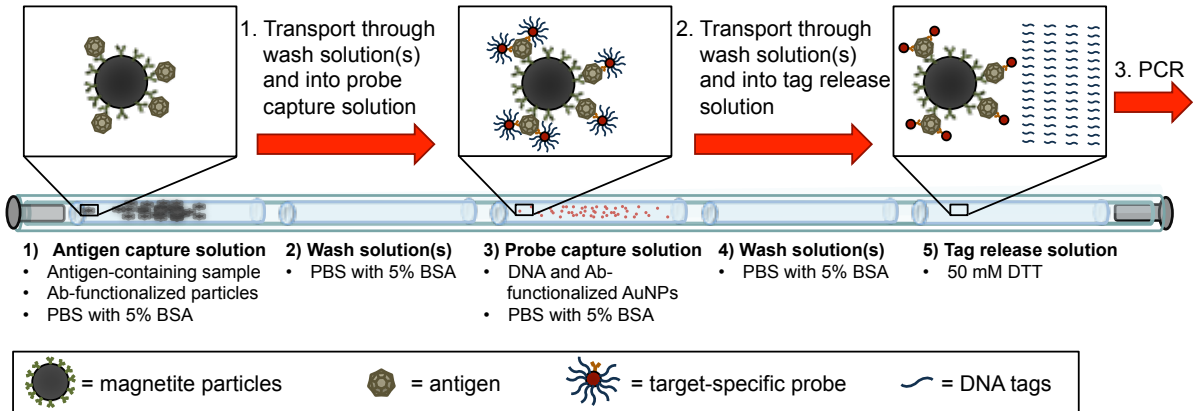
PCR-based detection of protein using DNA-tagged recognition agents and the Extractionator



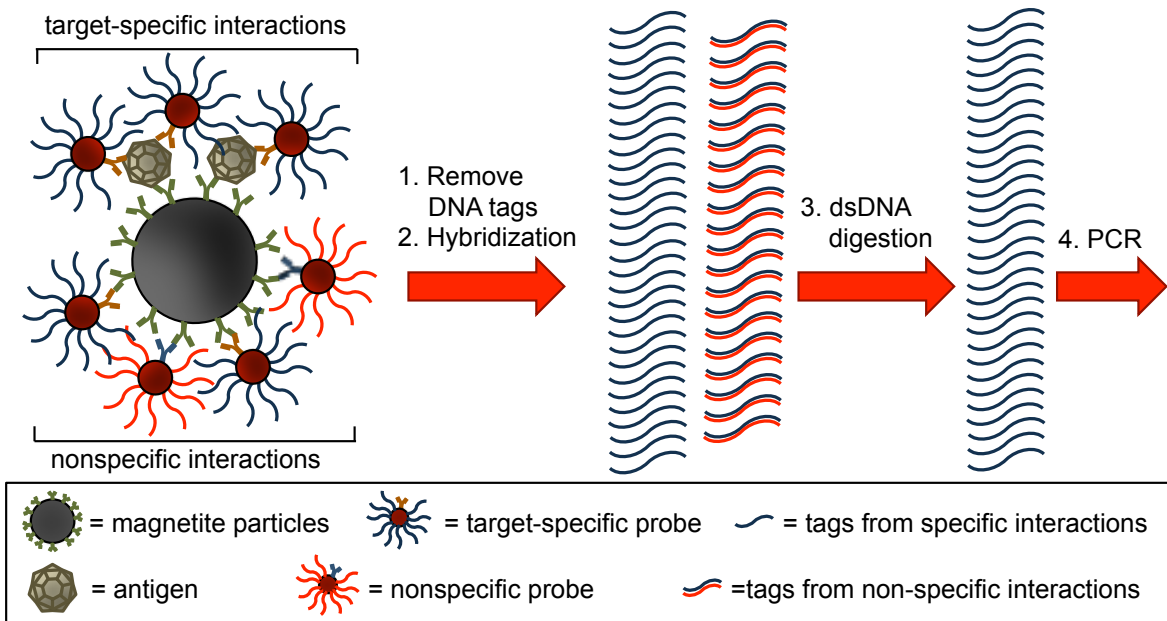
Y-DNA-based amplification design based on the Extractionator



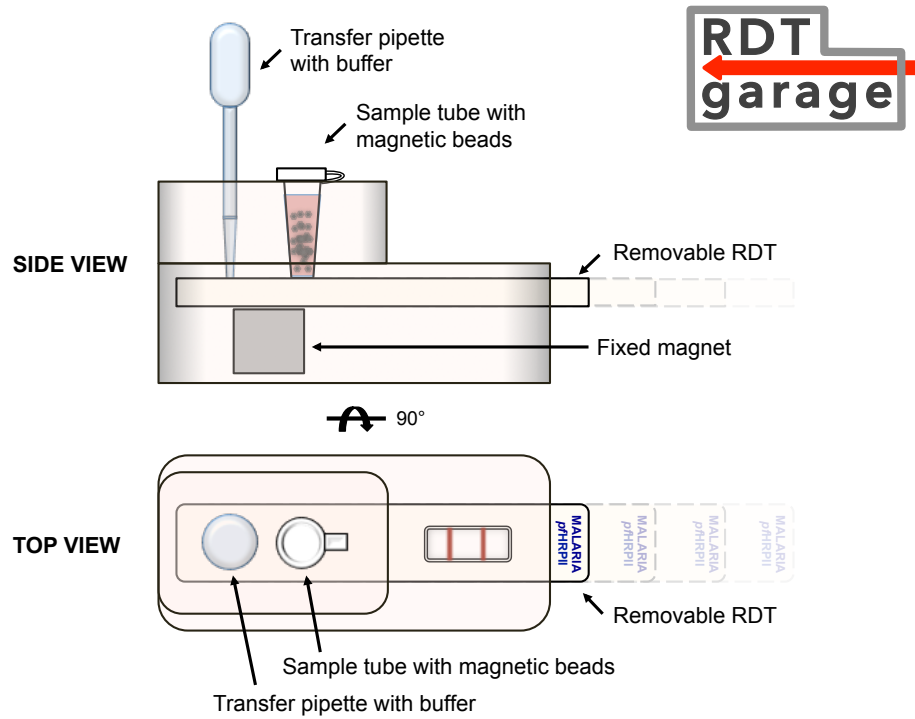
“Amplified Immuno-PCR” assay design using the Extractorator



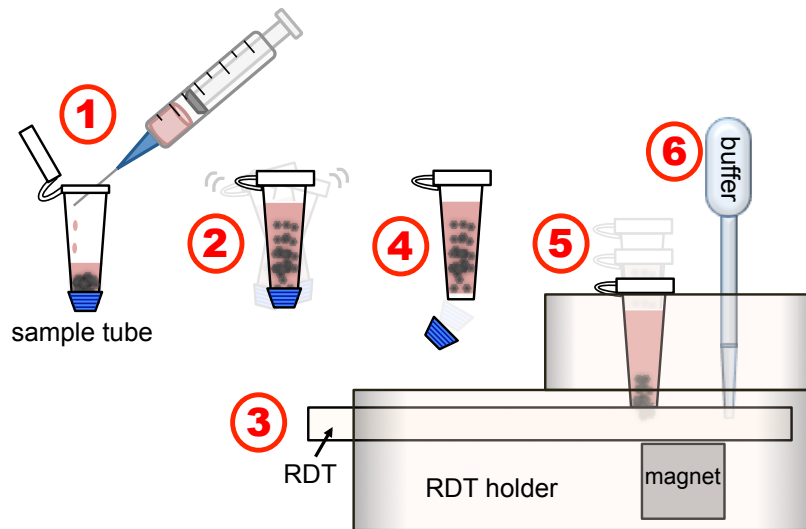
“DNA logic NOT operation” assay design



“RDT Garage” test enhancement based on magnetic bead-based biomarker concentration

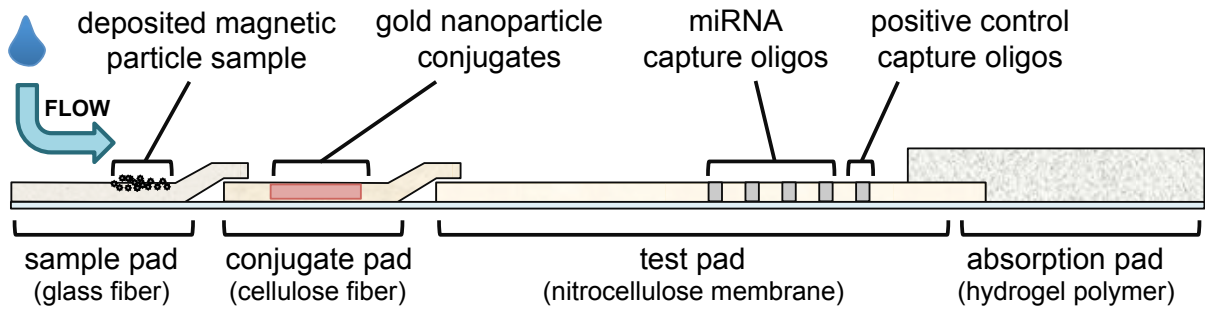


RDT Garage assay workflow



- | | |
|--------------------------------------|--------------------------------------------|
| ① Add sample to tube | ④ Break away tube cap |
| ② Mix sample with magnetic particles | ⑤ Insert tube to transfer particles to RDT |
| ③ Insert RDT into holder | ⑥ Add running buffer |

Lateral flow design for multiplexed microRNA detection



Appendix C.

Nucleic Acid Extraction Protocols and Reagents

RNeasy protocol

- 1) Add 5 μ l of the cell lysate to 350 μ l RLT and 350 μ l 70% EtOH. Vortex.
- 2) Place the lysate in RNeasy column with 2 ml tube. Centrifuge at 8000 g for 15 sec.
Discard flow-through.
- 3) Add 700 μ l RW1. Centrifuge at 8000 g for 15 sec. Discard flow-through.
- 4) Add 500 μ l RPE. Centrifuge at 8000 g for 15 sec. Discard flow-through.
- 5) Add 500 μ l RPE. Centrifuge at 8000 g for 2 min. Discard flow-through.
- 6) Centrifuge at 8000 g in empty 2 ml tube for 1 min. Discard flow-through.
- 7) Add 50 μ l RNase-free water to column and place in 1.5 ml tube. Let sit for 1 min.
Centrifuge at 8000 g for 1 min.
- 8) Discard the column, cap the 1.5 ml tube, and refrigerate at 4 °C prior to PCR.

MagAttract protocol

- 1) Add 5 μ l of cell lysate to 720 μ l RLT and 60 μ l silica-coated magnetic particles. Vortex on level 2 for 5 min.
- 2) Pull magnetic particles to one side with a magnet and remove supernatant. Add 900 μ l MW and vortex.

- 3) Pull magnetic particles to one side with a magnet and remove supernatant. Add 900 μ l RPE and vortex.
 - 4) Pull magnetic particles to one side with a magnet and remove supernatant. Add 900 μ l RPE again and vortex.
 - 5) Pull magnetic particles to one side with a magnet and remove supernatant. Add 1000 μ l RNase-free water while holding the magnetic particles in place with the magnet. Remove the magnet briefly to let the magnetic particles fall into the water, then pull them back to one side with the magnet and remove the water.
 - 6) Add 50 μ l RNase-free water and vortex. Place on the shaker for 5 min. Then refrigerate at 4 °C prior to PCR.
 - 7) Pull magnetic particles to one side with a magnet and collect the eluate.
- *Optional: Pre-heat the RNase-free water for elution to 65 °C.

Original self-contained extraction protocol

- 1) Into one end of 1/16th inch Tygon R-3603 tubing, sequentially pipette three 100 μ l RNase-free water rinses, two 300 μ l RPE washes, and one 300 μ l MW wash, each separated by surface tension valves (short air bubbles).
- 2) Add 5 μ l of cell lysate to 230 μ l RLT and 20 μ l silica-coated magnetic particles. Vortex on level 2 for 5 min.
- 3) Pipette the sample into the end of the tubing, separating it from the MW wash by a surface tension valve. Cap the end with a small PCR tube.

- 4) Cut the tubing off 1 mm from the last water wash on the end of the tubing opposite from the end that the reagents were added. Slide a small PCR tube containing 50 μ l RNase-free water onto the end.
- 5) Gather the magnetic particles from the first solution with a magnet and pull them down the tubing through each wash buffer. Stop in each buffer and mix the magnetic particles by waving the magnet quickly above the tubing before gathering them again and proceeding to the next buffer.
- 6) In each of the three water rinses, remove the magnet briefly to let the magnetic particles fall into the water, then gather them again and proceed to the next rinse.
- 7) Pull the magnetic particles into the small PCR tube containing the 50 μ l water by slightly twisting the tubing back and forth to get the magnetic particles to pass through the slightly constricted end of the tubing.
- 8) Remove the small PCR tube containing the water and magnetic particles from the tubing, cap it, place it into a 1.5 ml tube and vortex it on level 2 for 5 min. Then refrigerate at 4 $^{\circ}$ C prior to PCR.

Nucleic acid extraction reagents

Binding buffer

- 4 M guanidinium thiocyanate
- 25 mM sodium citrate (pH 7.0)

Wash buffer

- 4 M guanidine hydrochloride
- 25 mM sodium citrate (pH 7.0)

*Precipitation buffer**

- 5 mM KPO₄ pH 8.5
- 80% ethanol

*Prepare 1 M K₂HPO₄ and 1 M KH₂PO₄ solutions using RNase-free water.
Mix 9.5 ml of 1 M K₂HPO₄ and 0.5 ml of 1 M KH₂PO₄ to generate 1 M KPO₄ pH 8.5 buffer.

For 100 ml of buffer:

- 0.5 ml 1 M KPO₄ pH 8.5
- 80 ml 100% ethanol
- 19.5 ml RNase-free water
(from Frank Wellmer, "RNA amplification and labeling of RNA probes."
Meyerowitz lab, Caltech. Feb. 2004)

Wash and elution buffers

- Nuclease-free H₂O

Appendix D.

Synthesis of the Respiratory Syncytial Virus RNA Biomarker Protocol

Cell culture

- 1) Scrape some cells of *E. coli* containing the RSV plasmid standard and spread them onto an agar plate containing 50 µg/ml kanamycin antibiotic. Place them in 37 °C incubator overnight.
- 2) Isolate a colony and add it to 25 ml media containing 50 µg/ml kanamycin and shake overnight in an autoclaved 50 ml Erlenmeyer flask at 37 °C.
- 3) 16 - 20 h later, place the cell suspension in a 50 ml conical tube and spin for 15 min at 6,000 g. Aspirate off the media and either freeze at -20 °C or continue onto a QIAGEN plasmid midi prep.

Plasmid midi prep

- 4) Follow the protocol for the QIAGEN plasmid midi kit, starting at step 4.

*Use the ultracentrifuge in the Crowe lab with permission from Fran, the lab manager

*Use 17 ml SORVALL PET tubes for spinning at 20,000 g (see Reagan in the Williams lab)

*The 17 ml SORVALL PET tubes began to crack at 20,000 g once the isopropanol was added (step 13), so step 14 was carried out at 20,000 g in 1.7 ml Eppendorf tubes on the benchtop microcentrifuge

*We air-dried the pellet (step 15) for 20 min, until it didn't appear wet, and resuspended in 500 μ l TE buffer

5) Look up the extinction coefficient of our expected sequence using the online calculator found at <http://www.basic.northwestern.edu/biotools/oligocalc.html>, and, using the absorbance measured at 260 nm, calculated the μ g of DNA.

*Expect \sim 150 ng/ μ l

6) Run \sim 100 ng of the plasmid DNA on a 1% agarose gel to confirm the correct migration of the supercoiled and nicked form of the DNA.

*We use 1 μ l of 180 ng/ μ l DNA

Restriction digest

7) Perform a restriction digest with a restriction enzyme that is downstream from the inserted region according to the manufacturer's protocol (Use 5 - 10 μ g DNA to have enough for the T7 transcription).

*We use 50 μ l of 180 ng/ μ l plasmid DNA (9 μ g), 2 μ l BSA, 20 μ l NEB 4, 8.5 μ l BssHII, and 119.5 μ l water. We place it at 37 $^{\circ}$ C for \sim 2 h.

8) Run \sim 100 ng of the linearized plasmid DNA on a 1% agarose gel to confirm the correct migration/length.

*We run 4 μ l of the product and 1 μ l of the original plasmid on a gel and expect a \sim 1,200 bp fragment

Transcription

9) Perform the optional proteinase K digestion to ensure all RNases are degraded and cleanup with RNeasy

*We stop and clean up the restriction digest by adding 10 μ l 0.5 M EDTA, 20 μ l 3 M sodium acetate, and 400 μ l 100% ethanol to the 200 μ l digestion, putting it at -20 °C for 15 min, centrifuging at 21,100 g for 15 min, carefully removing the supernatant, resuspending in 140 μ l TE, and incubating for 2-3 h at 37 °C to dissolve the pellet.

*We add 20 μ l proteinase K to our 140 μ l TE containing our linearized fragment and incubate for 30 min at 50 °C. The proteinase K digestion is then cleaned up using an RNeasy kit, eluting the product in 50 μ l water.

10) Perform a T7 transcription using a MEGAscript kit from Ambion

*We combine 12 μ l of each of the kit reagents to our 42 μ l linearized DNA plus 5 μ l water, and place it at 37 °C for 4 h. The product is cleaned up using RNeasy with the optional on-column DNA digestion.

11) Run the product on a formaldehyde-agarose denaturing gel to ensure the correct migration/length.

*We add 1 μ l RNA to the gel

Appendix E.

HEp-2 Cell Culture Protocol

Media

- 1) Make up media by adding 5 ml 250 µg/ml AmphotericinB, 5 ml 200 mM L-Glutamine, 10 ml FBS, and 500 µl Gentamicin to 500 ml OPTI-MEM media (all of these reagents are purchased at the Core at the correct concentration except Amphotericin, which is sold as a lyophilized powder). Mix well then run it through a sterilization filter.

Starting frozen cells

- 2) Warm media and 1 ml HEp-2 cells (from liquid nitrogen) to 37 °C.
- 3) Add 1 ml HEp-2 cells to 9 ml media and place in a T150 flask. Add 40 ml media and place at 37 °C overnight.

*HEp-2s are relatively tolerant to DMSO; other cell types may require centrifugation to remove DMSO.
- 4) Change the media the next day by aspirating it off and replacing it with 45 ml of pre-warmed media. Let the cells grow for a few days until confluent.

Splitting cells

- 5) Once confluent, aspirate off the media and add 20 ml PBS without Mg²⁺ or Ca⁺. Rock the plate a few times then aspirate off the PBS. Repeat one more time

- 6) Add 5 ml of pre-warmed trypsin and incubate at 37 °C for 5 min. Shake it to remove the cells then add 15 ml media to inhibit the trypsin.
- 7) Add 3-3.5 ml of the cells suspended in trypsin/media to new T150 flasks then add 45 ml media to each flask and place in 37 °C incubator.
- 8) Two days later change the media so that the cells reach confluency with plenty of nutrients present.

Freezing cell stocks

- 9) Once the cells are confluent with fresh media from the day before, they are ready to freeze down.
- 10) For freezing down 4 T150s of cells, prepare 16 1.5 ml freezer tubes labeled with “HEp-2 (cell type), p367 (pass #), ¼ T150 (cell #), date, and initials,” and 8 ml media to resuspend cells and 8 ml media with 10% DMSO to prepare cells for freezing.
- 11) Aspirate media from the cell flasks and wash each flask twice with 20 ml PBS without Mg^{2+} or Ca^{+} .
- 12) Add 5 ml trypsin to each flask, incubate for 5 min, shake cells off flask, then add 15 ml media to each.
- 13) Place cells in 50 ml conical tubes, centrifuge at 100 g for 5 min, remove the supernatant, then combine in 8 ml media.
- 14) Add the media with 10% DMSO dropwise while shaking. The total solution should then consist of 1 ml cells suspended in media with 5% DMSO.
- 15) Add 1 ml cells to each of the 16 tubes, place in the ethanol insulated deep-freeze box, and put in -40 °C for at least 4 h then into the -80 °C freezer for at least 1 h or straight into the

-80 °C for at least 4 h. Then place the samples into the liquid nitrogen, filling out their correct location on the sheet above.

- 16) The next day thaw one of the samples and plate it to check the viability of the frozen cells. Repeat if necessary.

Freezing down cell lysates for RNA analysis

- 17) Prepare a denaturing solution of 4 M guanidinium thiocyanate, 25 mM sodium citrate (pH 7.0) 0.5% *N*-lauroylsarcosine (Sarkosyl), and 0.1 M 2-mercaptoethanol, according to Chomczynski and Sacchi (“The single-step method of RNA isolation by acid guanidinium thiocyanate–phenol–chloroform extraction: twenty-something years on” *Nature Protocols* 1:2 581-585, 2006) as follows:

17a) Dissolve 25.0 g guanidinium thiocyanate in 29.3 ml water at 65 °C.

17b) Add 1.76 ml of 0.75 M sodium citrate (pH 7.0) and 2.64 ml of 10% (wt/vol) Sarkosyl.

*This stock solution can be stored up to 3 months at room temperature.

17c) Add 57.6 µl of 98% 2-mercaptoethanol to 8.0 ml of stock solution.

*This working solution can be stored up to 1 month at room temperature.

CAUTION: Minimize handling of guanidinium thiocyanate (dissolve in the manufacturer’s bottle).

CAUTION: The 2- mercaptoethanol should be handled under a fume hood.

- 18) Prepare about 8 freezer tubes by labeling them “Uninfected HEp-2 cell lysates, 1/8th T150, date, initials.”

- 19) Prepare a freeze bath by getting dry ice from the 3rd floor store room outside and placing it in a small breaker of ethanol.
- 20) Scrape the cells off the flask into the media that they have been growing in. Place it in a 50 ml conical tube.
- 21) Centrifuge at 500 g for 5 min, then aspirate off the supernatant and resuspend in 8 ml denaturing solution and place in a 15 ml conical tube.
- 22) Place the tube in the freeze bath for ~5 min until frozen solid, then place in the 37 °C heat bath for ~5 min until thawed. Repeat this freeze/thaw cycle two more times.
 - 22a) Optional: Centrifuge at 100 g for 5 min and place the supernatant in a new 15 ml conical tube.
- 23) Add 1 ml of the lysate or supernatant to each of the 8 freezer tubes and store at -80 °C.
Record the location of the cell lysate stocks in the notebook on top of the freezer.
***At 100% confluence, there are ~110,000 HEp-2 cells/cm², so a T150 will have ~1.65 × 10⁷ cells.

Appendix F.

Respiratory Syncytial Virus Culture Protocol

Preparing the HEp-2 cells

- 1) Prepare a solution of 5 ml media containing 250 or 500 μl of 1.7×10^6 pfu/ml RSV A₂ (250 μl to if the infection will last 5 days, 500 μl if the infection will last 3 - 4 days).
- 2) Grow HEp-2 cells to 100% confluence in a T150 flask, then aspirate off the media and add the 5 ml media/RSV mixture. Incubate 1 h at 37 °C to allow the virus to attach. Then add 45 ml media and incubate at 37 °C for 3 - 5 days.

Harvesting the virus

- 3) To harvest the virus, prepare about 8 freezer tubes by labeling them “RSV A₂ infected HEp-2s, date, initials.”
- 4) Prepare a freeze bath by getting dry ice from the 3rd floor store room outside and placing it in a small breaker of ethanol.
- 5) Scrape the cells off the flask into the media that it’s been growing in. Place it in a 50 ml conical tube.
- 6) Centrifuge at 500 g for 5 min, then aspirate off the supernatant and resuspend in 8 ml media and place in a 15 ml conical tube.
- 7) Place the tube in the freeze bath for ~5 min until frozen solid, then place in the 37 °C heat bath for ~5 min until thawed. Repeat this freeze/thaw cycle two more times.

- 8) Centrifuge at 100 g for 5 min and place the supernatant in a new 15 ml conical tube.
- 9) Add 1 ml of the supernatant to each of the 8 freezer tubes and store at -80 °C. Record the location of the virus stocks in the notebook on top of the freezer.

Quantifying plaque-forming units

- 10) Grow HEp-2 cells to 100% confluence in a T150 flask. Aspirate off the media, wash twice, trypsinize, and resuspend the cells in a 5 ml trypsin/15 ml media mixture as described in steps 5) and 6) of the “HEp-2 cell culture protocol” above.
- 11) Remove 2.2 ml of the media and resuspend it in 23 ml media in a new 50 ml conical tube. Place 1 ml of the solution into each well of a 24-well plate and incubate for 2-3 days until 100% confluent.

*A 24-well plate has 1/3rd the surface area of a T150, so by taking 2.2 ml, or 1/9th, of the 20 ml and plating it across the 24-well plate, we are plating the cells at 1/3rd confluence.
- 12) To prepare a dilution plate, add 900 µl media to 6 wells of a 24-well plate and place it in the 37° incubator. Also pull out 1 ml of the virus stock and place it in the 37 °C water bath.
- 13) Aspirate the media off the 24-well plate of cultured HEp-2 cells. Add 1 ml PBS without Mg²⁺ and Ca⁺ to each well and let sit while preparing the dilutions.
- 14) Remove the dilution plate from the incubator and the virus stock from the water bath. Add 1 ml virus stock to an empty well. Then add 100 µl virus stock to the first 900 µl media and mix. Then pull 100 µl of that 1/10th dilution and add it to the next 900 µl media and mix. Continue this process until you have five serial dilutions besides the stock. You should also still have 900 µl media without virus added.

15) Aspirate the PBS off the 24-well plate and add 100 μ l plain media, without virus added, to the six wells along the first column. Add 100 μ l of the stock virus to the three other wells in the first row, 100 μ l of the 1/10th dilution to the three other wells of the second row, and so on until all six rows have serial dilutions of the virus. Label the plate with the dilutions used and write “RSV A₂ infected, (date),” then place them in the incubator for 1 h. Place the media containing methyl cellulose in the 37 °C water bath.

*Media containing methyl cellulose is prepared in advance by adding 3.75 g methyl cellulose and a stir bar to a 500 ml bottle and autoclaving. After autoclaving, add 500 ml sterile filtered media, stir overnight, and store at 4 °C.

16) After 1 h, add 1 ml methyl cellulose to each well and place in the 37 °C incubator for 3-5 days.

17) Count the plaque-forming units (pfus) by aspirating off the methyl cellulose and washing once with PBS without Mg²⁺ or Ca⁺. Aspirate off the PBS wash.

18) Add 1 ml of 80% methanol at -20 °C to each well and place at -20 °C for 1 h.

19) Make up a solution of 5% powdered milk (w/v) in PBS. Flick off the methanol, wash once with PBS, flick off the PBS, and then add 250 μ l of the 5% powdered milk solution and shake for 1 h at room temperature.

20) Flick off the 5% powdered milk solution and add 150 μ l of 30 μ g/ml primary antibody in 5% powdered milk solution (1:1000) to each well of the plate (for example, add 7.5 μ l of 30 mg/ml “F-mix” to 7.5 ml PBS, then add 150 μ l to each well of the plate). Let it shake at room temperature for 1 h.

21) Aspirate off the primary antibody, wash three times in PBS, remove the last wash by aspirating, and add 150 μ l of 0.5 μ g/ml secondary antibody in the 5% powdered milk

solution (1:2000) to each well of the plate (for example, add 3.75 μ l of 1 mg/ml “Antimouse HRP” to 7.5 ml PBS, then add 150 μ l to each well of the plate). Let it shake at room temperature for 1 h.

22) Aspirate off the secondary antibody, wash three times in PBS, remove the last wash by flicking, and add 150 μ l of TrueBlue peroxidase substrate to each well. Let it sit for 15-30 min at room temp.

23) Count the plaques in the row of wells that have the best resolution, and then calculate the pfus/ml of the stock by multiplying the average number counted in the row with the best resolution of plaques by $10^{(\text{row\#})}$.

Appendix G.

RNA and DNA Gel Electrophoresis Protocol

DNA gels

- 1) For a 1% agarose DNA gel, add 0.65 g agarose into 65 ml 1× TBE buffer. Place in microwave for 2 - 3 min, checking it every 10 - 30 sec. Allow it to cool until it is almost too hot to handle. If using ethidium bromide to stain the DNA, add 1 µl to warm agarose solution. Pour the gel into a gel casting tray, add a gel comb, and let it set up for 20-30 min.
- 2) Prepare the samples on a piece of Parafilm by mixing 50 - 150 ng DNA or 2 µl DNA ladder with 2 µl 6× loading buffer, 1.2 µl (10×) SYBR gold, and enough water to make 12 µl total volume. Load into the wells of the gel.
- 3) Run the gel at 120 V for 60 - 90 min.
- 4) Image on the Bio Doc-it gel imaging box using 302 nm wavelength UV.
- 5) Access the images by using the IP address (<ftp://10.8.68.153>), insert “biodocit” as the user name, leaving the password blank, and open the ftp files.

RNA gels

- 1) For a denaturing 2% formaldehyde-1.2% agarose RNA gel, add 0.78 g agarose into 55 ml water. Place in microwave for 2 - 3 min, checking it every 10 - 30 sec. Allow it to cool until it is almost too hot to handle. Add 3.5 ml 37% formaldehyde and 6.5 ml 10× MOPS

to the warm agarose solution. Perform the rest of the procedures in a hood. Pour the gel into a gel casting tray, add a gel comb, and let it set up for 20 - 30 min.

- 2) Prepare RNA gel loading buffer with 50% deionized formamide (deionize by stirring 100 ml formamide with 1 g Dowex MR3 for about 1 h in the hood), 7% formaldehyde, 0.5 mg/ml ethidium bromide, 1 mM EDTA, 20% glycerol, 1× MOPS, and 0.25% Bromophenol blue. Store deionized formamide and running buffer aliquots at -20 °C.
- 3) Prepare the samples on a piece of Parafilm by mixing 50 - 150 ng RNA or 1 - 2 µl DNA ladder with 15 µl loading buffer for 18 µl total volume, heat to 65 °C for 15 min, cool at 4 °C for 15 min, then load into the wells of the gel.
- 4) Run the gel at 60 V for 60 - 90 min.
- 5) Image on the Bio Doc-it gel imaging box using 302 nm wavelength UV.
- 6) Access the images by using the IP address (<ftp://10.8.68.153>), insert “biodocit” as the user name, leaving the password blank, and open the ftp files.

Appendix H.

Circular Dichroism Spectroscopy of Nucleic Acids Protocol

Starting the spectrophotometer

- 1) Open the liquid nitrogen valve to the instrument. Check that the flow into the instrument is correct using the gauges on the side on the instrument. Let purge for 20 minutes.
- 2) Turn on the “lamp power and cooling switch” and wait for the “lamp ready light” to turn on.
- 3) Press the red “start button” to fire the lamp. Check that the lamp is drawing current using the red LED indicator on the side of the instrument. If it is not drawing current, wait for the “lamp ready light” to turn on again, and repeat the process until the red LED indicator shows that it is drawing current.
- 4) Turn on the “CPU and Instrument switch.” no password is required. Start the CD-215 software by clicking on the icon on the desktop.

Running an experiment

- 5) Prepare the oligonucleotide at a concentration that would result in an optical density between 0.8 to 1, or at a base concentration of approximately 100 μM .
- 6) Insert the sample or blank into a clean 1.0 mm path length quartz cuvette, and place the cuvette in the sample holder of the instrument.

- 7) Set experiment parameters by clicking on “Select Experiment Configuration.” Enter the information for the experiment. Common experimental parameters for nucleic acids include: wavelength set from 320 nm to 200 nm, temperature set at 25.0 °C, wavelength step set at 0.5 nm, bandwidth set at 1.0 nm, and averaging time set at 1 second. Three to five scans is sufficient.
- 8) Select Data Set / Save Options, then click on Exit / Save Configuration.
- 9) Click on “Run Experiment” and wait approximately 20 minutes for three scans.
- 10) Once the scans are completed, the “Save Experiment Panel” will appear. Save the experiment. Saving, exporting, and loading data is done through the Data Browser under the Displays Menu.

Working up the data

- 11) Make sure the graph is displaying wavelength (Displays > Data Review > Wavelength).
- 12) Click File > Load Data Set. Read Data Set from disk. Find the first .DAT file to analyze.
- 13) Click Axis Definitions > Clear left Axis Definition. Clear all.
- 14) Axis Definitions > Left- Multi-Data Set. Select all three or five scans of the .DAT file.
- 15) Axis Definitions > Data Review Average. Select all three and click “average selected.”
Name the data set “(experiment) average” and click “Save average trace.”
- 16) Repeat steps 12) through 15) for the blank measurements and all the samples.
- 17) Click Math Operations > Wavelength experiment. Select data set A, find “(experiment) average.” Operation > smoothing. Data set name > “(experiment) smooth.” Click calculate.
- 18) Repeat step 17 for the blank measurements and all the samples.

- 19) Math operations > wavelength experiment. Select data set A, find the sample “(experiment) smooth.” Select data set B, find the blank “(experiment) smooth.” Operation > subtract data sets. Data set name > “(experiment) subtracted.” Click calculate.
- 20) File > load data set. Find “(experiment) subtracted” from list. Export data set > export to ASCII text.
- 21) If needed, the y-axis can be converted into molar ellipticity. Math operations > wavelength. Select data set A, find “(experiment) subtracted.” Operation > convert to Molar Ellipticity. Dataset name “(experiment) molar ellipticity.” Click calculate.

Turning off the spectrophotometer

- 22) Close the software and shut down windows. Turn off the “Lamp Power and Cooling Switch,” then the “CPU and Instrument Switch.”
- 23) Let liquid nitrogen flow through the system for an additional 5 - 10 minutes.
- 24) Turn off the liquid nitrogen.

Appendix I.

Nanomaterial Functionalization and Evaluation Protocols

Functionalizing 15 nm AuNPs with molecular beacons

Coupling

- 1) Aliquot 16 ml AuNPs into 16 Epp tubes, 1 ml per tube. Spin them down at full speed (21,000 g) for 20 min.
- 2) Remove as much of the supernatant as possible (save it in a 15 ml conical tube), and combine the samples.
- 3) Measure the absorbance of the concentrated samples by diluting 1 μ l of it into 99 μ l of the saved supernatant. Using the saved supernatant as a blank, measure the absorbance at 522 nm (wavelength). According to Beer's law, the absorbance equals molar absorptivity (L/mol cm) multiplied by path length (cm) multiplied by concentration (mol/L): $A=ebc$ ($e=3.64 \times 10^8$ for 15 nm AuNPs, and $b=1$ for most cuvettes). Calculate the concentration, and multiply it by 100 to get the concentration of the concentrated solution of AuNPs: $c=(A \times 100)/3.64 \times 10^8$.
- 4) Make a solution of 10 nM AuNPs and 2 μ M thiolated DNA in 1 ml dH₂O, cover it in foil (molecular beacons have a fluorophore), and let it rotate at least 2 h (preferably overnight).

*Mixing in 8 μ M thiolated PEG improved the ability for the molecular beacons to open.

*Overnight may be detrimental because the DNA might reform disulfide bonds

- 5) Add 110 μ l 0.1 M phosphate buffer (pH 7), 1.1 μ l Tween 20, then 22.2 μ l 5 M NaCl dropwise (half at a time, then vortex). Let it rotate for 2 h.
- 6) Add 22.4 μ l 5 M NaCl dropwise (half at a time, then vortex). Let it rotate for 2 h.
- 7) Add 22.6 μ l 5 M NaCl dropwise (half at a time, then vortex). Let it rotate for 2 h. The sample is now at 0.3 M NaCl. Save the sample at room temp overnight, or at 4 °C over a weekend, until cleanup.
- 8) Make a solution of 10 mM phosphate buffer pH 7, 0.3 M NaCl, 0.02% Tween 20 (4 ml 0.1 M phosphate buffer pH 7, 2.4 ml 5 M NaCl, and 0.8 ml Tween 20 into 32.8 ml dH₂O).
- 9) Centrifuge the fAuNPs at 13,300rpm for 15 min, remove the supernatant, and resuspend in the solution described in 8) above. Repeat two more times. Save the cleaned fAuNPs at 4 °C until further analysis.
- 10) Measure the concentration of the fAuNPs as described in 3) above, without diluting the sample 1/100, and using 522 nm wavelength.

Quantifying the number of molecules attached

- 11) Make reducing buffer as follows: mix monobasic phosphate buffer with dibasic phosphate buffer to get a pH of 8.3. Dissolve 0.617 g DTT into 40 ml of the phosphate buffer pH 8.3.
- 12) Take 150 μ l of the fAuNPs and spin them down at 13,300rpm for a few minutes. Remove the supernatant and resuspend in 30 μ l water. Measure the concentration of the fAuNPs as described in 3) above.
- 13) Aliquot the 30 μ l into three tubes and dilute it 10-fold into reducing buffer. Rock/shake the solutions for 1 h.

- 14) Set up a range of standard curve dilutions of known concentrations of the molecule that is attached to the AuNPs in 10% water and 90% reducing buffer. The range should contain the estimated concentration of the molecules on the AuNPs (For example, if you measured a concentration of fAuNPs of 50 nM in step 12) above, then you should have 5 nM fAuNPs. If you estimated about 100 molecules are attached to each AuNP, then you should have 500 nM molecules in solution after 1 h in reducing buffer. The standard curve dilutions could then be set up at 1000 nM, 800 nM, 600 nM, 400 nM, 200 nM, 100 nM, and 10 nM.)
- 15) After the 1 h in reducing buffer, spin the three samples at 21,000 g for a few min. Place 50-150 μ l of each sample to a well of a black 96-well plate. Add the same amount of the seven dilutions of the standard curve.
- 16) Turn on the Bio-TEK plate reader and wait for it to leave the plate reader out. Open the KC4 software, click "Wizard," click "Reading Parameters," select the correct excitation and emission wavelengths and the correct lanes, then click "Okay." Click "Layout," select the wells to be read, and click "Okay." Click "Okay," then click "Read." Repeat with a higher intensity if required. Plot the curve in Excel and do a linear regression, show the R^2 and the slope equation. Average the three sample values and plot them on the curve to determine the concentration of molecules. Divide by the fAuNP concentration to determine the number of molecules/AuNP.

Measuring limits of detection

- 17) Adjust the concentration of the target/complement strand of ssDNA to 10 \times , 1 \times , and 0.1 \times the known concentration of probe/molecular beacon on the AuNP (= concentration of

AuNPs × number of probes/molecular beacons per AuNP) by diluting it into PBS without Mg^{2+} or Ca^{+} .

- 18) Add 50 μ l of the fAuNPs plus 50 μ l target of each dilution (10 \times , 1 \times , and 0.1 \times), 50 μ l of fAuNPs plus 50 μ l PBS, and 100 μ l PBS in triplicate into a black 96-well plate. Cover the plate in foil and place on a shaker for 1 h.
- 19) Measure the fluorescence of the plate using the Bio-TEK plate reader as described in step 16) above.

Functionalizing magnetic microparticles with antibodies

Coupling

- 1) Wash 200 μ l amine derivatized 1 μ m magnetic microparticles three times with coupling buffer (50 mM phosphate buffer (pH 7.0), 0.15 M NaCl, and 5 mM EDTA) by pulling the particles to one side with a magnet, removing the supernatant and resuspending in fresh coupling buffer.
- 2) Activate the 200 μ l MMPs with 20 μ l of 1 mM Sulfo-SMCC (2 mg Sulfo-SMCC into 4.58 ml nuclease-free water). Rotate for 1 h, then wash 3 times with coupling buffer.
- 3) During the 1 h Sulfo-SMCC incubation, reduce 15 μ l of 30 mg/ml purified antibodies in PBS using 15 μ l of 1.2 mM DTT (2 mg into 10.8 ml PBS). Rotate for 30 min, then clean up using a NAP-5 column according to the manufacturer's guidelines. Catch the elution fractions (drops) in a 96 well plate, measure absorbance at 280 nm on the plate reader, and combine the 4 - 5 fractions with the highest absorbance.
- 4) Add the combined fractions of purified antibody to 100 μ l Sulfo-SMCC-activated MMPs. Rotate for 1 h, then wash 3 times with coupling buffer.

Validation by sandwich ELISA

- 5) Add 100 μ l of a 1:5,000 dilution of Synagis antibody to 9 or more wells of a 96 well UV-transparent plate. Shake for 1 h, then wash the wells 3 times with PBS.
- 6) Add 300 μ l of 5% BSA to each well to block for 1 h on a shaker. Don't wash.
- 7) Flick the BSA out, then add 100 μ l triplicates of either RSV infected HEp-2 cells, uninfected HEp-2 cells, media, or any other control. Shake for 1 h, then wash the plates 3 times with PBS.
- 8) Add a solution of 5 μ l of F mix conjugated magnetic microparticles plus 95 μ l of 5% BSA to each well. Shake for 1 h, then wash times with PBS.
- 9) Add 100 μ l of a 1:1,000 dilution of goat anti-mouse HRP secondary antibody to each well. Shake for 1 h, then wash 5 times with PBS.
- 10) Add 100 μ l of True Blue peroxidase to each well. Shake for 10 min, then quench with 100 μ l of 2 M H₂SO₄.
- 11) Read the absorbance at 450 nm for each well.

Coupling of antibodies and DNA to gold nanoparticles

Coupling

- 1) Reduce the disulfides present in the thiolated DNA solution by adding 100 nM DTT and 0.1 M phosphate buffer (pH 8.3). Rotate for 30 min. Desalt using Microcon YM-3 centrifugal filters. Elute in TE buffer and store at -80 °C.

- 2) Add 35 μl of 0.2 mg/ml Synagis antibody to 10 ml of a stock concentration (2.3 nM) of 15 nm gold nanoparticles at pH 9.3 (Slowly add 10 - 20 μl 1 M NaOH to the nanoparticles while monitoring the pH). Rotate for 30 - 45 min.
- 3) Add 50.8 μl of 107 μM of activated DNA to the 10 ml antibody/AuNP solution. Rotate for 45 min.
- 4) Slowly add 200 μl of 0.1 M NaCl (200 μl of 5 M NaCl), 10 mM phosphate buffer (63.4 μl of 1 M disodium phosphate and 39.6 μl of 1 M monosodium phosphate), and 0.02% Tween 20 (1 μl) to the antibody/DNA/AuNP solution. Rotate for 1 h.
- 5) Slowly add another 0.1 M NaCl (206 μl of 5 M NaCl) solution to make 0.2 M NaCl. Rotate for 1 h.
- 6) Slowly add another 0.1 M NaCl (210 μl of 5 M NaCl) solution to make 0.3 M NaCl. Rotate for 1 hor overnight.
- 7) Wash the antibody/DNA fAuNPs 3 times by spinning down at 21,100 g for 20 min and resuspending in 0.3 M NaCl, 10 mM phosphate buffer, and 0.02% Tween. Remove the third wash, and leave the fAuNPs at that concentration. Measure the absorbance at 260 nm of a 1:50 dilution using the nanodrop and calculate the concentration using $C=(A \times 50)/(3.64 \times 10^8 \times 0.1)$.

Tagging and tag validation

- 8) Heat 500 μl of a 10 nM fAuNP sample at 95 $^{\circ}\text{C}$ for 10 min to remove nonspecific binding, then wash and resuspend in new buffer.

- 9) Add 2 μM of tag DNA (10.89 μl of 107 μM RSV_76) to 10 nM AuNPs, or to buffer for a control, in 0.3 M NaCl, 10 mM phosphate buffer, and 0.02% Tween at a total volume of 500 μl . Rotate overnight.
- 10) The next day, spin the solutions at 16,100 g for 30 min and measure the concentration of DNA present in 90 μl of the supernatant using the Agilent 8453 UV-Vis at 260 nm (The difference between the concentration of tag DNA in the solution containing tag and buffer and the tag DNA in the solution containing tag, fAuNPs, and buffer is an indicator of how much tag DNA bound to the fAuNPs).
- 11) Wash the AuNPs 3 times by spinning down at 21,100 g for 20 min and resuspending in 0.3 M NaCl, 10 mM phosphate buffer, and 0.02% Tween. Calculate the concentration and dilute to 10 nM (~500 μl).
- 12) Heat 100 μl of 10 nM AuNPs with tag and 100 μl of 10 nM AuNPs without to 95 $^{\circ}\text{C}$ for 10 min, then spin down at 21,100 g for 15 min.
- 13) Remove the supernatant and record the absorbance on the Agilent 8453 UV-Vis at 260 nm to calculate the concentration of tag that was released by heating.

Quartz crystal validation of antibody-AuNP attachment

- 14) Clean a 5 MHz Au/Cr or Au/Ti quartz crystal by washing it 3 times for 5 min in Piranha (3 H_2SO_4 :1 H_2O_2), rinsing it in water and ethanol between washings. Dry the crystal after rinsing in ethanol with nitrogen.
- 15) Place the crystal with the large-circle-side up, resting the metal surfaces on the electrodes of the Maxtek, Inc. Research Quartz Crystal Microbalance. Tighten the lid then place on

the ring stand with the inlet on the bottom and the out let on top. Prime the chamber by running PBS through it at speed setting 85. Then turn it down to ~50, or ~30 $\mu\text{l}/\text{min}$.

16) Open the Maxtek RQCM software and use the “View Status” and “Run Experiment” (using RRs parameters) to monitor the frequency and resistance during calibration.

17) Tune the capacitance by adjusting the course knob to the lowest setting where it will lock and allow tuning with the fine knob. Turn the fine knob up until the yellow flashing light flashes very slowly (~once per 5 sec).

18) Once it is locked and tuned at 5(+/-0.02) MHz and a resistance of 350(+/-15) ohms, make sure the delta frequency stays +/-0.5 during a 5 min time period in the “Run Experiment” mode.

*If it doesn't equilibrate, check that there are no bubbles in the chamber and that the crystal is good. *Take note of the Run # at the top of the screen

19) After recording a equilibrated base line with PBS for 5 min, add RSV infected HEp-2s at 2.0×10^5 pfu/ml until it stabilizes (~10 min), then add PBS until it stabilizes (~10 min), then add 1%BSA until it stabilizes (~5 min), then add PBS until it stabilizes (~5 min), then add 2-4 nM fAuNPs until it stabilizes (~5 min), then add PBS until it stabilizes (~10 min).

*To ensure no bubbles are introduced into the balance, turn the pump off before switching reagents.

*Take note of each time point that each reagent was added.

20) Collect the data by opening the Maxtek RQCM software, open “View Results”, find run number, click “Convert Binary to ASCII”, click “yes”, and click “okay”. Lookup the

location on the hard drive, paste into flash drive, and change extension from “.dat” to “.txt”.

- 21) Graph the data by opening Excel, click “data”, click “from text”, then open the file. Insert two new columns between “delta frequency” and “Mass #1”. Call the D column “delta resistance”, add the formula $=I2-I1$, then drag it down all the rows of that column. Call the E column “Mass (μg)”, add the formula $=(-C2+(D2*2.095))/165$, then drag it down all the rows of that column. Highlight column A and column E and create a scatter plot graph.

Nanoparticle amplified Immuno-PCR

Pulldown and tag release

- 1) Add 5 μl fMMPs to 100 μl RSV infected lysates and 200 μl of 5% BSA. Rotate for 1 h, then wash 3 times with coupling buffer.

*Use serial dilutions of the lysates to find limit of detection

*Make an experimental control by using uninfected cell lysates in a separate tube

- 2) Mix the fMMPs with 5 μl of 5 nM fAuNPs and 300 μl of 5% BSA. Rotate for 1 h, then wash 2 times with 5% BSA plus 3 times with PBS. Resuspend in 300 μl nuclease-free water.
- 3) Heat to 95 $^{\circ}\text{C}$ for 10 min, pull the fMMPs to one side, then remove the supernatant and analyze using PCR.

PCR amplification of released tags

4) Add 5 μ l of the supernatant from step 3 to 12.5 μ l 2 \times Rotor-Gene SYBR Green PCR Master Mix, with 0.2 μ M forward and reverse primers, and nuclease-free water to 25 μ l total volume. Do this in triplicate.

*Make a PCR negative control by adding no template/sample in triplicate

5) Using a Rotor-Gene Q 5-Plex qPCR machine, create the following protocol:

DNA polymerase activation: 95 °C for 3 min

PCR (40 cycles): 95 °C for 15 sec (melt)

60 °C for 1 min (anneal/extension)

72 °C for 15 sec (read fluorescence)

Melt curve: 50 °C to 99 °C

6) Calculate the limit of detection using the linear range to calculate 3 standard deviations above the background.

CURRICULUM VITAE

Nicholas M. Adams

100 Sadler Ct.
Nashville, TN 37210

n.adams@vanderbilt.edu
(435) 669-5961

EDUCATION

- Doctor of Philosophy, Chemical and Physical Biology** 2013
Vanderbilt University, Nashville, TN
Advisors: David W. Wright and Frederick R. Haselton
Dissertation title: *Development of Simple Methods for RNA Biomarker Extraction and Detection*
- Bachelor of Science, Biology** 2009
Dixie State College, St. George, UT
Advisor: David W. Jones

RESEARCH EXPERIENCE

- Ph.D. Candidate in Chemical and Physical Biology Program** 2010 - 2013
Vanderbilt University, Nashville, TN
Advisors: David W. Wright and Frederick R. Haselton
- Research Assistant in Molecular Genetics** 2008 - 2009
Dixie State College, St. George, UT
Advisor: David W. Jones
- Undergraduate Research Program in Regenerative Medicine** 2008
University of Utah, Salt Lake City, UT
Advisor: Patrick A. Tresco
- Undergraduate Research Scholar in Virology** 2007
Virion Systems, Inc., Rockville, MD
Advisor: Gregory A. Prince

PUBLICATIONS

1. **Nicholas M. Adams**, Kwo-Kwang Abraham Wang, Alison C. Caprioli, Lana C. Thomas, Besik Kankia, Frederick R. Haselton, and David W. Wright. Quadruplex Priming Amplification for the Detection of mRNA from Surrogate Patient Samples. *Analyst*, 2014, 139 (7), 1644 - 1652. DOI: 10.1039/C3AN02261G
2. **Nicholas M. Adams**, Ian R. Olmsted, Frederick R. Haselton, Darryl J. Bornhop, David W. Wright. The Effect of Hybridization-Induced Secondary Structure Alterations on RNA Detection Using Backscattering Interferometry. *Nucleic Acids Research*, 2013, 41 (9). DOI: 10.1093/nar/gkt165
3. **Nicholas M. Adams**, Amy E. Creecy, Catherine E. Majors, Bathsheba A. Wariso, Philip A. Short, David W. Wright, Frederick R. Haselton. Design Criteria for Developing Low-Resource Magnetic Bead Assays Using Surface Tension Valves. *Biomicrofluidics*, 2013, 7, 014104. DOI: 10.1063/1.4788922

4. Jonas W. Perez, **Nicholas M. Adams**, Grant R. Zimmerman, Frederick R. Haselton, and David W. Wright. Detecting Respiratory Syncytial Virus Using Gold Nanoparticle Amplified Immuno-PCR. *Nanobiotechnology Protocols*, Rosenthal, S, Ed. New York: Humana Press, 2013.
5. **Nicholas M. Adams**, Stephen R. Jackson, Frederick R. Haselton, David W. Wright. Design, Synthesis, and Characterization of Nucleic-Acid-Functionalize Gold Surfaces for Biomarker Detection. *Langmuir*, 2012, 28 (2): 1068 - 1082. DOI: 10.1021/la2028862
6. Hali Bordelon*, **Nicholas M. Adams***, Amy S. Klemm, Patricia K. Russ, John V. Williams, H. Keipp Talbot, David W. Wright, Frederick R. Haselton. Development of a Low Resource RNA Extraction Cassette Based on Surface Tension Valves. *ACS Applied Materials and Interfaces*, 2011, 3 (6): 2161 - 2168. DOI: 10.1021/am2004009. *These authors contributed equally.

Manuscripts in Preparation

7. Hali Bordelon, **Nicholas M. Adams**, Kwo-Kwang Abraham Wang, Laura E. Albert, David W. Wright, Frederick R. Haselton. The Effects of Magnetic Bead Surface Functionalization on Nucleic Acid Extraction and Detection.
8. Hali Bordelon*, Anna L. Bitting*, Mark Baglia, Keersten M. Davis, Amy E. Creecy, Philip A. Short, Laura E. Albert, Aditya Karhade, David W. Wright, Frederick R. Haselton, **Nicholas M. Adams**. Automated Extraction of Nucleic Acid and Protein Biomarkers Using Surface Tension Valves. *These authors are contributing equally.
9. **Nicholas M. Adams**, Keersten M. Davis, Frederick R. Haselton, David W. Wright. Battery-Powered Tube Vortexer Made from a Personal Massager for Mixing Samples in Resource-Limited Settings.

PRESENTATIONS

1. *Development of a Simple and Self-Contained mRNA Biomarker Extraction and Detection Assay*. Biomedical Engineering Society Annual Conference, Seattle, WA, 2013 (oral presentation)
2. *A Franchise Model for Sustainable Diagnostic Test Delivery*. Vanderbilt Institute for Global Health Seminar, Nashville, TN, 2013 (oral presentation with Rick Haselton)
3. *Health Centers of Peru*. Engineering World Health Seminar, Nashville, TN, 2013 (oral presentation)
4. *Self-Contained Processing of Patient Samples Using Surface Tension Valves*. Technologies for Brighter Futures Tech Fair, Lima, Peru, 2013 (oral presentation)
5. *Probe Design for Label-Free RNA Detection Using Backscattering Interferometry*. Vanderbilt Institute of Chemical Biology Research Symposium, Nashville, TN, 2012 (oral presentation)
6. *Design Criteria for Developing Low-Resource Magnetic Bead Assays Using Surface Tension Valves*. Biomedical Engineering Society Annual Conference, Atlanta, GA, 2012 (poster presentation with Rick Haselton)
7. *Low Resource Detection of Pathogen Biomarkers*. Chemical and Physical Biology Program Retreat, Nashville, TN, 2012 (oral presentation)
8. *Extraction of Disease Biomarkers using Surface Tension Valves*, Vanderbilt Institute of Chemical Biology Research Symposium, Nashville, TN 2011 (poster presentation)

9. *The Extractionator: A Self-Contained RNA Extraction Cassette for Biological Samples*, Vascular Biology Research in Progress, Nashville, TN, 2011 (oral presentation)
10. *Low Resource Extraction and Processing of Biological Samples Using Surface Tension Valves*, 11th Annual Nanoscience Forum, Nashville, TN, 2010 (poster presentation)
11. *Development of an Effective Decellularization Method for the Central Nervous Tissue*, Undergraduate Research Forum, St. George, UT, 2009 (oral presentation)
12. *Immune Response of Respiratory Syncytial Virus-Infected Cotton Rats*, Andrew H. Barnum Research Forum, St. George, UT, 2007 (oral presentation)

FELLOWSHIPS AND RECOGNITION

Fellowships and Scholarships

National Science Foundation Graduate Research Fellowship Program	2011 - 2013
National Institutes of Health Training Grant in Vascular Disease	2010 - 2011
Vanderbilt University Fellowship	2009 - 2010
National Science Foundation S-STEM Scholarship	2007 - 2009
Sterling Scholar Scholarship	2002 - 2007

Awards and Honors

First place presentation, Chemical and Physical Biology Retreat	2012
Educational award honorable mention, International Precious Metals Institute	2012
Third place for presentation, 11 th Annual Nanoscience forum	2010
<i>Summa Cum Laude</i> Baccalaureate	2009
Student of the Year in Biology	2009
Awards of Excellence in Natural Science and Mathematics	2008/2009
Dr. Andrew H. Barnum Scholar Award	2007
Science Rebel Award	2007

MENTORSHIP AND TEACHING EXPERIENCE

Undergraduate and Rotation Student Mentorship	2011 - 2013
Vanderbilt University, Nashville, TN	
Students mentored: David Rizzo, Cat Majors, Amy Creecy, and Abraham Wang	
Guest Lecturer: BME 305 Introduction to Research	2011 - 2012
Vanderbilt University, Nashville, TN	
National Science Foundation Undergraduate Research Mentorship	2010 - 2012
Vanderbilt University, Nashville, TN	
Students mentored: Grant Zimmerman and Lana Thomas	
Short Term Training Program for Minority Students Mentorship	2010 - 2012
Vanderbilt University, Nashville, TN	
Students mentored: Ricardo Francis, Bathsheba Wariso, and Jesus Bendito	
Undergraduate Research Preparation Program Mentorship	2008 - 2011
Dixie State College, St. George, UT	
Students mentored: Jace Jensen, Meghan Robertson, and Kong Davis	

TECHNICAL SKILLS

Research

- Writing and preparing manuscripts for peer-reviewed journals
- Writing and preparing proposals for government and foundation grant applications
- Gene transfection and expression in an *Escherichia coli* model
- Culture of bacteria, mammalian cell, and respiratory syncytial virus
- Extraction, amplification, detection, and analysis of nucleic acids
- Design, synthesis, and characterization of functionalized gold nanoparticles
- Circular dichroism spectroscopy for proteins and nucleic acids
- Scanning electron microscopy of nanomaterials
- Quartz crystal microbalance analysis of nanomaterials

Mechanical

- Diagnostic device design, development, and fabrication
- Electrical wiring and theory
- Metal fabrication and welding
- Automotive and diesel mechanics

OUTREACH AND COMMUNITY SERVICE

Scientific Outreach

2008 - 2013

- Scientific demonstrations for school children and scout troops
- Graduate school preparation assistance for underrepresented students

Service Mission in Costa Rica

2003 - 2005

- Community service project planning with local leaders
- Conversational English lessons to adults and children

FOREIGN LANGUAGES

Demonstrated proficiency in conversational and written Spanish